**US Army Corps
of Engineers**®
Engineer Research and
Development Center

Coastal Inlets Research Program

Design Water Levels and Waves for Repairs of Buffalo Harbor North and South Breakwaters and LaSalle Park Seawall, Buffalo, New York

Zeki Demirbilek, Lihwa Lin, Okey G. Nwogu, Weston P. Cross, Colleen M. O'Connell, Shanon Chader, Michael C. Mohr, Geoffrey K. Hintz, Sheila E. Hint, and Michael G. Draganac

May 2019

The U.S. Army Engineer Research and Development Center (ERDC) solves the nation's toughest engineering and environmental challenges. ERDC develops innovative solutions in civil and military engineering, geospatial sciences, water resources, and environmental sciences for the Army, the Department of Defense, civilian agencies, and our nation's public good. Find out more at www.erdc.usace.army.mil.

To search for other technical reports published by ERDC, visit the ERDC online library at http://acwc.sdp.sirsi.net/client/default.

Design Water Levels and Waves for Repairs of Buffalo Harbor North and South Breakwaters and LaSalle Park Seawall, Buffalo, New York

Zeki Demirbilek and Lihwa Lin

Coastal and Hydraulics Laboratory
U.S. Army Engineer Research and Development Center
3909 Halls Ferry Road
Vicksburg, MS 39180-6199

Okey G. Nwogu

University of Michigan
Department of Naval Architecture and Marine Engineering
2600 Draper Road
Ann Arbor, MI 48109-2145

Weston P. Cross, Colleen M. O'Connell, Shanon Chader, Michael C. Mohr, Geoffrey K. Hintz, Sheila E. Hint, and Michael G. Draganac

U.S. Army Corps of Engineers, Buffalo District
1776 Niagara Street
Buffalo, NY 14207

Final report

Abstract

Details of modeling approach for developing estimates of design water levels and waves for two U.S. Army Corps of Engineers (USACE) Buffalo District repair projects are described in this report. The estimates are for (1) the existing Buffalo Harbor (BH) South Breakwater (SB) and its two repair alternatives, and the existing BH North Breakwater, and (2) the LaSalle Park seawall along the northeast shore of the harbor that connects to the Niagara River canal. Two classes of wave models were used to develop these estimates for structural repairs: (1) CMS-Wave, a spectral wind-wave generation, growth, and transformation model, and (2) a nonlinear Boussinesq-type wave model BOUSS-2D. Estimates were developed for the 10-year maximum design water level condition of 3 meters (m) (9.8 feet ft) Low Water Datum and the 20-year design storm conditions with incident wave heights of 3.85 m (12.6 ft) and 4.15 m (13.6 ft), peak period of 10 seconds, and three incident wave directions of 233, 240, and 247 degrees. Study details, including data used, numerical modeling investigations, and analysis of results, are presented in this report.

Contents

Figures and Tables

Figures

Tables

Preface

This study was performed by the Coastal and Hydraulics Laboratory (CHL) of the U.S. Army Engineer Research and Development Center (ERDC) at the request of the U.S. Army Corps of Engineers (USACE), Buffalo District, under the Coastal Inlets Research Program (CIRP), Program Element number 280H46. CIRP is administered at CHL under the USACE Navigation Research, Development, and Technology Transfer Program.

At the time this study was conducted, Mr. Jeffrey A. McKee was the USACE Headquarters Navigation Business Line Manager overseeing the CIRP; Mr. W. Jeff Lillycrop, CHL, was the ERDC Technical Director for Civil Works and Navigation RD&T; Mr. Charles E. Wiggins, CHL, was the ERDC Associate Technical Director for Navigation; and Ms. Mary Cialone was the CIRP Acting Program Manager. The general administrative supervision was provided by Mr. James Gutshall, Chief, Harbors, Entrances, and Structures Branch; Dr. Jacqueline Pettway, Chief, Navigation Division, and Mr. Jeffrey R. Eckstein, Acting Director of CHL.

At the time of publication of this report, Dr. Ty V. Wamsley was Director of CHL, and Mr. Jeffrey R. Eckstein was Deputy Director of CHL.

COL Ivan P. Beckman was Commander of ERDC, and Dr. David W. Pittman was the ERDC Director.

1   Introduction

1.1   Background

1.1.1   Study area of North Breakwater (NB) and South Breakwater (SB) structures

The NB, Old Breakwater North Light (OBNL), Old Breakwater (OB), West Breakwater (WB), and SB were designed to protect portions of the Buffalo Harbor (BH) from incident storm waves in Lake Erie to improve navigation and increase overall utilization of the harbor. These breakwaters shown in Figure 1-1 through Figure 1-6 play an important role in the economic vitality, resilience, and sustainability of the BH complex. The NB and SB structures have been in service for nearly 120 years. The U.S. Army Corps of Engineers (USACE), Buffalo District (LRB), is concerned about the deteriorating condition of these structures and has received funds to develop repair plans for the SB and NB.

The Google® images of the existing SB and NB in Figures 1-1 to 1-5 show their locations in Lake Erie in Buffalo, NY. The south side of the SB is influenced by the nearby Confined Disposal Facility #4 (CDF4), including its curved dike, two breakwaters, the South Entrance Arm Breakwater (SEAB), the Stony Point Breakwater (SPB), as well as by the South Entrance Channel to the BH. The contaminated material storage facility CDF4 is fully enclosed by three structures: a curved dike, the SEAB, and SPB.

The initial LRB plan included design and construction specifications for partial repair of a damaged segment of the southerly portion of the SB structure. The SB structure is a long, continuous structure in these figures, and the NB (see Figure 1-1) is a group of four separate structures. Future repairs to the NB are expected to be considered upon the completion of repairs to the SB.

The location and size of these two groups of structures are depicted in Figures 1-1 through 1-6. Some segments of these structures with approximate dimensions are also provided in these figures and will be referenced later in this report.

The existing NB was constructed in 1899–1901 with a length of 671 meters (m) (2,200 feet [ft]) and design height of 4 m (13.5 ft) above Low Water Datum (LWD). Figures 1-2 and 1-3 show the longitudinal extent of the NB structure. Half of this timber crib substructure was built 11 m (36 ft) wide, and the other half was built 7.3 m (24 ft) wide. Water depth also varies in Figure 1-3 along the four primary segments of NB. At the south end of NB, water depth is 6.7 m (22 ft) LWD but decreases northward where depth reduces to 1.5 m (5 ft) at the north end of NB.

The NB structure was constructed as concrete shell-filled with stones for the above water portion of the NB. It was placed on semi-submerged concrete blocks resting on the timber crib substructure. The most severe damage to the NB occurred due to a storm in 1982. Several inspections have since been made to document damaged areas along the lake side of the NB structure.

Figure 1-1. Locations of NB and SB in Buffalo Harbor, NY.
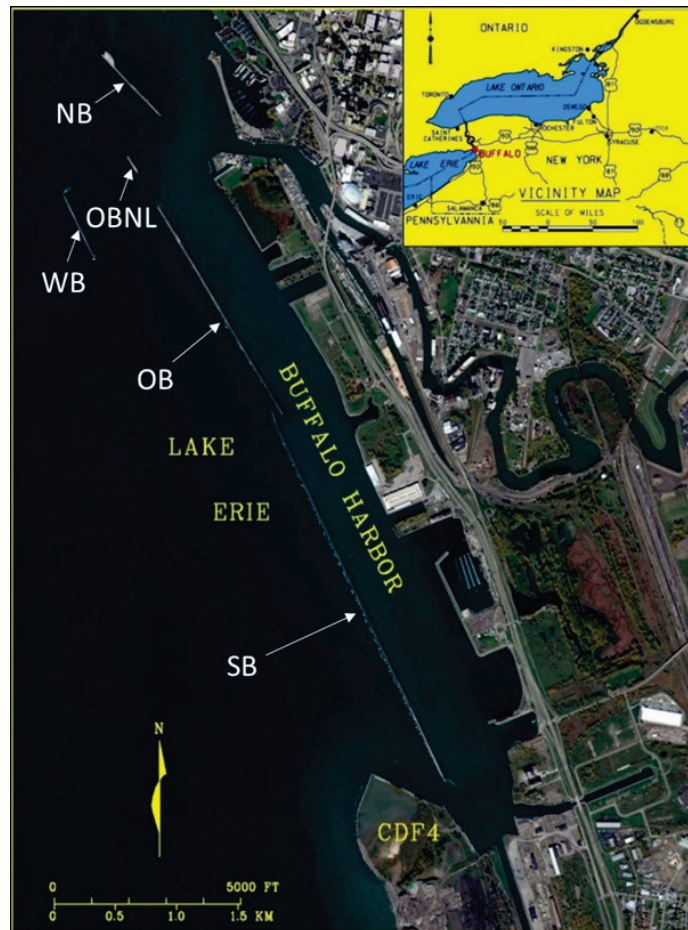
Figure 1-2. Location of the SB and NB structures in BH, NY.
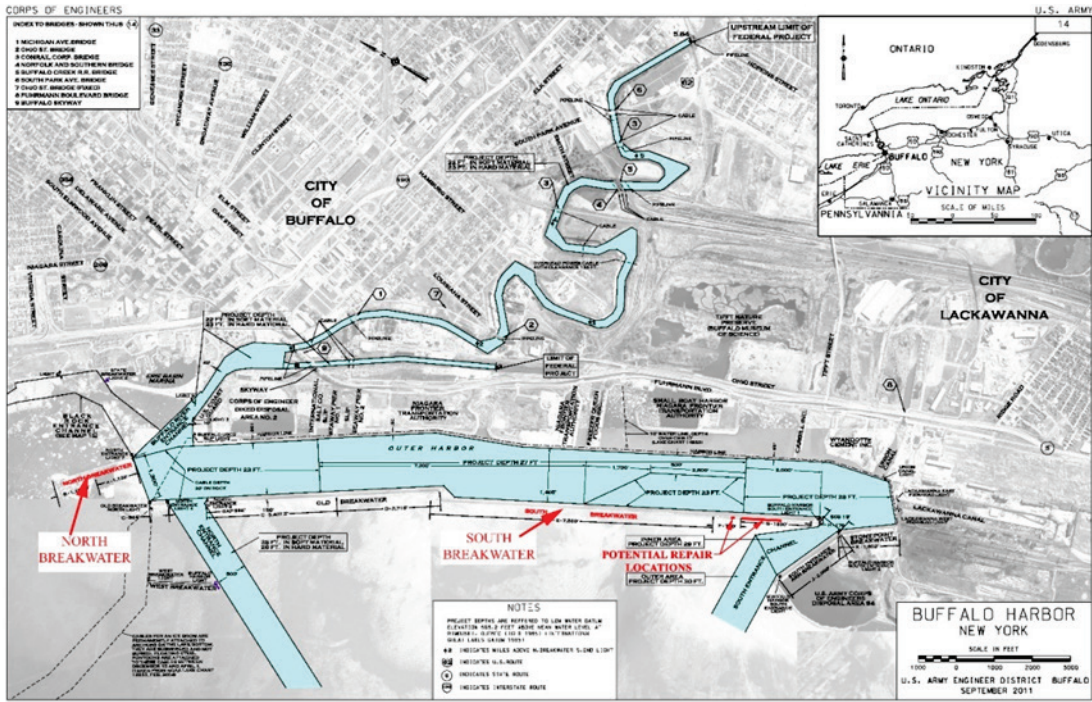
Figure 1-3. The NB structure with four segments

The SB structure was constructed during 1898–1902 and had a total length of 3,109 m (10,200 ft). The 838 m (2,750 ft) long southern portion of the structure had timber cribs below water, a concrete superstructure above, and a laid-up stone facing. Originally, a three-tiered timber superstructure with stone filling was used as the crest. Damage by severe storms, water level variations, and gale winds required a restoration of a 550 m (1,800 ft) long crest section, including a concrete shell with rubble interior. Figures 1-4 and 1-5 depict the proposed repair location of the SB relative to the south part of BH. It also includes a recently completed study area of the CDF4 adjacent to the south entrance of harbor because the close proximity of CDF4 affects the south side of the SB structure.

Figure 1-4. Location of the SB in BH.

Figure 1-5. The proposed repair location of the SB.
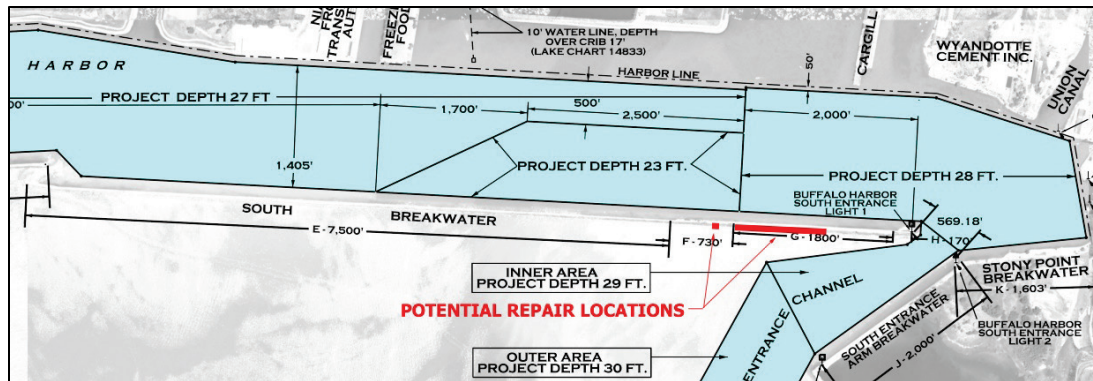
The SB superstructure consists of three parts: (1) three rows of semi-submerged cast-in-place concrete blocks resting on the timber cribs, (2) a banquette deck of concrete blocks with parapet walls and parapet deck, and (3) rubble stone fillings. Each of the five sections of crib super-structure was 55 m (180 ft) long and consisted of five 11 m long (36 ft) pieces. Several repairs were made to the SB structures following damages by a few severe storms.

1.1.2 Study area of LaSalle Park structures

LaSalle Park (LP), located in the north side BH, is part of the land boundary on the east side of the Black Rock Canal as shown in Figure 1-6. The canal is separated from the high-flow of the Niagara River to the west by a dike/wall called "Bird Island Pier" that provides a narrow, calm waterway for vessels to safely move up and down the canal (Figure 1-7). The shore-side of the canal along the LP has a seawall that protects the land and buildings from flooding and erosion caused by waves. Parts of this wall have experienced damages that require repair.

Figure 1-6. LP and vicinity area in north Buffalo Harbor, NY.

Figure 1-7. LP repair reach (red and blue lines).

The shoreline of LP with a total length of approximately 1,452 m (4,764 ft) consists of a bulkhead that extends from the foot of Porter Ave to the seaplane ramp (Figure 1-7). The crest elevation of the structure varies between 2.8 m (9.1 ft) and 3.1 m (10.2 ft) LWD. Although the existing bulkhead has protected the park infrastructure for more than 90 years, it is presently severely deteriorated and in need of repair in several locations

to prevent flooding and shore erosion. The bulkhead superstructure consists of concrete monolith caps while the substructure is either a stone-filled timber crib or timber piles. The City of Buffalo Colonel Ward water pumping station (Figure 1-8), a water filtration plant, and a public park are also located in the LP area.

Figure 1-8. City of Buffalo Colonel Ward water pumping station and water filtration plant.

Figure 1-7 shows the LP repair reach in red and blue lines. The heavy blue line represents the bulkhead substructure. The 232 m long (805 ft) segment represents the stone-filled timber crib with a concrete cap. The 229 m long (550 ft) segment shown with the heavy red line represents the timber piles section with concrete cap. Typical sections of a stone-filled timber crib and timber piles are shown in Figure 1-9 and Figure 1-10, respectively. Figure 1-11 and Figure 1-12 show the dock wall face and degradation of the structure from a dive inspection in June 2011. The Bird Island Pier is an effective attenuator of waves propagating across Lake Erie from the southwest direction. Without the Bird Island Pier, extreme waves with overtopping could potentially damage the LP structures.

Figure 1-9. Typical section of stone-filled timber crib substructure with concrete cap.
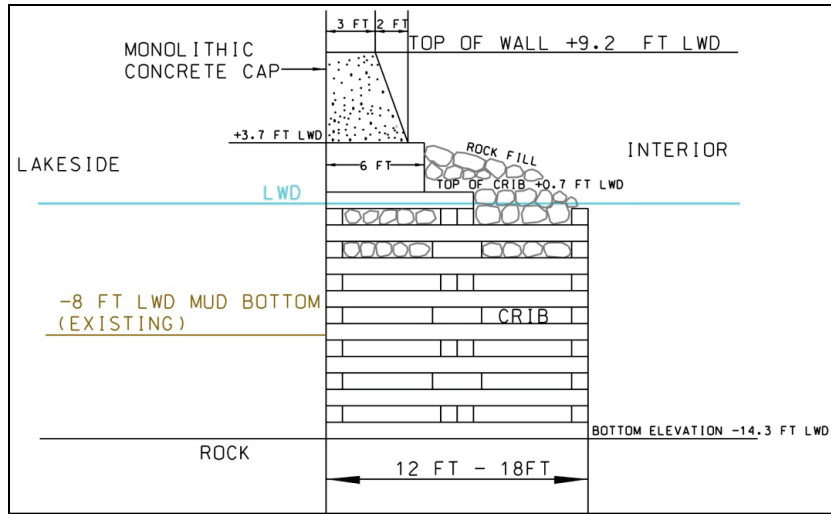
Figure 1-10. Typical section of timber pile substructure with concrete cap,
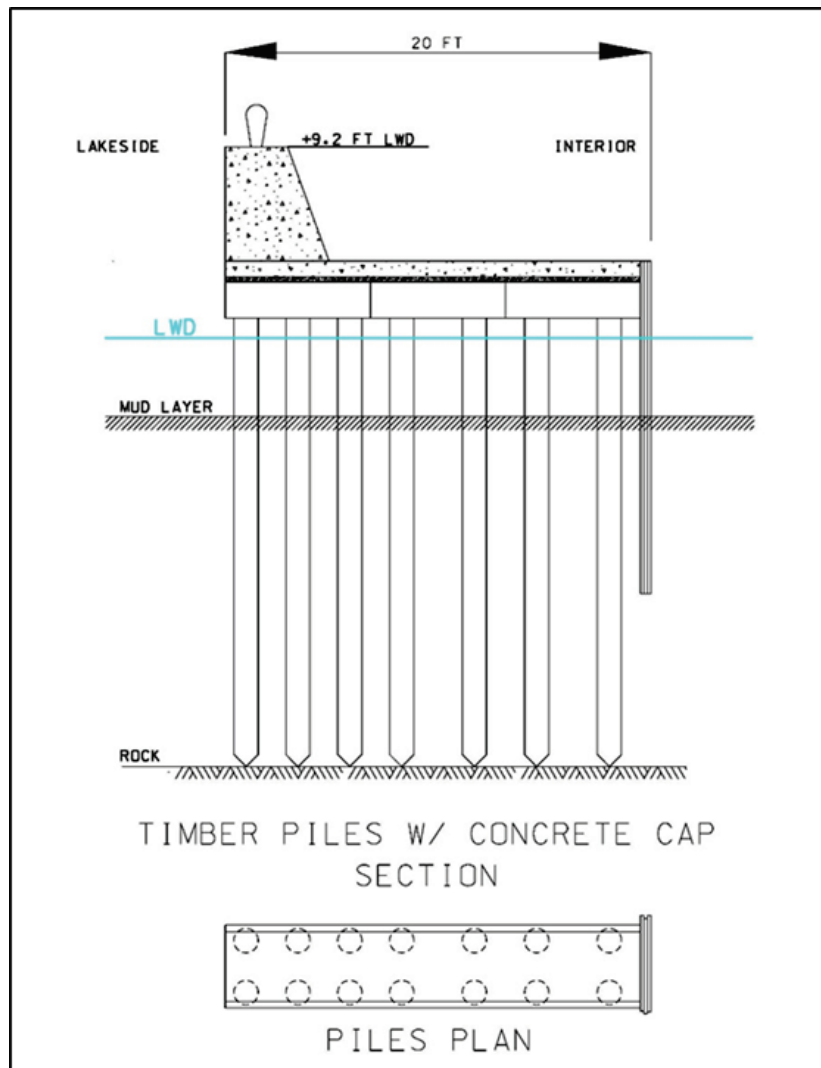
Figure 1-11. Stone-filled timber crib substructure with concrete cap photograph.

Figure 1-12. Timber pile substructure with concrete cap photograph.

The timber crib sections of the structure have lost significant stone fill due to storm surge, waves, and ice damage. Stone fill is being lost through voids in the seawall face. Noticeable settlement of the park lawn surface is occurring along these reaches, as well as the presence of large sink holes. The proposed repair includes grouting the voids in the crib, installing drainage behind the concrete monolith, and concrete repair (Figure 1-13). Wave forces and ice impacts were not evaluated at the timber crib substructure section due to the nature of the repair; structural computations are not required for this repair design.

Figure 1-13. Typical repair section of timber crib.
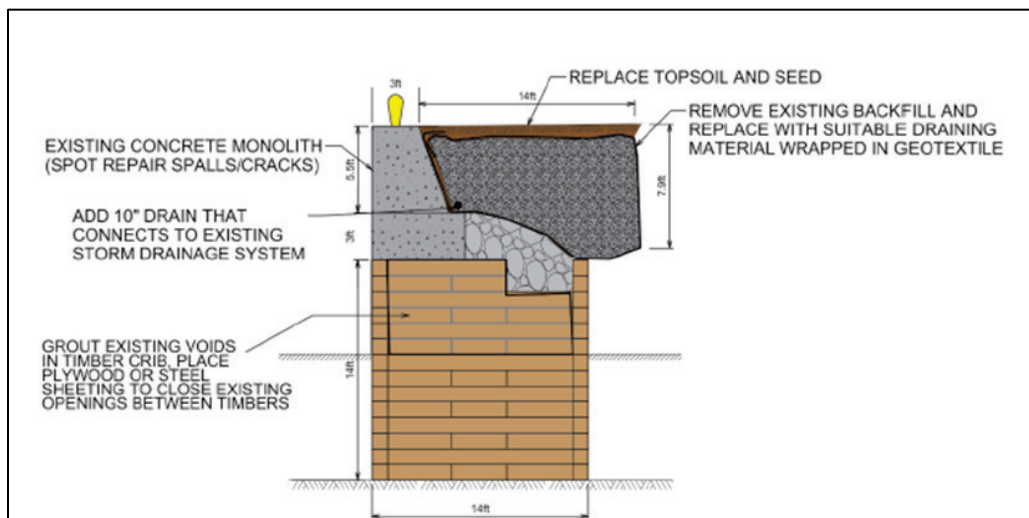
Wave forces and impacts were computed for the timber pile section, since the repair includes encasing the existing structure with 0.6 m (2 ft) diameter concrete-filled cylindrical piles and a concrete cap (Figure 1-14 and Figure 1-15). The timber piles have deteriorated; many of the piles are spilt and are no longer connecting or supporting the existing concrete cap. Figure 1-14 through Figure 1-16 present the proposed front and plan views of repair typical sections.

Figure 1-14. Typical section of encased timber piles.
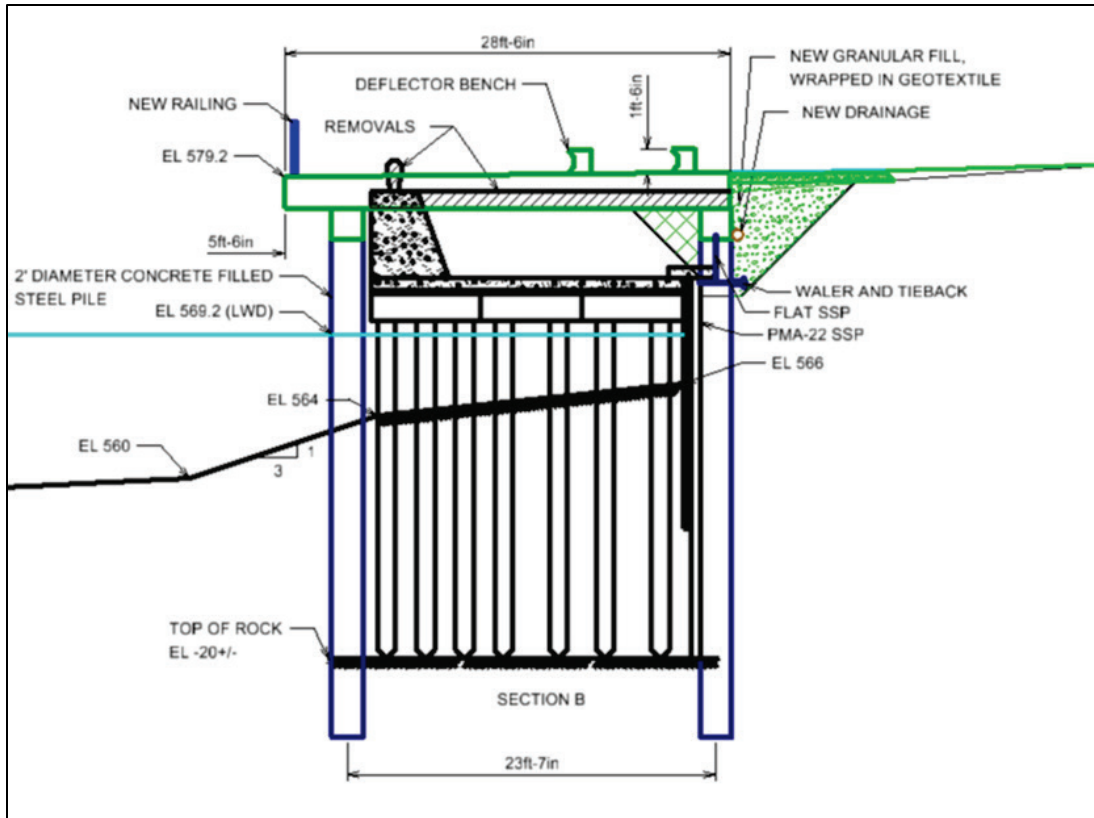
Figure 1-15. Front view of proposed repair for encased timber pile sections.
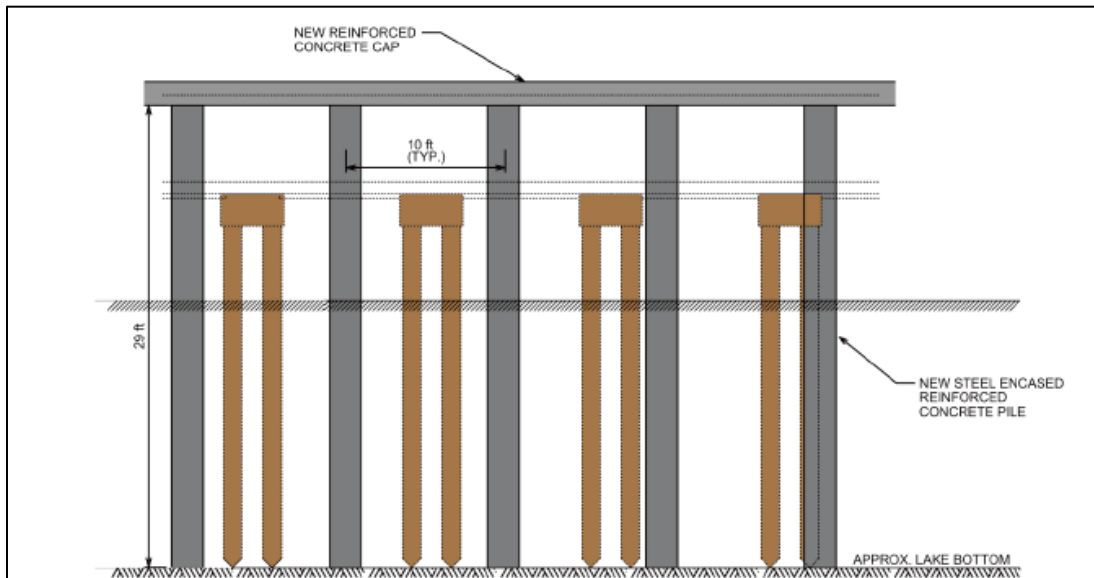
Figure 1-16. Plan view of proposed repairs for encased timber pile sections.
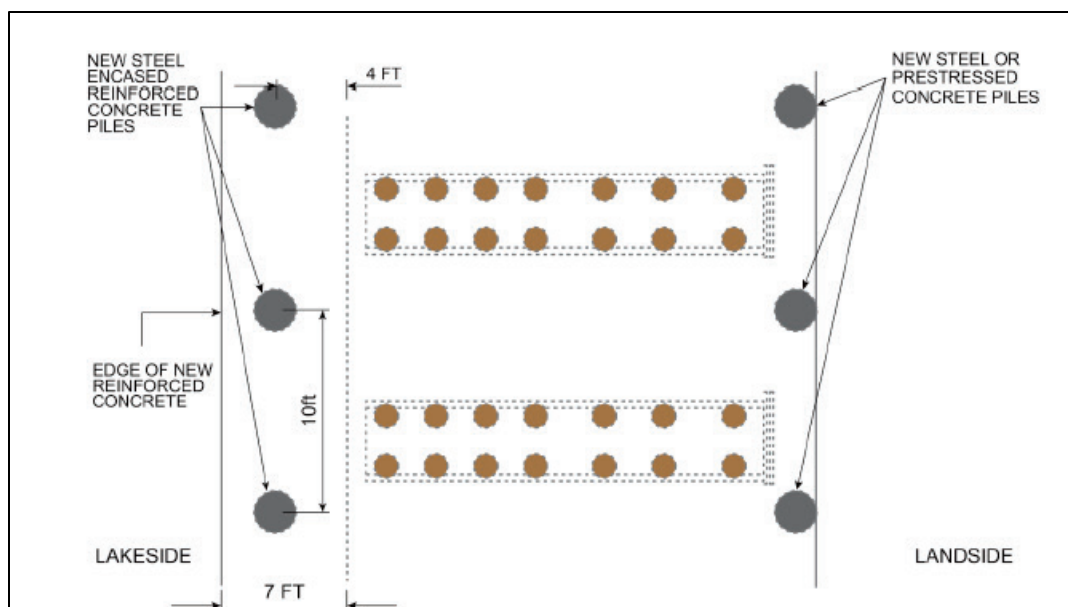
1.1.3   Related recent studies

Estimates of waves, wave overtopping, water levels, and currents were developed in a recent wave and hydrodynamic modeling study for potential repairs of the CDF4 protection structures (Demirbilek et al. 2017). The combination of BOUSS-2D and CMS-Wave models was used to develop these estimates. The NB and SB project teams requested the U.S. Army Engineer Research and Development Center (ERDC), Coastal and Hydraulics Laboratory, to use the same models to develop design wave estimates for a 20-year return-period storm and 10-year water level that were used in the CDF4 study. Three incident storm wave directions with a 3 m (9.8 ft) 10-year design water level were used in the CDF4 study. The same input metocean conditions are also used for the SB and NB existing breakwaters and two new SB project alternatives (Alt1 and Alt2).

Because the LP seawall repair was not part of the NB and SB modeling study, it was added to the scope of study in March 2018 at the request of LRB. To include the LP area in modeling, an additional local grid was required to cover the north sections of BH. Both studies used the same incident wave and water level described in the next section of this report. Estimates were provided for the existing NB and SB and two segments of the SB and the LP seawall for repairs.

To address the needs in the present studies, wave processes in the exterior and interior areas of the BH complex were modeled with two classes of wave models: CMS-Wave, a spectral wind-wave generation and transformation model, and a fully nonlinear Boussinesq-type wave model (BOUSS-2D). Appendices A and B provide additional information about each wave model, their features, and example applications. (More detailed information about each model is available in the following references: Demirbilek et al. 2017, 2016a,b, 2015a,b,c,d; Demirbilek and Rosati 2011; Lin et al. 2011a,b.)

1.1.4 Environmental conditions at the study site

All structures located in BH, including the NB, SB, and LP seawall, are affected by wind waves generated in Lake Erie. These waves are also the primary source of wave overtopping at the CDF4 system (Demirbilek et al. 2017). Lake Erie, approximately 388 km (241 miles) long, 92 km (57 miles) wide, and on average 19 m (62 ft) deep, is the eleventh largest lake in the world. It has sufficient fetch to create large wind waves. BH is located in the northeastern end of Lake Erie, coinciding with the dominant direction of lake storms along the longest fetch from southwest to northeast. The storms developing in Lake Erie produce large waves in parts of BH, which can cause significant seiche and wind setup with water surface elevation up to 3 m (9.8 ft).

There are no wave or current measurements in BH. The existing data sources of meteorological and oceanographic forcings include the National Oceanic and Atmospheric Agency (NOAA) buoys and gauges available in Lake Erie, the Great Lakes Observing System, the Great Lakes Coastal Forecasting System (GLCFS), and the USACE Wave Information Study (WIS) wave hindcast data. For consistency with the CDF4 study, the same water level, wind, and wave conditions were used in the present study. Demirbilek et al. (2017) describe details of the environmental conditions in the previous CDF4 study, and therefore only a brief description of climate is included in this report.

The bathymetry and structural data used in modeling were provided by LRB. Data obtained from different airborne lidar and boat surveys conducted were assembled, merged, and used in the present modeling studies. Datasets included high-resolution multibeam surveys collected by the LRB survey crews and lidar data collected by the Joint Airborne Lidar Technical Center of Expertise (JALBTCX). Incident waves are not affected by the Lake Erie bathymetry until reaching the harbor and proximity of

structures. Strong wave-structure interactions occur with multiple structures designed to protect north, middle, and south parts of the harbor complex. Only those waves overtopping or passing around these structures reach the interior of harbor. Breaking waves overtopping the protective structures and waves inside and outside shallow areas of northeast lake generate wave-induced currents, which can affect structures and navigation within the harbor. The numerical modeling study used the most recent bathymetric, wind, and wave data available.

1.2 Objective

Estimates are required of the design water levels and waves for repairs of the existing Buffalo Harbor SB and its two repair alternatives, the existing NB and LP seawall along the northeast shore of the harbor that connects to the Niagara River Canal. The SB and NB structures have been in service for nearly 120 years and are in a highly deteriorated condition. The shore-side of the canal along the LP has a seawall that protects and stabilizes the land and buildings from flooding and erosion caused by waves. Parts of this seawall have experienced extensive damage and require repair.

The LRB is concerned about the condition of these structures, and requested services of the USACE ERDC to develop estimates of the hydrodynamics and wave climate for design of repairs to these structures that play an important role in the economics of the region and in the resilience and sustainability of the Buffalo Harbor complex.

1.3 Approach

Two types of wave models (BOUSS-2D, and CMS-Wave) were used to develop estimates of waves and hydrodynamics for repair of the SB, NB, and LP structures. To develop these estimates inside the harbor required a regional-scale transformation of design incident waves in Lake Erie (Demirbilek et al. 2017). This was accomplished using a spectral wind-wave generation and transformation model that provided estimates of wind waves in the nearshore areas. For waves penetrating into the harbor and their strong interactions with harbor structures, a Boussinesq-type nonlinear, time-domain wave model BOUSS-2D (B2D hereafter) was used. B2D is a phase-resolving model developed specifically for modeling waves in nearshore applications including wave-structure interactions and for a variety of navigation project needs (e.g., channel widening, deepening, and infrastructure modifications in ports, harbors, and marinas). This model was used to include wave runup and overtopping in the wave estimates.

Although B2D is capable of modeling flooding of the land, this was not in the scope of present studies and not considered.

The long-term wave climate in Lake Erie developed in the previous CDF4 project (Demirbilek et al. 2017) was used in the present study. The design incident wave conditions are based on the WIS hindcast time series (1979–2012) for Lake Erie and transformed to the BH using CMS-Wave. The CMS-Wave model results were used as input wave forcing at the boundary of B2D model domain for developing estimates of design wave conditions for repair studies at the SB and NB and the LP seawall.

A combination of B2D and CMS-Wave was necessary for quantifying the impacts of waves on damaged structures in BH. CMS-Wave is used for the generation and growth of wind-waves in Lake Erie and to provide input conditions to B2D. An added benefit of using two wave models was to check and identify potential errors in setting up models and analysis of model results. Following the CDF4 study, this is the second wave overtopping study conducted using a combination of CMS-Wave and B2D models in BH.

An in-depth analysis of wind, water level, and wave conditions in Lake Erie was conducted by LRB in the previous CDF4 project. That study determined representative storms for the 10-year water level and 20-year wave to be modeled in this study. Demirbilek et al. (2017) provide a detailed description of the LRB analysis, including selection of return period events for future design waves and water levels for structural design and repair, and environmental and maintenance studies in BH. The design conditions inside and outside the BH for significant storm events for the present repairs at SB and NB structures and LP seawall are based on the climate analysis performed for the CDF4 project.

The tasks performed to provide design wave estimates for the SB, NB, and LP structural repair studies included (1) regional meteorological and oceanographic conditions (e.g., winds, waves, water levels) for the present study based on the 20-year design wave and 10-year water level from the previous CDF4 study, (2) assembly of new bathymetric, shoreline, and structural data for interior and exterior regions of BH and inclusion of structural surveys at the vicinity of repair areas, (3) calculation of waves outside and inside of the BH, (4) investigation of details of wave estimates

for repairs with and without overtopping of structures, and (5) analysis of model results and summary of key findings documented in this report.

The existing structural configurations of NB and SB and those of the two SB repair alternatives were investigated. Figure 1-5 shows the two SB repairs of the Section F and Section G. The first repair alternative considered placing a rubble-mound submerged plateau along the lakeside that served as a frontal low-stability berm. The second alternative considered the rounded ends that connect the berm to the SB structure to avoid wave focusing at both joining ends. Both alternatives are included in this analysis.

As noted earlier, the modeling areas for the SB and NB structures were located north of the CDF4, indicating that the grids used in the CDF4 study could not be used for the NB, SB, and LP modeling studies. New grids were required for CMS-Wave and B2D models. Furthermore, these new grids had to have a fine grid resolution for a proper representation of the breakwaters, complicated harbor bathymetry and its enclosing land boundaries. After several iterations, it was decided to use one large grid domain that included both SB and NB structures. This was done by covering most of the middle harbor and parts of south and north harbor. This domain excluded some of north side of harbor and did not cover most of LP and the Black Rock Canal to the north.

Chapter 2 describes data used in the present study. Chapter 3 and Chapter 4 provide details of modeling for CMS-Wave and B2D, respectively. Conclusions are provided in Chapter 5.

2 Data for the Study

2.1 Bathymetry and coastline data

The bathymetry data used in this structural repair study were provided by the LRB. The data were assembled from various sources covering the harbor, land, nearshore, and offshore areas, and included some recent surveys of the damaged segments of breakwaters. The bathymetry for the exterior and interior of harbor, channels, structures (breakwaters, dikes, jetties, seawalls etc.), and shorelines were from the JALBTCX 2007 lidar data and recent multi-beam surveys conducted by LRB. The multi-beam surveys are the primary source, and the lidar data were used to fill in the gaps. Data for the offshore area was extracted from the National Geophysical Data Center (NGDC) GEODAS database (https://www.ngdc.noaa.gov/mgg/greatlakes/erie.html). Parts of coastline data were extracted from the NGDC (http://www.ngdc.noaa.gov/mgg/ shorelines/) and were augmented with several georeferenced image files downloaded from Google Earth Pro 7.3 (http://earth.google.com). All datasets were converted to the Lake Erie's LWD, which is 173.5 m (569.2 ft) above the International Great Lakes Datum (IGLD) 1985.

2.2 Water level and river discharge data

Hourly water level data from 1960 to the present time were available from NOAA Coastal Station 9063020 (BUFN6), located on the south side of the Buffalo River (http://tidesandcurrents.noaa.gov/) near the upriver end of the U.S. Coast Guard base (42° 52.6' N, 78° 53.4' W). Daily discharge data for the Niagara River were available at Buffalo from U.S. Geological Survey (USGS) Station 4216000 (42° 52.67' N, 78° 54.98' W) since 1926 (https://waterdata.usgs.gov/nwis/rt). River discharge data were used in the CMS. The average annual discharge is approximately 5,800 m^3/second (sec) (204,000 ft^3/sec). Table 2-1 presents the mean monthly and annual discharges. The Buffalo River discharge was estimated from three major tributaries: Buffalo Creek, Cayuga Creek, and Cazenovia Creek from USGS-collected river stream data and drainage areas (Irvine et al. 1991). The annual discharge is approximately 20 m^3/sec (700 ft^3/sec). Table 2-2 presents the annual mean discharges for the Buffalo River and three major tributaries. Figure 2-1 shows the location map of NOAA 9063020/BUFN6 (green label) and USGS Station 4216000 (white label), WIS hindcast

output stations (red label) and an Environmental and Climate Change Canada (ECCC) Buoy 45142 (blue label).

Table 2-1. Mean monthly and annual discharge for the Niagara River at Buffalo, NY.

Month/Annual	Mean Discharge (ft³/sec)*
January	196,000
February	193,000
March	199,000
April	207,000
May	216,000
June	215,000
July	211,000
August	207,000
September	203,000
October	199,000
November	200,000
December	201,000
Annual	204,000

* based on 1926–2015 data from NOAA Coastal Station 9063020

Table 2-2. Buffalo River average annual discharge.

Location	Period of Record	Drainage Area (miles²)	Average Annual Discharge (ft³/sec)
Buffalo Creek at Gardenville, NY	October 1938 to current year	142	207.2
Cayuga Creek near Lancaster, NY	September 1938 to September 1968, annual maximum only--1972-74, May 1974 to current year	96.4	139.6
Cazenovia Creek at Ebenezer, NY	June 1940 to current year	135	242.1
Total above		373.4	588.9
Buffalo River at mouth		446	**703.4***

* pro-rated by drainage area

Figure 2-1. Location of NOAA (green), USGS (white), WIS (red), and ECCC (blue) coastal stations.

2.3 Wind and wave data

Coastal wind and wave data in the study area are available from various sources. NOAA Station 9063020 provides the hourly wind data since 1960. Offshore wave data are available from Meteorological Service of Canada (MSC) (http://www.meds-sdmm.dfo-mpo.gc.ca/isdm-gdsi/waves-vagues/index-eng.htm) Moored Buoy 45142 (Port Colborne; 42° 44.6' N, 79° 17.6' W). The GLCFS archived hourly nowcasts for Lake Erie are available for the period of 2006 to present (http://data.glos.us/glcfs/). The USACE WIS has the long-term wind and wave hindcasts for 1979 to 2012. (Data for 2013–2014 were not available at the time of this study.) Figure 2-1 shows the location of Buoy 45142 and WIS stations for the northeastern end of Lake Erie. In the present modeling study, WIS Station 92243 (42° 48' N, 78° 57.6' W), which is the closest WIS station to BH, was used for the incident wave conditions (14 m water depth).

2.4 Storm data for modeling

Storm analysis was based on WIS Station 92243 hindcast data (1979–2012). Storm duration was the time maximum significant wave heights were greater than 4 m (13 ft). The storms with maximum significant wave heights greater than 4 m (13 ft) and mean wave directions within Class Angle 2 encompassing 219 and 279 degrees (deg) azimuth (Figure 2-2) were selected for analysis by LRB. The analysis showed that all major storm (significant wave height [Hs] greater than 4 m [13 ft]) approached BH during the peak of the storm from 247 deg with a standard deviation of 1 deg. Table 2-3 presents storm events selected from WIS Station 92243. Table 2-4 presents the 2-year, 10-year, 20-year, and 50-year recurrence of storm waves within Class Angle 2 sector (specified by LRB) at WIS Station 92243.

Figure 2-2. Class Angle 2 wave directions.
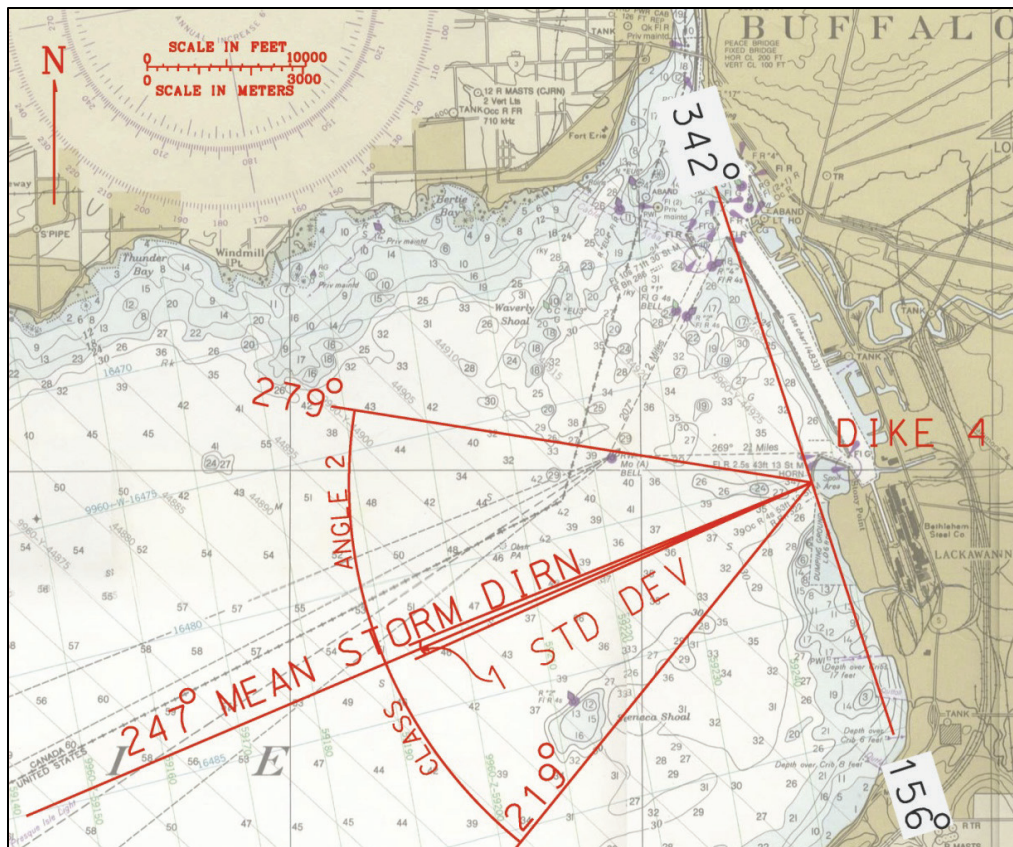
Three storm conditions were specified by LRB for wave modeling in the previous CDF4 study (Demirbilek et al. 2017). These were (Tables 2-3 and 2-4): (1) 2-year wave and 2-year water level (Storm Condition 1), (2) 20-year wave and 10-year water level (Storm Condition 2), and (3) the 11

January 2008 storm (Storm Condition 3). Appendix C presents the detail of these storm data selection and analyses. In the present SB, NB, and LP modeling, Storm Condition 2 was selected for the design wave and water level forcing. As specified by LRB, the 20-year wave condition was averaged from the following three approximately 20-year recurrence storms: 1 February 2002, 18 January 2012, and 25 December 2013. The details of averaging three storms are described in Appendix C. A constant wind and wave direction of 247 deg was used for Storm Condition 2.

Table 2-3. List of selected storm wave events from WIS Station 92243.

Rank	Start Timestamp*	End Timestamp*	Peak Wave Timestamp*	Peak Wave H_S (m)	T_p (sec)**	Θ_p (deg)**
1	12022419	12022607	12022501	4.85	9.7	249
2	12011717	12011816	12011801	4.73	9.2	248
3	02020115	02020206	02020120	4.72	10.1	247
4	12030304	12030418	12030313	4.68	10.0	247
5	12012814	12013017	12012822	4.68	9.4	248
6	06120120	06120300	06120203	4.59	10.2	247
7	12010116	12010305	12010203	4.57	10.0	247
8	08122715	08122907	08122819	4.48	10.0	248
9	11101416	11101810	11101521	4.37	10.2	248
10	82011015	82011206	82011112	4.37	10.2	247
11	85120120	85120313	85120213	4.36	10.0	247
12	03111303	03111410	03111314	4.33	10.9	247
13	82010412	82010521	82010503	4.30	10.8	246
14	09120914	09121212	09121005	4.29	10.8	246
15	87121514	87121706	87121608	4.27	11.0	246
16	00121715	00121820	00121803	4.22	10.0	247
17	90110603	90110623	90110611	4.15	10.4	247
18	11042811	11042903	11042816	4.11	9.2	246
19	08010905	08011005	08010913	4.11	8.5	249
20	06020507	06020712	06020514	4.10	9.6	246
21	89010804	89010923	89010820	4.06	9.7	248
22	12011308	12011411	12011315	4.01	9.2	247

* timestamp given in yymmddhh (yy for year, mm for month, dd for date, hh for hour, Greenwich Mean Time   (GMT))

** wave period T_p and direction Θ_p associated with the peak wave height H_S

Table 2-4. Class Angle 2 recurrence of storm wave
heights and associated wave period.

Return Period (year)	H_S (m)	Tp (sec)
2	4.2	9.8
10	4.7	10.2
20	4.8	10.4
50	5.1	10.6

The 2-year storm water level condition was averaged (with storm water
level peak aligned at the same time) from three approximately 2-year
recurrence storms: 13 November 2003, 7 October 2009, and 25 December
2014. Similarly, the 10-year storm water level condition was averaged from
three approximately 10-year recurrence storms: 12 December 2000, 10
March 2002, and 1 December 2006. Table 2-5 presents the water levels for
2-year, 10-year, 20-year, and 50-year recurrence intervals. These water
levels were based on data collected at the NOAA gauge.

Table 2-5. Water levels at NOAA Station 9063020 for
several recurrence intervals.

Return Period (year)	Water Level (m), IGLD 1985
2	175.80
10	176.45
20	176.56
50	176.74

Table 2-6 presents the hourly wave height, wave period, wave direction,
wind speed, wind direction, and water level for Storm Condition 2, which
covers a 50-hour (hr) duration. Storm Condition 2 has a maximum wave
height of 4.8 m (15.7 ft) at Hour 14, coincident with the highest water level
of 176.45 m (578.7 ft) (IGLD 1985) or 3.0 m (9.8 ft) above the LWD.

Table 2-6. Hourly data for the 20-year wave and 10-year water level storm
(Storm Condition 2).

Time (hr)	H_S (m)	T_p (sec)	θ_p (deg)	U_{10} (m/sec)	Wind Direction (deg)	Water Level (m) IGLD 1985
0	0.34	2.94	247	3.4	247	173.84
1	0.34	3.10	247	3.4	247	173.77
2	0.34	3.13	247	3.4	247	173.77
3	0.34	3.17	247	3.4	247	173.75
4	0.36	3.23	247	3.5	247	173.77
5	0.40	2.91	247	3.7	247	173.77
6	0.50	3.21	247	4.1	247	173.69
7	0.62	3.43	247	4.7	247	173.76
8	0.79	3.89	247	5.4	247	173.83
9	1.36	5.12	247	7.9	247	173.85
10	2.16	6.20	247	11.1	247	174.29
11	2.95	7.22	247	14.1	247	174.72
12	3.77	8.48	247	17.0	247	174.83
13	4.45	9.63	247	19.2	247	175.51
14	4.80	10.40	247	20.2	247	176.45
15	4.54	10.63	247	19.4	247	176.27
16	3.96	10.45	247	17.6	247	175.58
17	3.50	10.10	247	16.0	247	175.25
18	3.17	9.72	247	14.9	247	175.29
19	2.91	9.30	247	13.9	247	174.99
20	2.77	9.06	247	13.4	247	174.74
21	2.63	8.73	247	12.9	247	174.58
22	2.41	8.51	247	12.1	247	174.65
23	2.16	8.16	247	11.1	247	174.46
24	1.94	7.94	247	10.2	247	174.19
25	1.74	7.66	247	9.4	247	174.33
26	1.61	7.47	247	8.9	247	174.61
27	1.54	7.33	247	8.6	247	174.70
28	1.47	7.23	247	8.3	247	174.49
29	1.37	7.22	247	7.9	247	174.44
30	1.24	7.23	247	7.4	247	174.56
31	1.12	6.84	247	6.8	247	174.52
32	1.03	6.75	247	6.5	247	174.43

Time (hr)	H_S (m)	Tp (sec)	Θp (deg)	U_{10} (m/sec)	Wind Direction (deg)	Water Level (m) IGLD 1985
33	0.97	6.83	247	6.2	247	174.37
34	0.92	6.68	247	6.0	247	174.33
35	0.87	6.62	247	5.8	247	174.20
36	0.83	6.45	247	5.6	247	174.04
37	0.80	6.11	247	5.5	247	173.99
38	0.77	6.00	247	5.3	247	174.00
39	0.72	6.04	247	5.1	247	174.04
40	0.69	5.97	247	5.0	247	174.01
41	0.66	4.86	247	4.8	247	174.03
42	0.65	4.81	247	4.8	247	174.08
43	0.64	4.79	247	4.8	247	174.16
44	0.62	4.75	247	4.7	247	174.24
45	0.60	4.70	247	4.6	247	174.18
46	0.61	4.60	247	4.6	247	174.17
47	0.62	4.66	247	4.7	247	174.14
48	0.65	4.80	247	4.8	247	174.12
49	0.71	5.00	247	5.1	247	174.07
50	0.80	5.01	247	5.5	247	174.01

3   CMS-Wave Modeling

3.1   Description of wave models

Two classes of wave models were used to investigate the storm wave conditions at BH. CMS-Wave is a steady-state two-dimensional (2D) spectral wave model (Lin and Demirbilek 2012; Lin et al. 2011a,b; Demirbilek and Rosati 2011; Lin et al. 2008; Demirbilek et al. 2008). It is one part of an integrated Coastal Modeling System (CMS) for coastal and inlet processes modeling applications. (CMS-Wave was the main modeling effort, not CMS-Flow. CMA-Flow modeling was considered only for potential change in the local water level at certain parts of the harbor resulting from river discharge and/or wave/current interactions.) B2D is a Boussinesq-type 2D wave model (Demirbilek and Nwogu 2007; Demirbilek et al. 2007a,b,c; Demirbilek et al. 2005a,b; Nwogu and Demirbilek 2001). CMS-Wave is used to transform deep or intermediate-water incident waves to the nearshore to develop input conditions for B2D.

CMS-Wave can be used in half-plane or full-plane mode to transform offshore waves to nearshore project sites. The half-plane is the default mode, and the model runs efficiently in this mode as waves are transformed primarily from offshore toward the coast. CMS-Wave is based on the wave-action balance equation that includes wind-wave generation, wave propagation, refraction, shoaling, diffraction, reflection, breaking, and dissipation. The computational efficiency of CMS-Wave and recent improvements to the capabilities of the model (Lin and Demirbilek 2012; Lin et al. 2011a,b; Demirbilek and Rosati 2011) allow for simulating large spatial domains and a large number of wave conditions in coastal engineering applications. The advantages also include dynamic coupling with CMS-Flow, a 2D circulation and sediment transport model in the CMS, and the use of nesting of multiple grids for simultaneous modeling of regional and local processes. CMS-Flow is used with CMS-Wave to account for wave-current interactions and variation of water levels. (Additional information about CMS-Wave is provided in Appendix A.)

B2D is a nonlinear, time-domain wave model capable of representing various wave processes occurring from intermediate to shallow water. It is a computationally resource-demanding model. Large domain modeling around this harbor was not possible with B2D because of the large number of conditions to be simulated. It was necessary to augment B2D

modeling with CMS-Wave, a spectral wave model capable of efficiently providing wave estimates over a large domain for many wave conditions. Because of complementary features of B2D and CMS-Wave, these two models are frequently used together in coastal studies. CMS-Wave was used in the present study to transform the offshore hindcast waves from the WIS Station 92243 to the seaward boundary of B2D. (Appendix B provides additional information about the B2D model, its capabilities, and example applications. Details of the B2D modeling for this study are presented in Chapter 4.)

3.2 Modeling grids and domains

Table 2-4 presents the offshore incident wave conditions along the CMS-Wave grid offshore boundary (based on the WIS hindcast data). The CMS-Wave model results were used as input wave to force B2D for developing estimates of design waves at the SB and NB and LP seawall.

CMS-Wave modeling consisted of two grids: a *parent* grid that covered the eastern end part of Lake Erie and a *child* grid covering the BH complex. The parent and child grids include all breakwaters, seawalls, and CDF4 present in the BH complex. Figure 3-1 shows the CMS-Wave parent grid domain (red box) and child grid domain (yellow box). The parent grid had 13 nesting cell output locations (orange circle) for saving model wave spectra for the child grid. The offshore westward boundary of the parent grid extends beyond WIS Station 92243. The parent grid covered a rectangular area approximately 11 kilometers (km) (7 miles) (cross-shore) × 17 km (11 miles) (alongshore). The grid cell size in the parent grid varied from 20 to 200 m (65 to 650 ft), and water depths varied from 0 to 14.6 m (0 to 48 ft). The parent grid was used to transform the offshore incident wave to the BH nearshore to develop and provide the wave condition for the CMS-Wave child grid and B2D grid. These CMS-Wave parent and child grids were also used for CMS-Flow.

The CMS-Wave child grid is within the parent grid; it contains a smaller domain and finer resolution. The child grid includes details of the coastal structures and neighboring nearshore and channel areas. The CMS-Wave child grid covered a rectangular area approximately 4.1 km (2.6 miles) cross-shore × 10.1 km (6.3 miles) alongshore. The child grid cell size varied from 5 to 50 m (16 to 160 ft) with smaller cells around the SB, NB, and LP seawall. Figure 3-2 shows a closer view of the CMS-Wave child grid domain and bathymetry encompassing BH.

B2D is run on four grids: SB grid, NB grid, BH grid, and LP Seawall grid. B2D grid domains are shown in Figure 3-3 with the CMS-Wave child grid domain. The BH grid domain (not marked in Figure 3-3) has the combined domains of SB and NB grids.

Figure 3-1. CMS-Wave parent grid domain (red box) and child grid domain (yellow box).
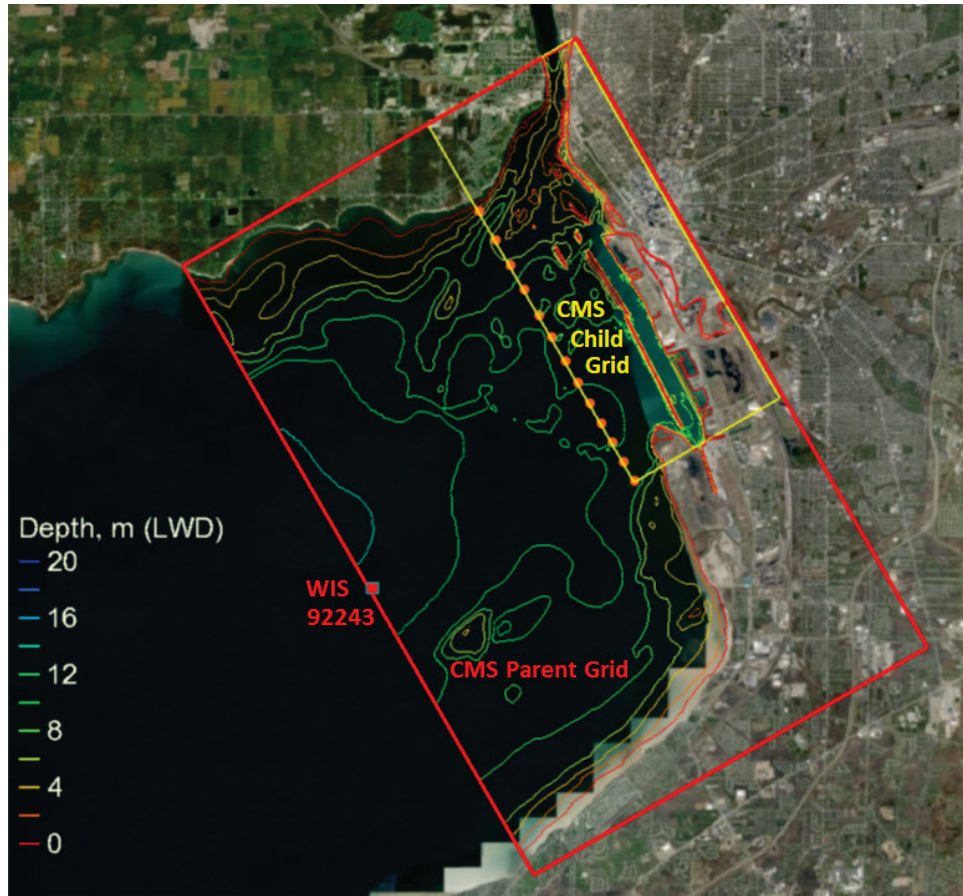
Figure 3-2. CMS-Wave child grid domain (white box) with bathymetry contours.
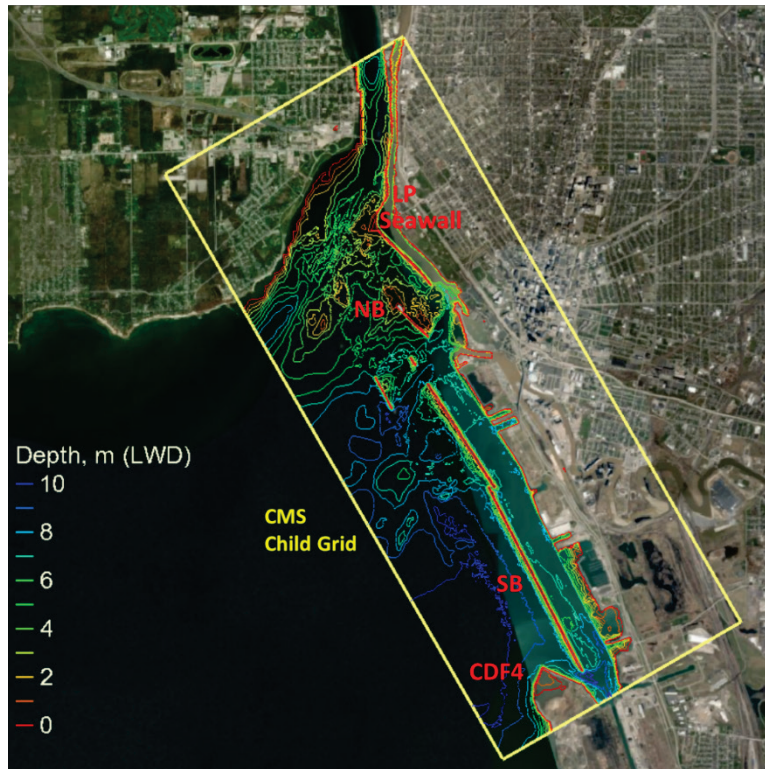
Figure 3-3. CMS-Wave child grid domain and B2D grid domains.
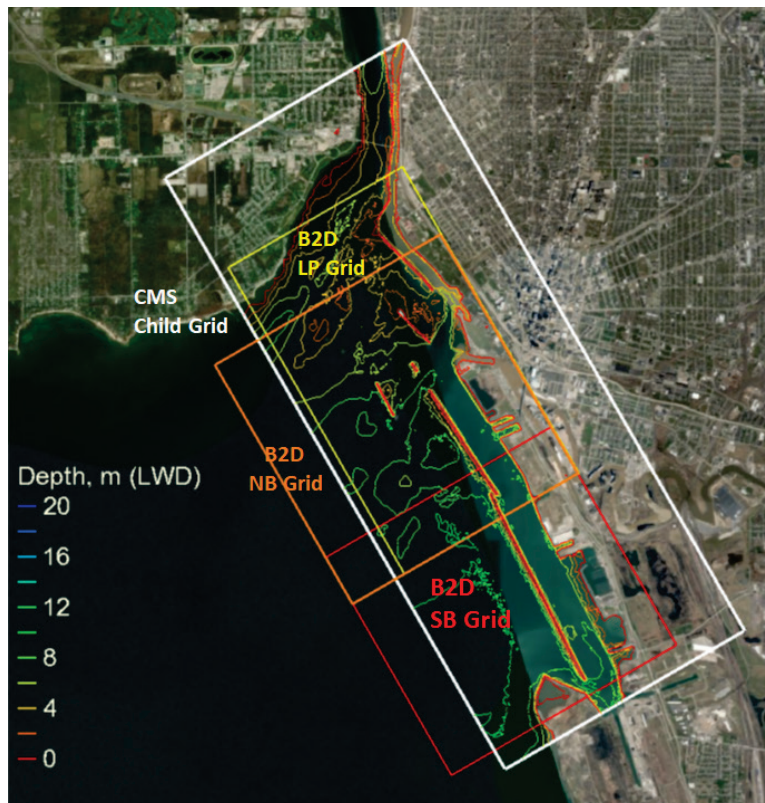
3.3   Model simulations

CMS-Wave was run and coupled with CMS-Flow on the parent and child grids to determine water level change in the entire harbor complex. As described in Section 2.4, the 20-year design storm wave with a constant wave direction of 247 deg, and 10-year water level is used in the present wave modeling. The average annual maximum river discharge of 11,400 m^3/sec (403,000 ft^3/sec) was specified for the Niagara River and 1,060 ft^3/sec (30 m^3/sec) for the Buffalo River. CMS-Flow was used to account for spatial variation in water level and wave/current interactions.

CMS-Wave was run for the grid nesting of a parent grid and a child grid in the half-plane mode. The parent grid simulation provides the wave forcing boundary condition to the child grid. Wave spectra were specified in CMS-Wave using 40 frequency bins (covering the range of 0.06 to 0.45 hertz [Hz] at 0.01 Hz increment) and 35 direction bins (covering a half-plane for incoming wave direction in the range of 152.5 to 327.5 deg azimuth with 5 deg increment). Wave runup and infra-gravity wave options were activated in the parent and child grid simulations. The diffraction intensity was set to 4 (default) for the maximum diffraction allowed in CMS-Wave. A constant Darcy-Weisbach coefficient of 0.005 and a constant reflection coefficient of 0.5 (default) were used for bottom friction and forward reflection calculations, respectively (Demirbilek et al. 2017). Sensitivity analyses were performed in that previous study, and details are presented in Section 4.5 of that previous document.

CMS-Wave and CMS-Flow were coupled at 1 hr intervals. The CMS-Flow explicit-solver version of the model was used for hydrodynamics modeling. A 0.25 sec computational time-step was used in in CMS-Flow and model was run on the same parent and child grids as used in CMS-Wave. A constant Mannings coefficient of 0.025 (default) was used for bottom friction in CMS-Flow (Demirbilek et al. 2017). A constant 3 m (9.8 ft) design water level was specified along the CMS-Flow offshore boundary. The current and water level fields computed from CMS-Flow were used as hydrodynamic forcing to CMS-Wave while the wave radiation stress fields computed from CMS-Wave were used as wave forcing to CMS-Flow. The wave radiation stresses computed from two consecutive CMS-Wave runs were linearly applied in the CMS-Flow simulation.

Wave model results were saved over the entire computational domain, including three engineering wave parameters (significant wave height,

peak period, and mean direction). Model results including wave parameters and spectra of the CMS-Wave parent grid were extracted at points as inputs to drive the CMS-Wave child grid and also at points near the B2D wavemaker boundary as inputs for the B2D simulations. Calculated directional spectra were saved at seven transects with 358 output locations along the front and around the sides of the seawall and breakwaters in the CMS-Wave child grid. Figure 3-4 shows the seven transects on which wave information is extracted from CMS-Wave child grid. CMS-Wave results were used to check/compare with B2D results.

Figure 3-4. Seven primary transects (T1–T7) in the CMS-Wave child grid.
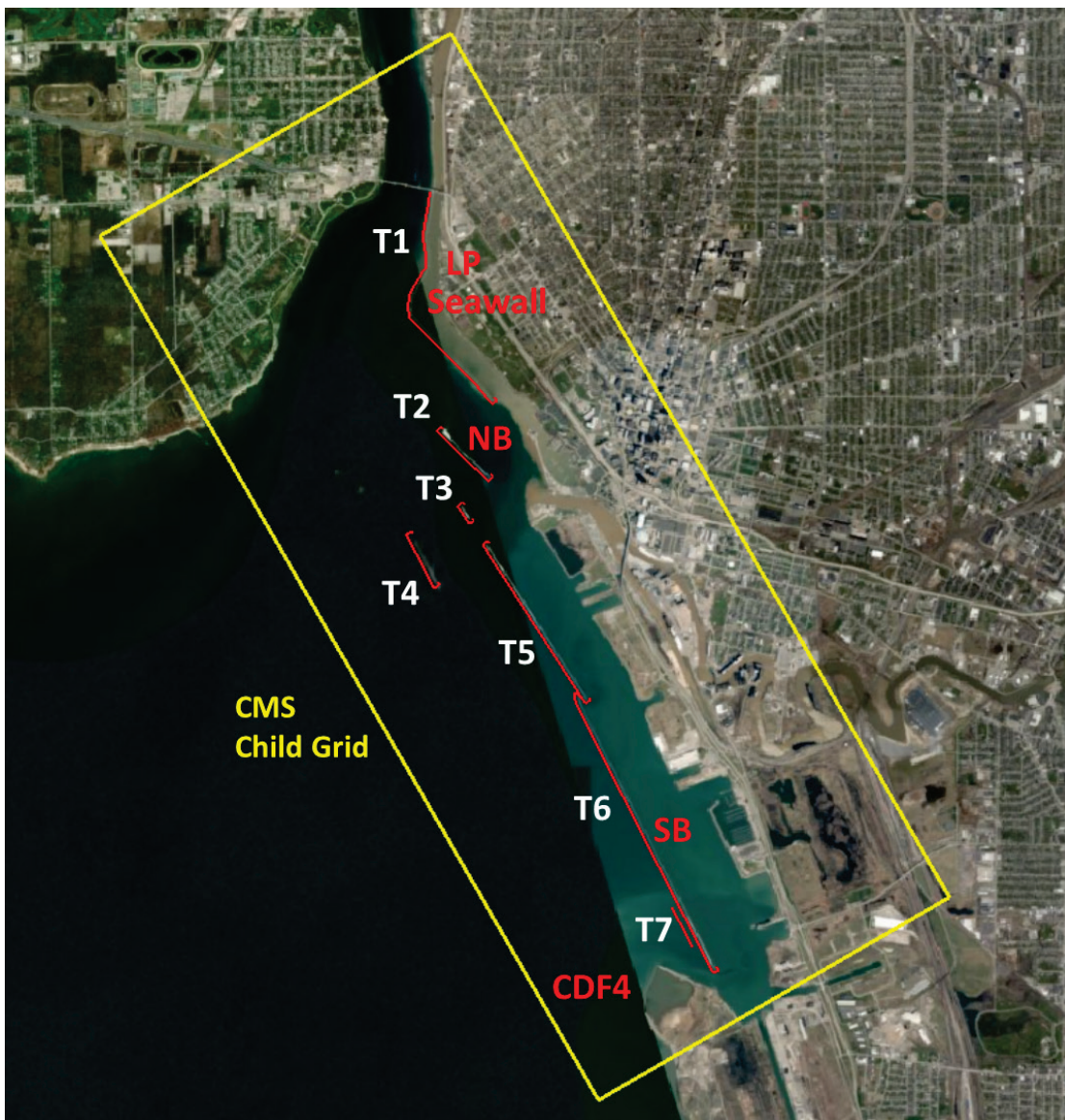
Figures 3-5 and 3-6 show the model maximum velocity and wave height fields in the parent grid during the simulated storm condition of 20-year wave and 10-year water level. The model maximum depth-averaged current velocity at the upstream of Niagara River reaches 1.51 m/sec (5 ft/sec). Niagara River flow is always from Lake Erie into Lake Ontario. The incident wave height and period along the CMS-Wave parent offshore boundary are 4.8 m (15.7 ft) and 10 sec. Figure 3-7 shows the corresponding wave height field along seven transects lines for model wave output in the CMS-Wave child grid. The model wave height along the open-water boundary varies from 1.5 m (5 ft) near the north boundary to 3.8 m (12.5 ft) at south boundary.

Figure 3-5. Model maximum velocity field in the CMS-Flow parent grid.
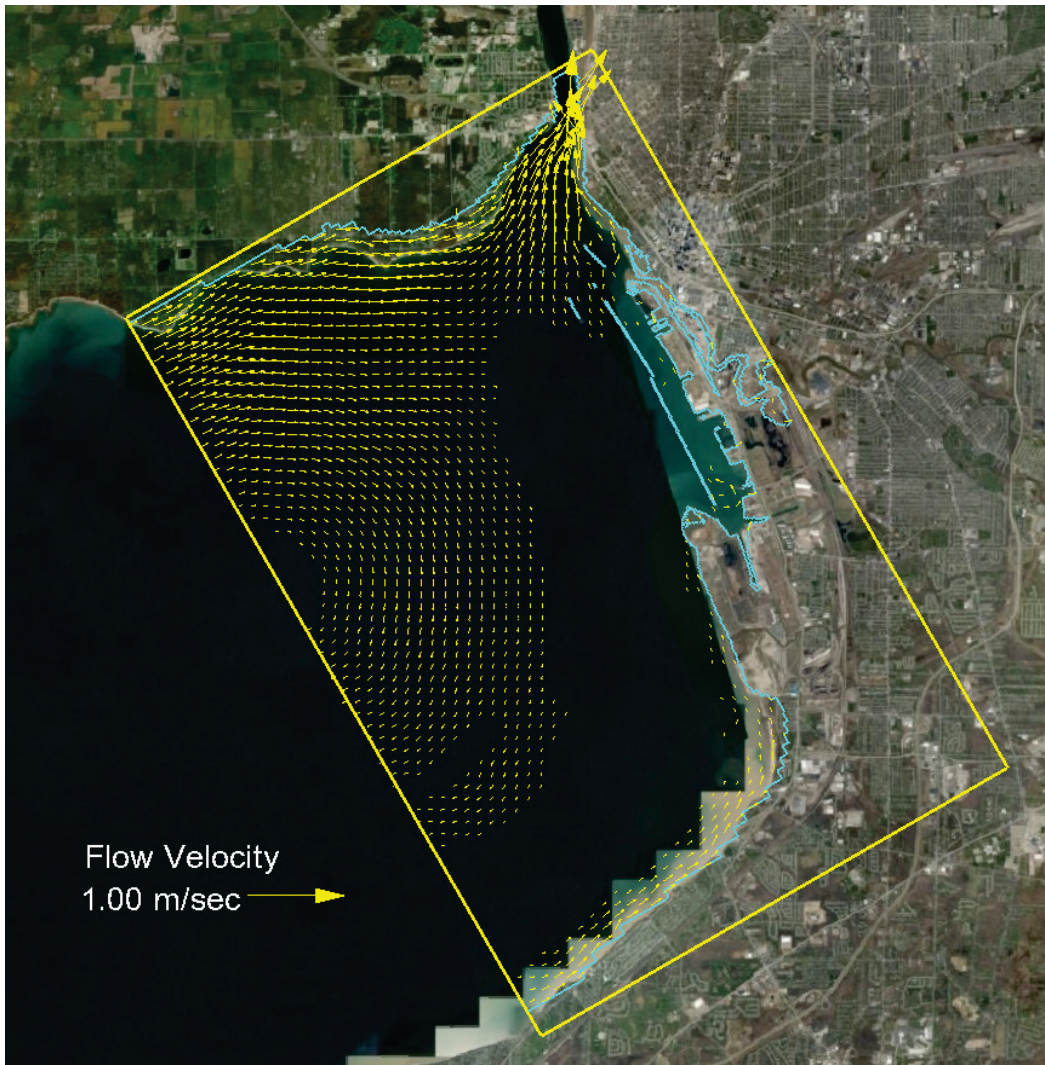
Figure 3-6. Model maximum wave field in the CMS-Wave parent grid.
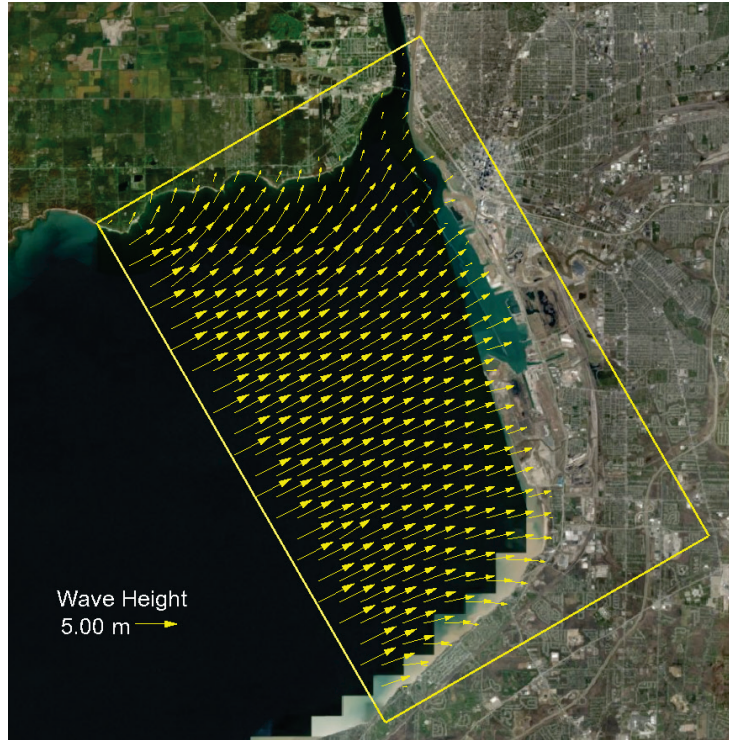
Figure 3-7. Model maximum wave field in the CMS-Wave child grid.
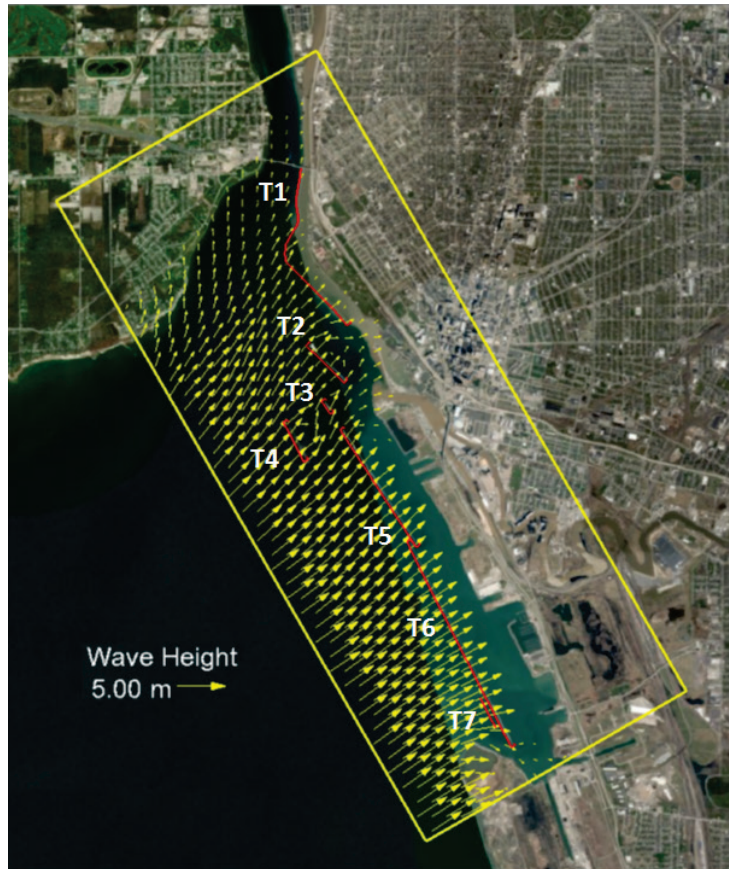
Figures 3-8 and 3-9 show examples of wave heights during the peak of the design storm condition along T1 (LP seawall) and T2 (NB) and T5 (Old Breakwater) and T6 (SB), respectively, for the simulated storm condition. Because Old Breakwater and SB are exposed to the lake, waves along T5 and T6 are generally much larger than those along T1 and T2. In front of the Old Breakwater and SB, the maximum wave height is approximately 3.3 m (10.8 ft). Model wave heights varied from 3.5 m (11.5 ft) to 4.2 m (13.8 ft) along the B2D grid boundary while the peak wave period remained constant at 10 sec. The incident wave direction also varied, ranging from 233 deg to 247 deg, with a mean direction of 240 deg, along the wavemaker in B2D grids.

Figure 3-8. CMS-Wave model wave heights along Transects T1 and T2.
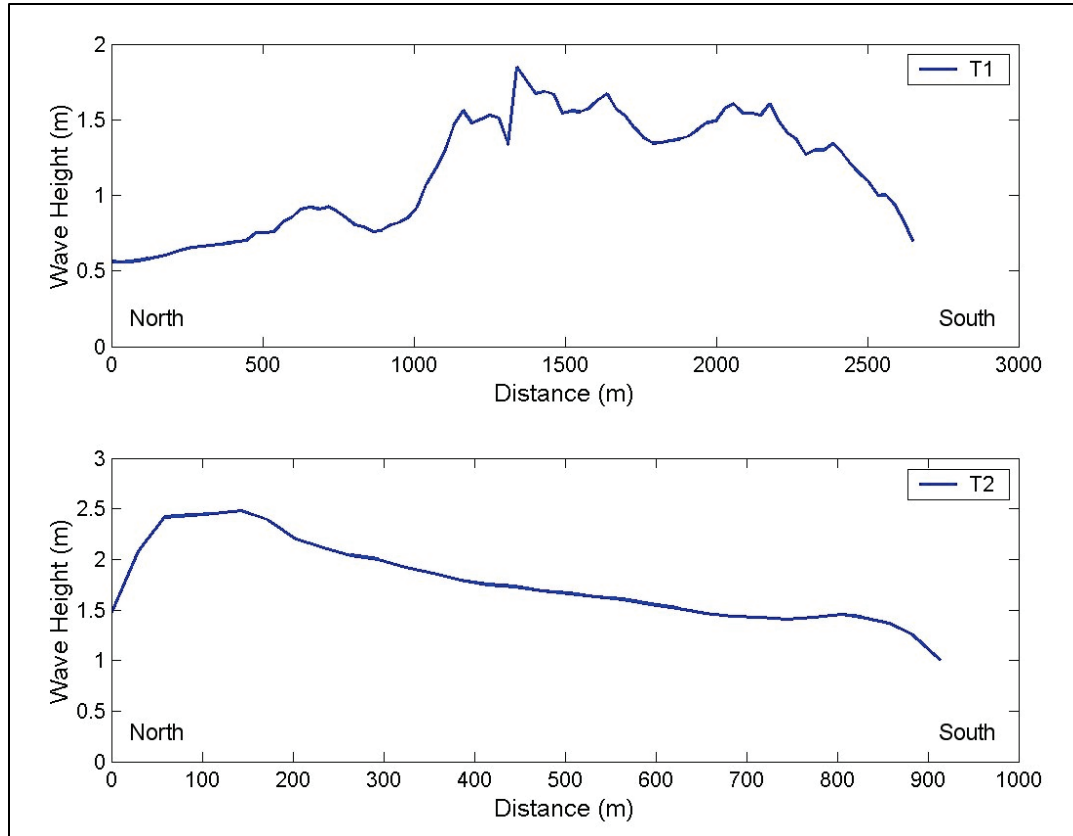
Figure 3-9. CMS-Wave model wave heights along Transects T5 and T6.
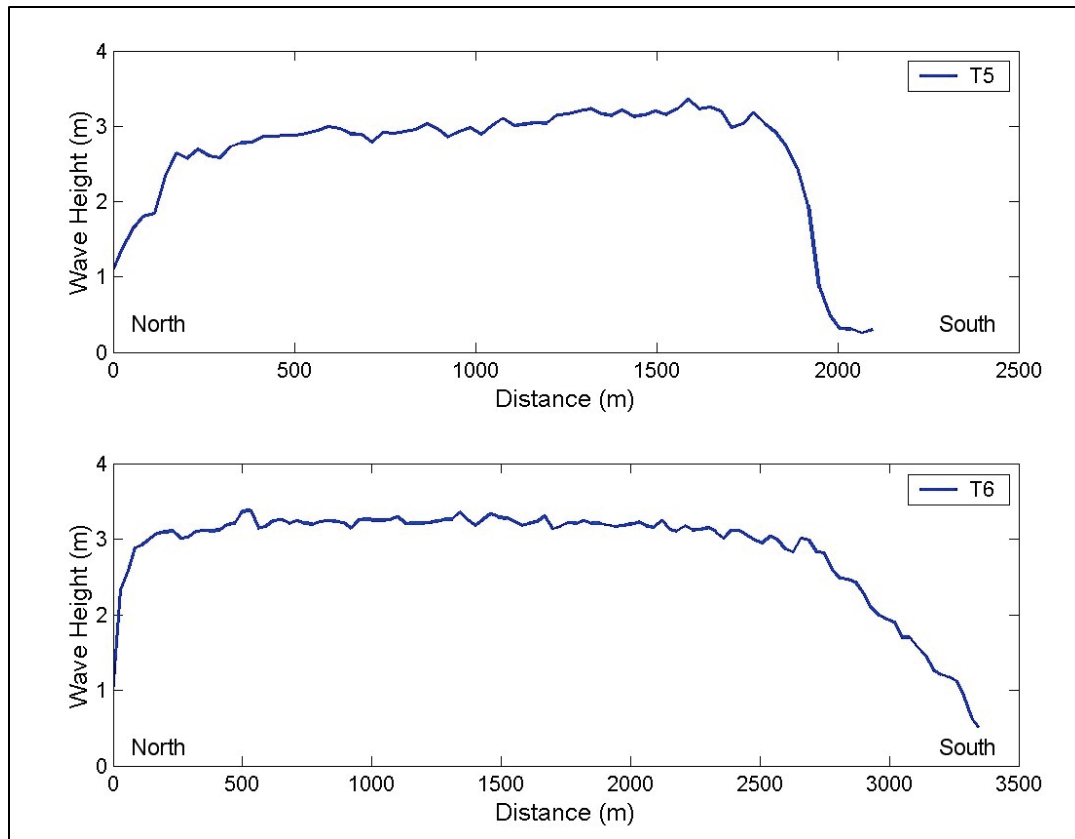
The CMS-Flow results showed water levels did not change much at the offshore depth of the CMS-Wave child grid and B2D grids. For a conservative design approach, the maximum water level of 3 m (9.8 ft) LWD was used in all B2D grids to develop design wave estimates for structural repairs inside the harbor and along the LP shoreline.

4 Boussinesq Wave Modeling

4.1 Modeling approach

Boussinesq wave modeling performed to address the needs of the SB, NB, and LP seawall projects is described in this chapter. A 20-year design wave with 10-year water level was used to develop design wave estimates for repairs of these structures. Details of the return period conditions for BH complex and Lake Erie were described by Demirbilek et al. (2017). A summary of previous study is provided in Chapter 3 and Appendix C of this report.

A spectral wave model (CMS-Wave) was used with a Boussinesq-type wave model (B2D) to provide wave estimates for the planned structural repairs. Because field wave data were not available to calibrate and validate numerical models, B2D and CMS-Wave were applied in this study based on default parameters used in the previous study (Demirbilek et al. 2017). Sensitivity tests were conducted during both the previous and present studies.

For modeling nearshore waves at breakwaters situated in the harbor, several B2D modeling domains were considered. All grid domains were bounded approximately by the 15 m (49.2 ft) depth contour and shorelines. Using the Boussinesq wave equations, B2D represents short- and long-period linear and nonlinear wave processes in deep, intermediate, and shallow water depths. The solution of these nonlinear wave equations is computationally demanding. It requires smaller grid domains (less than 30 km^2) (11.6 miles^2) and a limited number of wave conditions. For additional information about Boussinesq wave theory and nonlinear shallow water wave processes possible in practical applications, readers should consult recent project publications (Demirbilek et al. 2007a, 2008, 2009, 2017, 2015a,b,c,d, 2016a,b; 2017; Nwogu and Demirbilek 2001, 2006, 2008, 2010) and other sources listed in the References section.

A coupled B2D and CMS-Wave modeling approach is unavoidable in coastal applications involving large modeling domains or evaluation of several alternatives or many simulations. Lin and Demirbilek (2012, 2005) describe details of this approach, including the calibration and validation of models with field data for several example applications. In the

framework of this approach, B2D is used for modeling nearshore waves and for evaluation of wave-structure interaction processes at and around the structures (e.g., wave refraction, shoaling, diffraction, reflection, breaking, nonlinear wave-wave and wave-current interactions, and wave runup/overtopping).

These are impermeable structures at BH. Neither structural construction details, layer information, permeability, nor cross-section data are required. The crest elevation, width, and front and back slopes based on structural survey data define the external geometry of the structures. Sensitivity tests were performed on local roughness of the structures.

Demirbilek and Vincent (2015) indicate the characteristics of nonlinear shallow-water waves can be defined by three dimensionless quantities: H/h, L/h, and H/L, where h is the mean water depth, H is the wave height, and L is the wavelength. The Boussinesq wave theory uses two of these fundamental parameters, H/L and H/h, which define dispersion and nonlinearity of the waves in any water depth. In general, wave nonlinearity increases with the wave height as depth decreases. This leads to an increase in wave asymmetry and eventual wave breaking and deformation of the wave profile. B2D provides estimates of wave parameters (height, period, and direction), wave-induced currents (circulation), and infragravity (IG) waves, which are potential source of severe harbor oscillations or surging problems (Demirbilek et al. 2005a,b, 2007b,c; Nwogu and Demirbilek 2001, 2006; Nwogu 1993, 1994, 2006). IG waves were not detected in this study. The lengths of B2D grid domains are generally less than a few kilometers. Because wind generation and growth are not included in B2D, the wind effect is neglected in the B2D results (Nwogu and Demirbilek 2001).

Not all features of nonlinear shallow-water wave processes can be described accurately by a state-of-the-art nonlinear wave model such as B2D. However, in coastal applications, B2D is capable of capturing the most complex characteristics of nonlinear shallow-water waves (Demirbilek et al. 2007b,c, 2015a,b, 2016; Nwogu and Demirbilek 2001, 2006, 2008; Nwogu 1993, 2006). The model was used in this study to investigate changes in characteristics of nonlinear waves in the harbor resulting from interactions with the SB, NB, and LP structures, including wave runup/overtopping.

4.2   Model grids for existing breakwaters

The structures in BH included in various B2D grids are depicted in Figures 4-1 through 4-8. Pertinent data for all grids were provided by LRB, including bathymetry, shorelines, structures, and other prominent features of harbor and structures of interest.

Figure 4-1 shows the first three grids used in this study for wave modeling of SB and NB structures. These three grids are marked as "SB grid" (yellow), "NB grid" (blue), and "BH grid" (red). The BH grid includes several major structures present in the harbor. Note this BH grid covered only the south part of the LP area of interest because the LP region of harbor was initially not part of the modeling study. When the LP area was added later to the modeling study after SB and NB modeling tasks were completed, a fourth grid (LP grid) was necessary to cover the area of interest in the LP region.

Figure 4-1. The three B2D grids for SB (yellow), NB (blue) and BH (red).
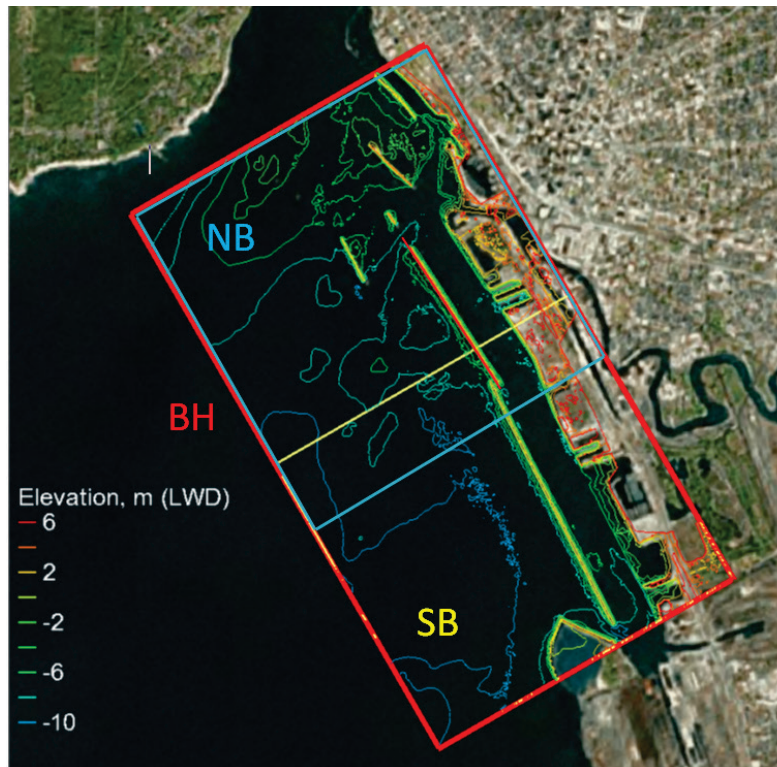
The breakwaters shown in Figure 4-2 in the B2D domain are identified by numbered transects (T1 to T7) fronting each structure. (Figure 3-4 shows T1 to T7 in the CMS domain.) These transects were used to extract and post-process model wave estimates on lakeside of structures. All

breakwaters visible in Figures 4-1 and 4-2 are isolated. As indicated by overlapping segments of T5 and T6, parts of the NB and SB are very close to each other. Furthermore, several breakwaters are sheltered by neighboring structures located on their lake side. The extent of sheltering depends on relative positions of transects (T1 and T2), (T3 and T2), (T4, T3 and T5), (T6 and T5), and (T7 and T6). Consequently, SB and NB grids could not be limited to include only their own breakwaters. In the region where structural segments were close but separated, all neighboring segments had to be included in the NB and SB grids. For example, the most northern segment of SB structure was included in the NB grid, while the most southern part of OB structure was incorporated in the SB grid. Test simulations showed close proximity of structures to lateral grid boundaries was affecting B2D solutions. Sensitivity runs included one larger grid domain (BH grid) that contained both SB and NB structures.

Figure 4-2. Existing breakwaters in Buffalo Harbor B2D domain with Transects T1 to T7.

Initial investigations using the NB and SB grids helped to determine if presence of structures near and passing through the lateral grid boundaries introduced problems. These investigations demonstrated that close proximity of structures to grid boundaries or using the so-called "mixed grid

boundaries," which contain structures and damping layers should be avoided. Any type of structural arrangements near grid boundaries could lead to numerical instabilities caused by strong localized wave-structure interactions. Different wave estimates were obtained in and around the shared area of the SB and NB grids, which were attributed to presence of structures in the shared area in both grids. These problems were avoided by using a single grid that included both SB and NB structures. This requirement led to use of the "BH grid" (red grid in Figure 4-1).

The BH grid domain of Figure 4-3 was comparatively much larger than domains of the NB and SB grids. An adequate grid resolution was required to properly represent all breakwaters contained inside the BH grid domain. A series of sensitivity tests were made with different grid resolution. Tests indicated that the BH grid should be centered to the mid-sections of harbor, with a constant grid cell size of 6 m (19.7 ft). The BH grid covered a large area approximately 3.9 km (2.4 miles) (cross-shore) × 7 km (4.4 miles) (alongshore). The domains of NB and SB grids were 3.9 km (2.4 miles) × 4.1 km (2.6 miles) and 3.9 km (2.4 miles) × 3.7 km (2.3 miles), respectively. The (i, j) triad is displayed at the origin of grids.

Figure 4-3. The BH grid containing entire SB and NB structures.
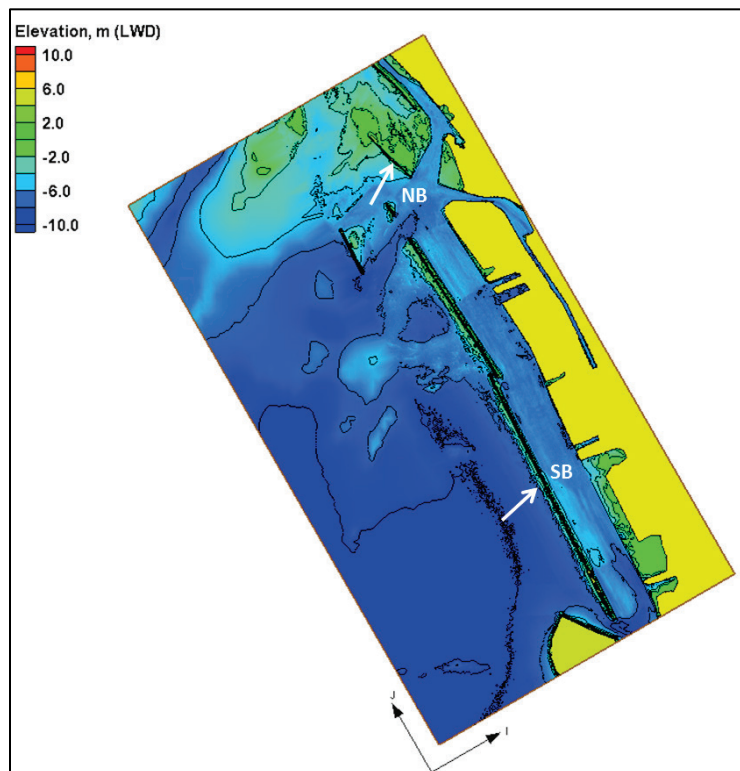
A final BH grid emerged as shown in Figure 4-3 emerged after several iterations and refinements of test grids. This grid was used in wave estimates for the existing SB and NB structures and associated repairs. However, note that the north region of harbor and the canal that connects to the Niagara River were not included in the BH grid. Consequently, a new B2D grid was required for wave estimates requested at the LP seawall area. The "LP grid" shown in Figure 4-4 was developed for wave estimates at the LP seawall and vicinity. For consistency with other B2D grid, a 6 m (19.7 ft) constant cell size was also used in the LP grid. Figure 4-5 shows a zoomed image of the north canal area.

Figure 4-4. The LP grid for north harbor region.
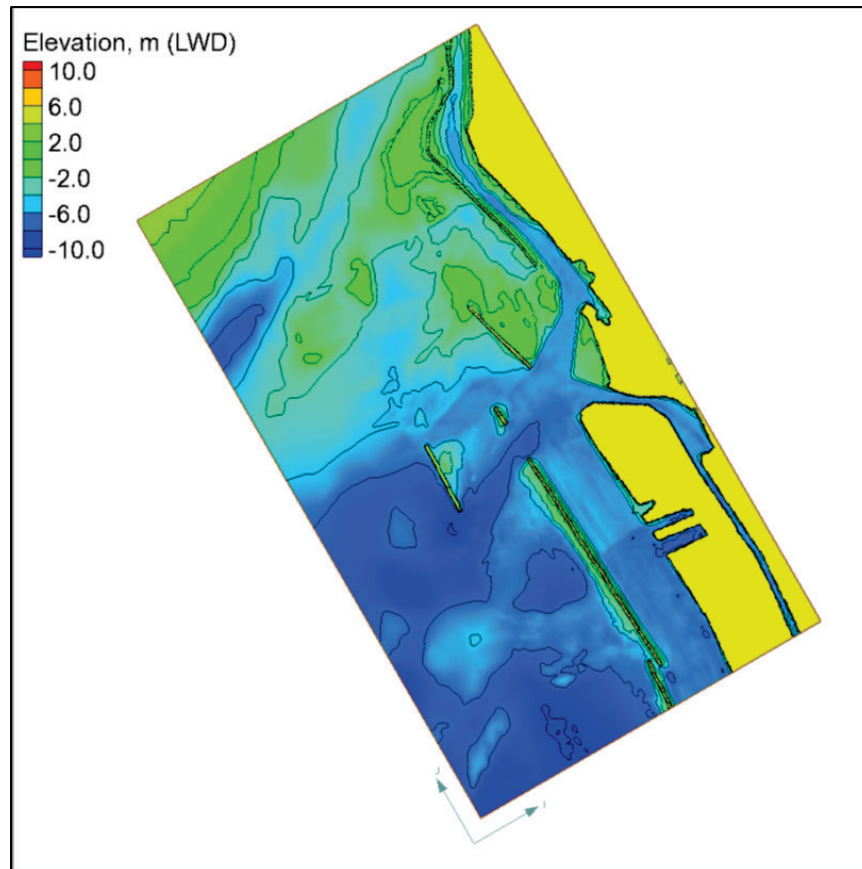
Figure 4-5. Zoomed image of the north canal area of LP grid.
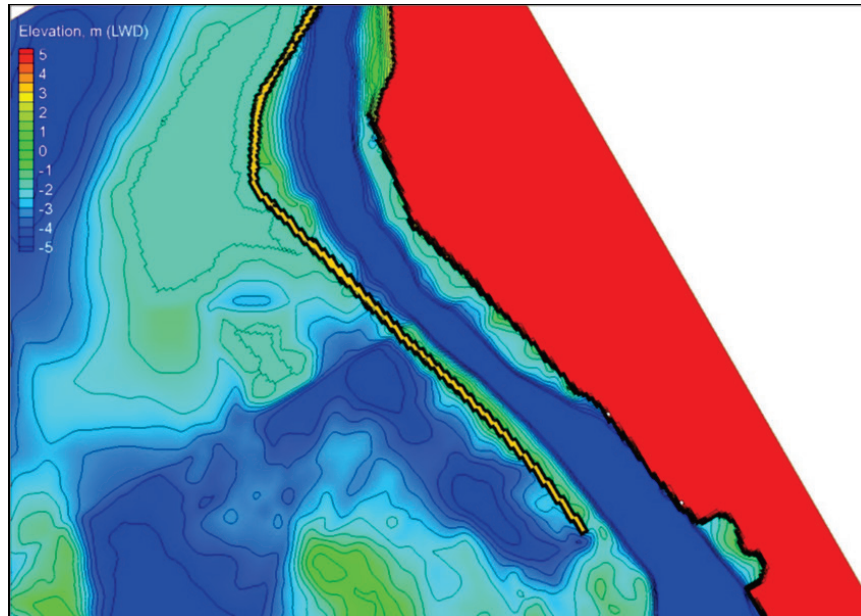
4.3   Model grids for structural repairs

Two repairs to the south side of the SB structure were considered by the LRB project team. Figure 4-6 shows Alt 1 repair, which involves placement of a submerged berm in front of a damaged section of the breakwater. Alt2 is similar to Alt 1 except that the north and south ends of the berm were smoothed and rounded at connections to the SB. The BH grid was modified to include Alt1 and Alt2. Figures 4-7 and 4-8 show the zoomed images of Alt 1 and Alt 2 modifications.

Test runs were performed to check the berm location, shape (geometry), size, and elevation to minimize local wave focusing by the berm. The smoothing of the north and south ends of the berm (30 m [98 ft] each end) in Alt2 was necessary to reduce excessive localized wave focusing that was observed in Alt1.

Figure 4-6. The SB repair area with a submerged berm in front (Alt1 grid).
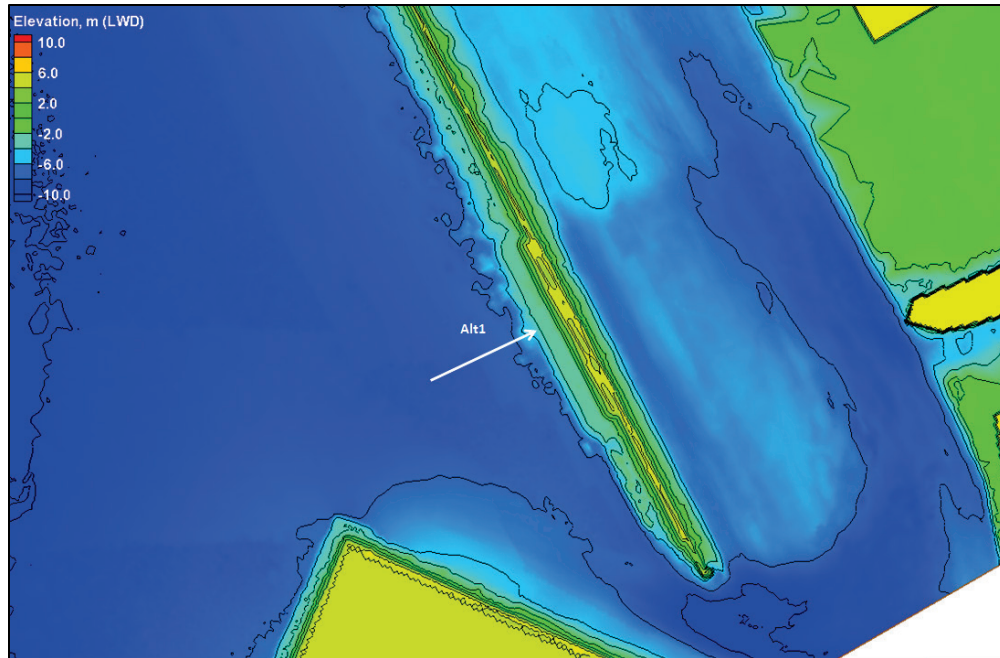
Figure 4-7. Zoomed image of contours in the SB repair area and vicinity (Alt1 grid).
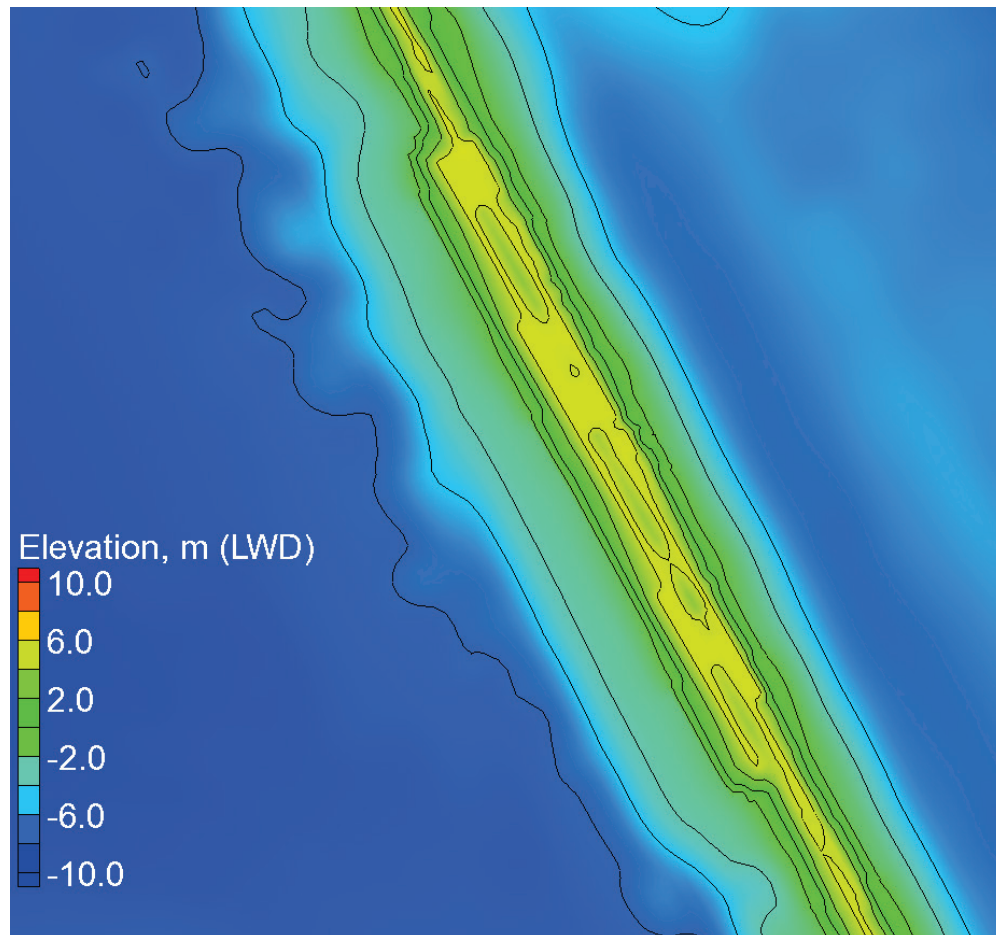
Figure 4-8. Zoomed image of contours with rounded ends connecting to the SB (Alt 2).
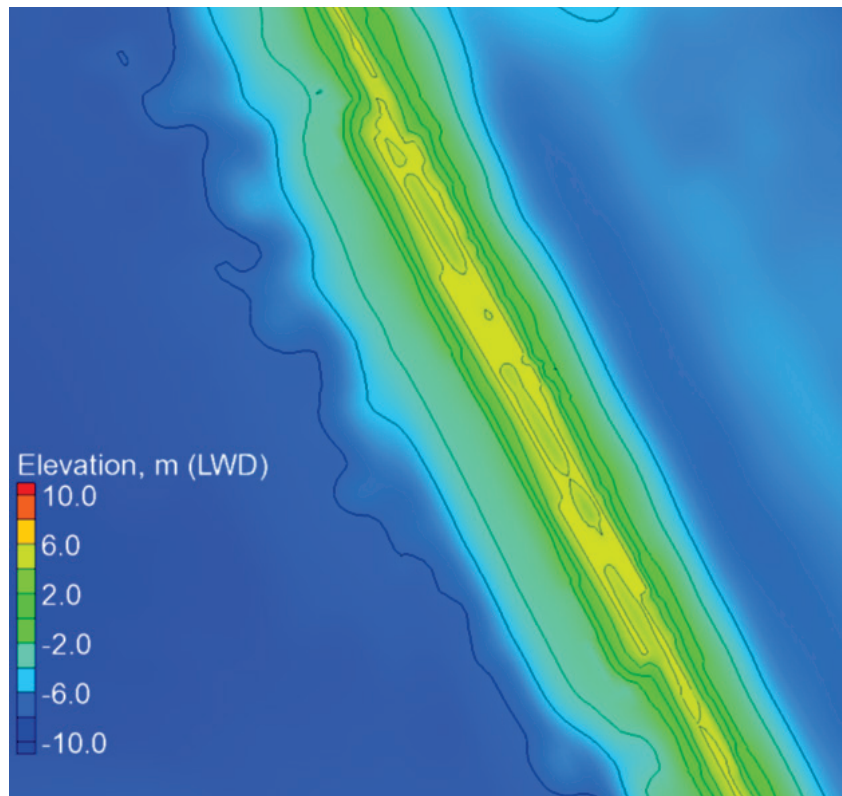
The modifications of the north and south ends of the berm in Alt 1 has sharper connections to the SB, which causes large wave heights in the vicinity of these areas. With smoothened berm end connections in Alt2, the intensity of wave focusing was reduced.

4.4 Input wave and water level conditions

The metocean forcing conditions in Lake Erie were simulated with CMS-Wave and CMS-Flow using coupled parent and child grids described in Chapter 3. The parent and child grids are shown in Figures 3-1 and 3-2, with parent grid including parts of the Lake Erie, entire BH and all breakwaters in the harbor. The parent grid was used to transform hindcast conditions at the WIS Station 92243 to project site. The CMS-Wave wave height, period, and direction and water levels from the parent grid were saved seaward of the B2D wavemaker boundary as input conditions.

The lakeside boundary of B2D grid is the *wavemaker* boundary where incident wave input conditions were specified. Wave height, period, and direction parameters were extracted from CMS-Wave seaward of the B2D

wavemaker boundary. Detailed analysis of CMS-Wave results indicated that wave heights were not constant along the B2D grid boundary, where wave heights varied from 3.5 m (11.5 ft) to 4.15 m (13.6 ft). Values of the peak wave period were constant at 10 sec. The incident mean wave direction varied as well, and wave directions varied from 233 deg to 247 deg with a 240 deg incident angle at the center of the wavemaker boundary. The 10-year water level of 3 m (9.8 ft) was used in B2D simulations to develop wave estimates for structural repairs in the harbor and along the LP shoreline. Table 4-1 provides the spectral wave parameters and water levels (WL) used as inputs to B2D simulations for all structural repairs.

Table 4-1. Input waves and water levels used in B2D simulations.

Grid	H_s (m)	T_p (sec)	θ (deg)	WL (m)
BH grid (for SB and NB structures)	4.15	10	233, 240, 247	3.0
LP grid (for seawall)	3.85	10	233, 240, 247	3.0

Wave parameters (Hs = 3.85 m [12.6 ft] and 4.15 m [13.6 ft], Tp = 10 sec, and θ = 233°, 240°, 247°) in Table 4-1 represent a 20-year maximum design wave condition at harbor entrance. The largest incident waves affecting the harbor area were mostly from the southwest direction. However, smaller waves from south, west, northwest, and north directions can also reach this harbor. For this reason, three incident wave directions from southwest are considered in Table 4-1. These incident wave directions in Table 4-1 should capture impacts of slightly oblique waves on design estimates if such incident waves penetrate into harbor where structures are located.

4.5 Model setup and test runs

A constant depth zone is required for the wavemaker in B2D followed by a transition zone connecting to the rest of the grid domain. The wavemaker was tested at three depths: 14 m (45.9 ft) as the external wavemaker, and 12 m (39.4 ft) and 10 m (32.8 ft) as two internal wavemakers. Interior wavemakers were tested to reduce the computational burden. Testing of internal and external wavemakers indicated the wavemaker type had minor effect on model results. An internal wavemaker could sometimes introduce model computational instability and become sensitive to backward reflected waves and damping placed along the structures and shorelines.

Consequently, an external wavemaker was used in the production runs for selected wave conditions for computational stability of the model.

A series of sensitivity tests were conducted for input parameters that influence model solution and numerical stability. These included the Chezy (bottom friction) coefficient, Smagorinsky (turbulence) coefficient, and the width and strength of damping or sponge layers used to represent the reflectivity of structures and land boundaries. Tests indicated the numerical stability of computations was sensitive to the characteristics of the damping layers used in simulations, including their location, width, and coefficient. Partially absorbing, lateral damping layers 5 to 25 m (16.4 to 82.0 ft) wide along parts of the lateral grid boundaries were tested.

Damping layers were placed along the interior and exterior faces of structures in the initial tests. Dampers were used along the lakeside face of the breakwaters without wave runup/overtopping. No dampings were used in simulations with wave runup/overtopping. For all simulations, fully absorbing damping layers were used at the down-wave boundary along the harbor shorelines.

Test runs were performed to finalize damping layer properties affecting interaction of waves with land and structures. These test runs were necessary in the absence of field data to determine the extent of change in model results. The damping layer placed on the down-wave boundary along the Buffalo Harbor land boundary was used to absorb waves reflecting back from the boundary. Both the model computational solution and numerical stability improved with absorbing or low reflection from the harbor shorelines and with no damping layers placed on the front face (lakeside) of the breakwaters. These findings were applied to final production runs of the SB, NB, and LP structures and repair alternatives investigated.

4.6 Model calibration and test runs

Field data were unavailable to calibrate and validate the B2D model. Consequently, the key computational parameters used in the simulations were based on values used in a previous study (Demirbilek et al. 2017). B2D is robust and has been used successfully in many district studies with the default parameters. Publications in References and Appendix C of this report provide additional information about numerous successful practical applications of B2D that have used default parameters. A brief summary is provided next.

In the present study, sensitivity tests indicated appropriate values of Chezy and Smagorinsky coefficients were 24 and 0.2, respectively. These produced stable solutions over a wide range of sensitivity tests considered for the three storm conditions.

The value of the time-step used in the simulations varied with the incident wave and water level inputs, ranging from 0.05 sec to 0.1 sec. The effects of Chezy and Smagorinsky coefficients and damping layers on model results and computational stability were based on sensitivity tests. Tests for model stability indicated the model was less sensitive to computational parameter settings. Additional simulations were made using different values of non-storm conditions to ascertain the effect of numerical parameters on model results (Demirbilek et al. 2007, 2015a,b, 2016, 2017; Nwogu and Demirbilek 2001).

Figure 4-9 through 4-12 show examples and highlight features of the 2D spatial variation of structures and waves from the NB grid, including wave focusing zones along the NB. Large wave heights occur in these zones of wave convergence where potential future damages can occur. Figures 4-13 through 4-16 show examples of several wave converging zones from the SB grid. See Section 4.7.3 of this report for details. The following observations are made from these B2D results.

Figure 4-9. NB structure B2D test grid.
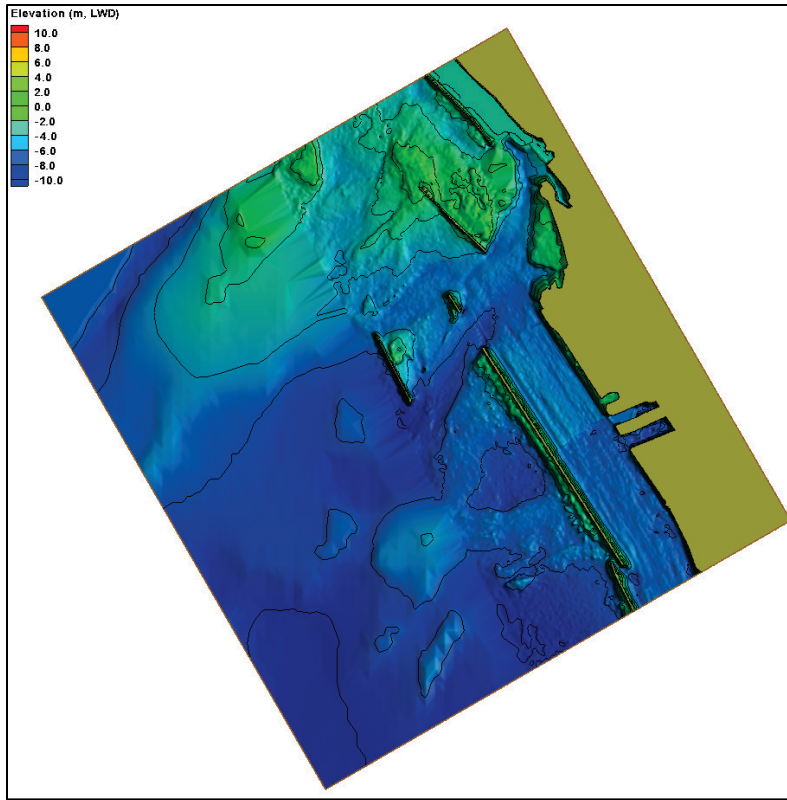
Figure 4-10. Details of NB structure in the B2D test grid.
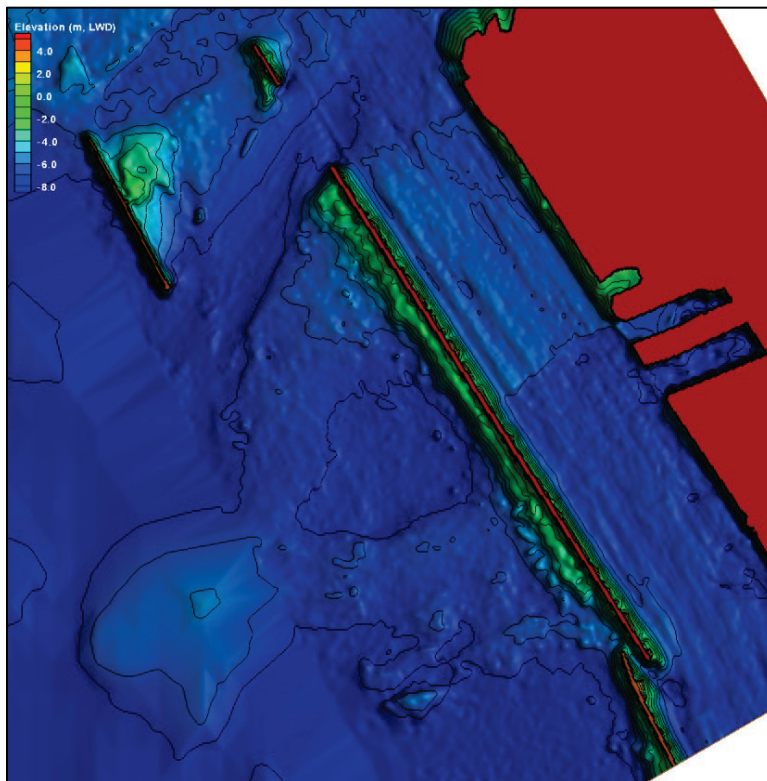
Figure 4-11. Example of 2D wave field with the NB B2D test grid.
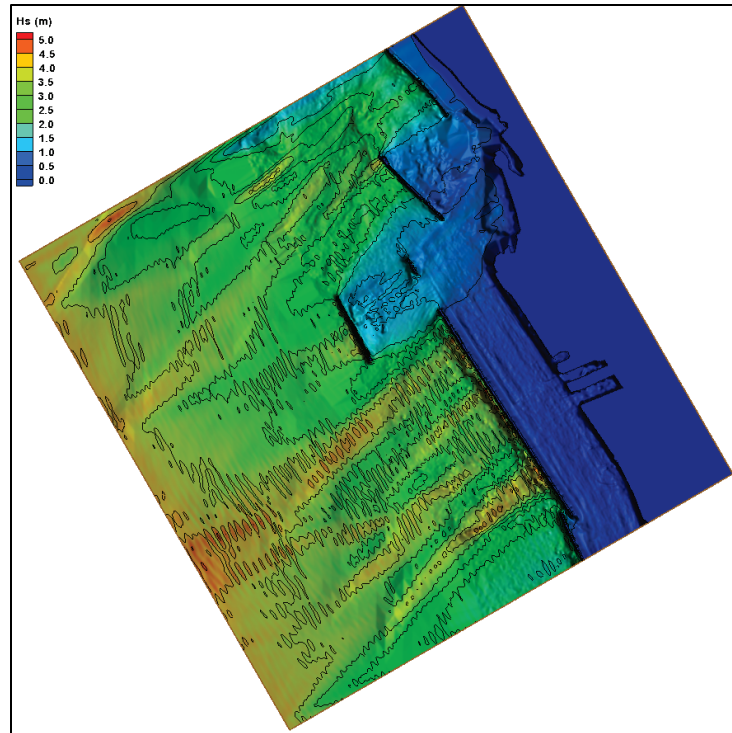
Figure 4-12. Wave focusing areas visible in the NB B2D test grid.
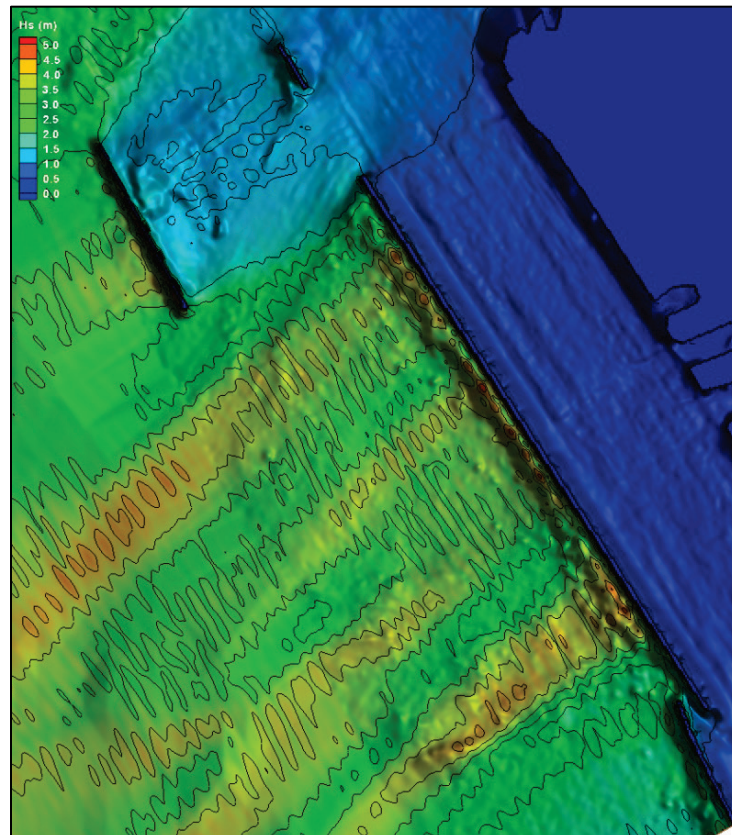
Figure 4-13. The initial B2D test grid for the SB structure.
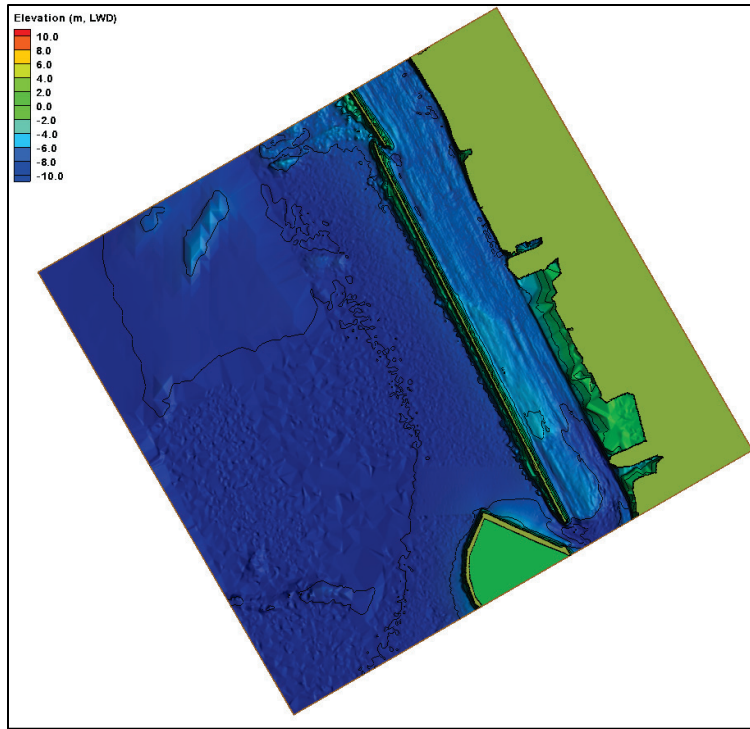
Figure 4-14. Details of the north side of SB structure in the initial B2D test grid.
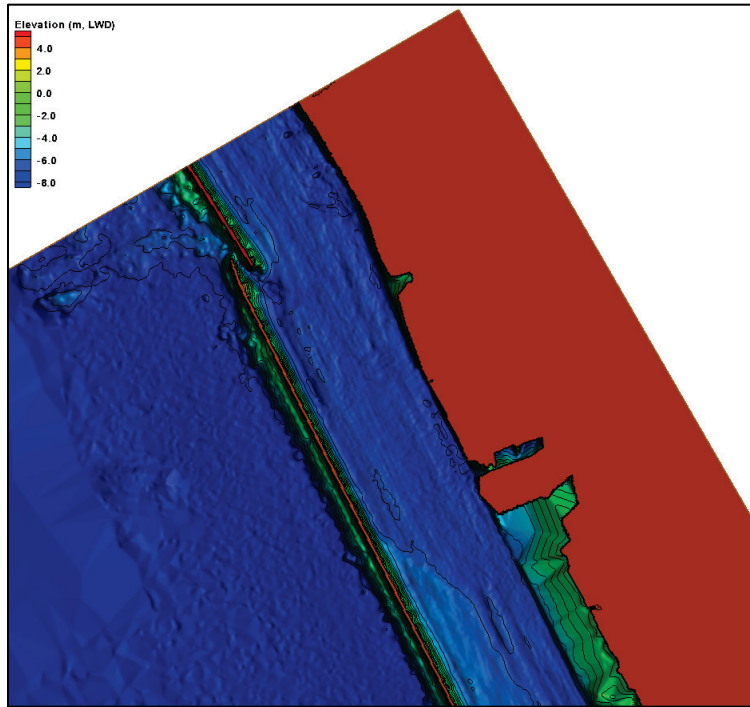
Figure 4-15. Example of two-dimensional wave field with the SB B2D test grid.
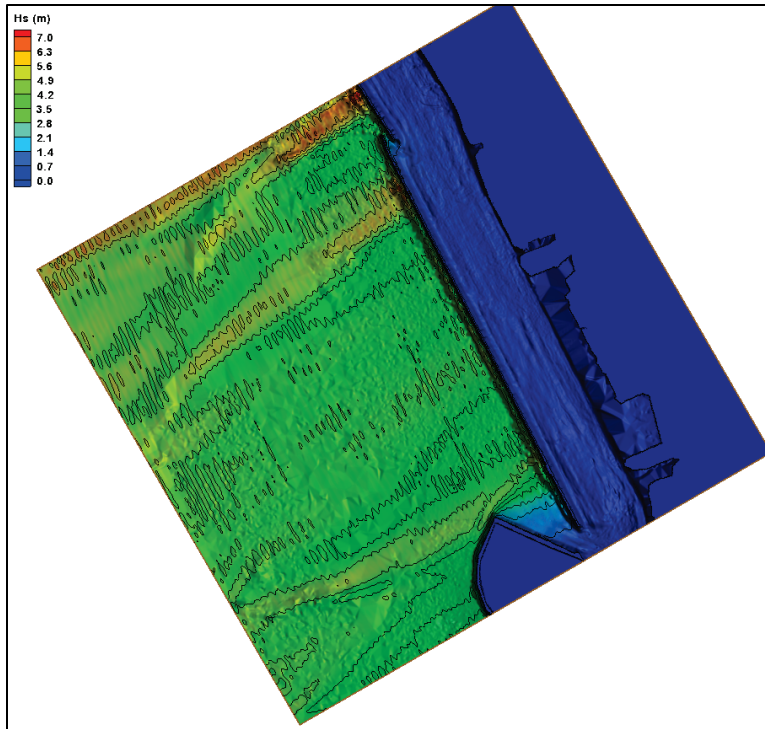
Figure 4-16. Wave focusing areas visible in the SB B2D test grid.
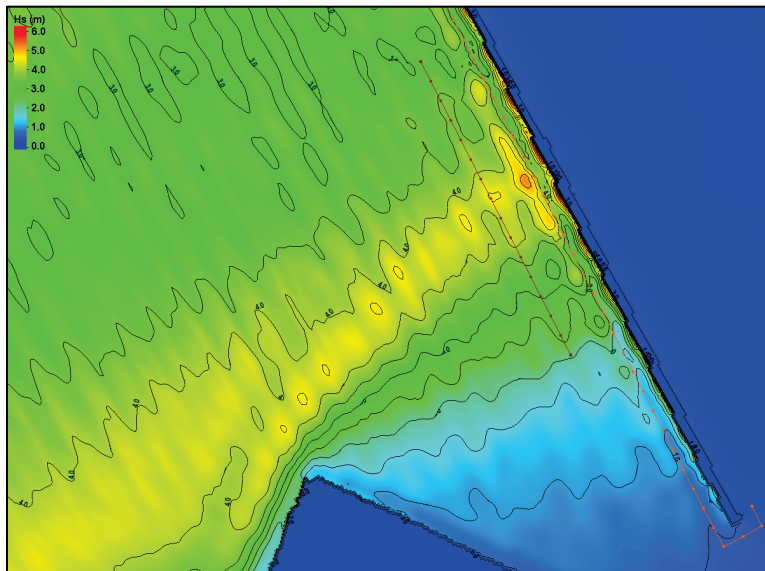
First, these results indicate certain locations along breakwaters may experience damages in areas where wave focusing is occurring (Figures 4-12 through 4-16). This is evident at the south segment of SB where a damaged section of SB has been identified by the LRB for repair. Second, different wave estimates are obtained in the overlapping area of SB and NB grids due to the presence of structures passing through or near the lateral grid

boundaries. For this reason, the need for using one grid for the harbor region became apparent, and the B2D modeling continued hereafter by using the BH grid. The BH grid covered a larger domain (4 km [2.5 miles] by 7 km [4.3 miles] with 6 m [19.7 ft] cell size) and simulation time (CPU~16 hr) was greater as compared to the run time (~ 9 hr) for the SB (3.7 km [2.3 miles] by 3.9 km [2.4 miles] with 6 m [19.7 ft] cell size) and NB (3.9 km [2.4 miles] by 4 km [2.5 miles], with 6 m [19.7 ft]) cell size.

The B2D output files of the mean water level (i.e., wave setup), mean wave direction, significant wave height, mean velocity (current), and time series of water surface elevation and pressure at the probe (save) locations were post-processed and analyzed by spectral analysis. The B2D model interface in the Surface-water Modeling System (SMS) (http://www.aquaveo.com) was used to view, extract, and post-process model results (i.e., wave parameters such as wave height, period, direction, water level, and wave-induced current).

4.7 Modeling details

4.7.1 Output locations and files

B2D results were saved over the entire grid and along several transects (profiles) shown earlier. The first seven transects (T1 to T7) are shown in Figure 4-2, and three additional cross-shore transects (T8 to T10) covering the Alt1 and Alt2 berm area are depicted in Figure 4-17. Model results extracted along these 10 transects are used in calculations to determine the rock size, wave forces, etc., in the breakwater repair.

Figure 4-17. Cross-shore transects for SB repairs (Alt1 and Alt2).
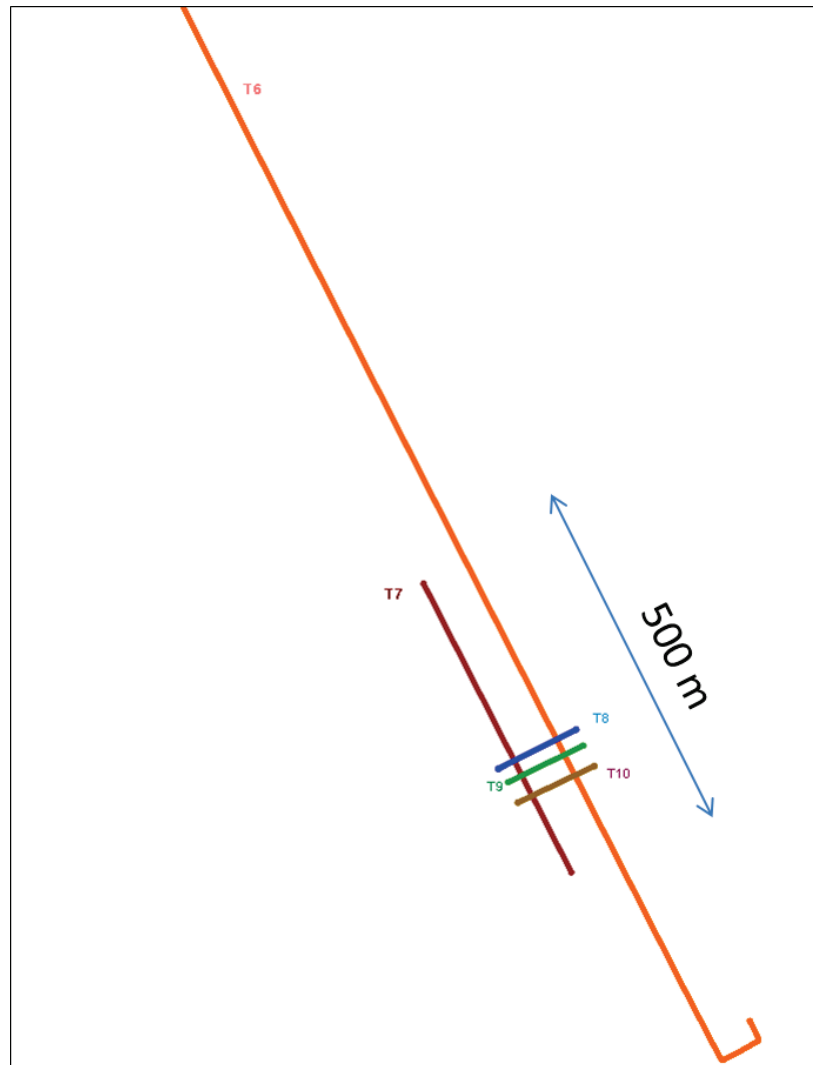
4.7.2   Results for SB repairs

Results from the B2D simulations for wave and water level of H_s = 4.15 m, T_p = 10 sec, WL = 3 m (9.8 ft) LWD are provided for three incident wave directions to show details of waves at the breakwaters. Because the SB repair area covers a small segment of the damaged breakwater, model results away from this local area will not be affected by the proposed repair. Consequently, it suffices to show model results for one repair alternative (Alt2). Model results farther from the repair area in other parts of the BH grid domain both for the existing SB and NB structures can be viewed as *without project* estimates.

4.7.3 Two-dimensional (2D) wave height fields for SB repairs

Figures 4-18, 4-19, and 4-20 show calculated wave height fields for three incident wave directions (233°, 240°, and 247°) simulated with the BH grid. Spatial variations of wave fields for each wave direction over the entire BH grid are different. The difference is not surprising. Although these simulations used the same wave height, period, and water level at the wavemaker boundary in the lake, a 7 deg difference in the incident wave direction can produce such a change in model results. Wave period was based on the transformed WIS station data at the B2D grid boundary. The three directional sectors (each 7 deg wide) were used to simulate unidirectional sea states that can produce the strongest wave focusing and larger wave heights at and around the breakwaters.

One common feature of waves propagating toward the breakwaters is a noticeable change of where wave focusing strips (bands) start emerging and how they intensify or diminish before reaching the breakwaters. They develop into high wave zones that impact the SB and NB structures. The positions of these high wave zones move up and down along the breakwaters as the incident wave direction changes. The bands of more severe wave focusing develop in the south, middle, and north sections of the SB and NB structures. Severe wave overtopping of breakwaters was observed in animations at these high wave concentration areas.

The intensification in wave heights is a consequence of combined wave-bathymetry-structure interactions, indicating stronger wave shoaling, refraction, reflection, and diffraction in the BH. The 2D bathymetry looks smooth, but in three dimensions it has irregularities, and there are areas with 0.3 to 0.9 m (1 to 3 ft) elevation differences. Such bathymetric features will affect wave shoaling and refraction of waves propagating over these areas. The nonlinear wave effects become stronger towards the structures because of combined effects of wave reflection, diffraction, and breaking.

Water levels associated with storms also play a major role on waves near the structures. Not only the wave height and period were the same, but the peak water level used for three wave conditions was identical (3 m [9.8 ft]); the water level effect on wave-structure interaction is of less concern. Consequently, the incident wave direction appears to be the dominant factor in addition to large wave height controlling the pattern of wave focusing in the harbor (Figures 4-18, 4-19, and 4-20). The strong wave focusing seen in these figures from B2D modeling was not as apparent in

the CMS-Wave model simulations of Figures 3-8 and 3-9. This is expected because wave-action models such as CMS-Wave are a comparatively weaker compared to phase-resolving models (Lin et al. 2008).

Figure 4-18. B2D model wave height field for incident wave from θ = 247 deg.
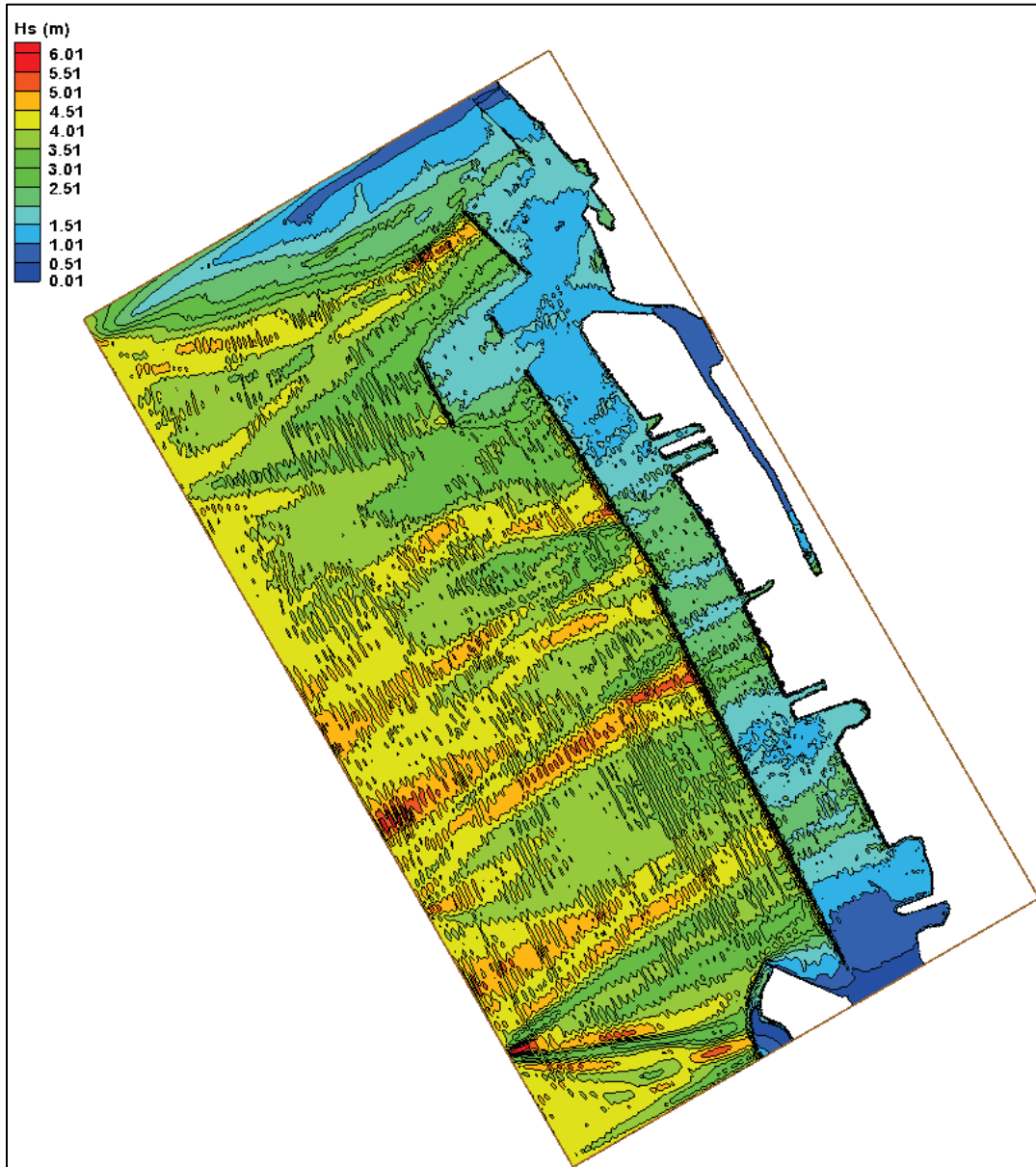
Figure 4-19. B2D model wave height field for incident wave from θ = 240 deg.
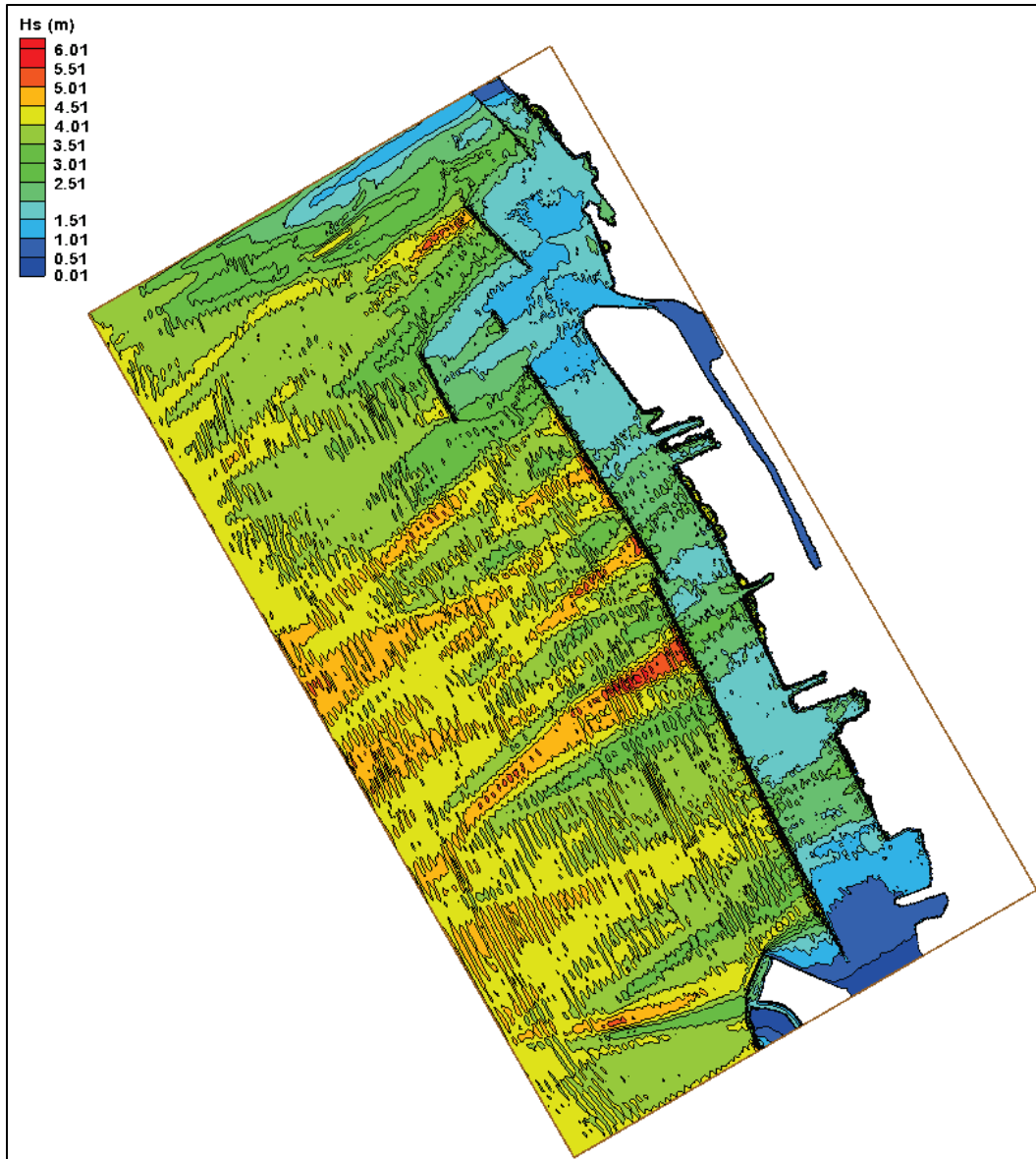
Figure 4-20. B2D model wave height field for incident wave from θ = deg.
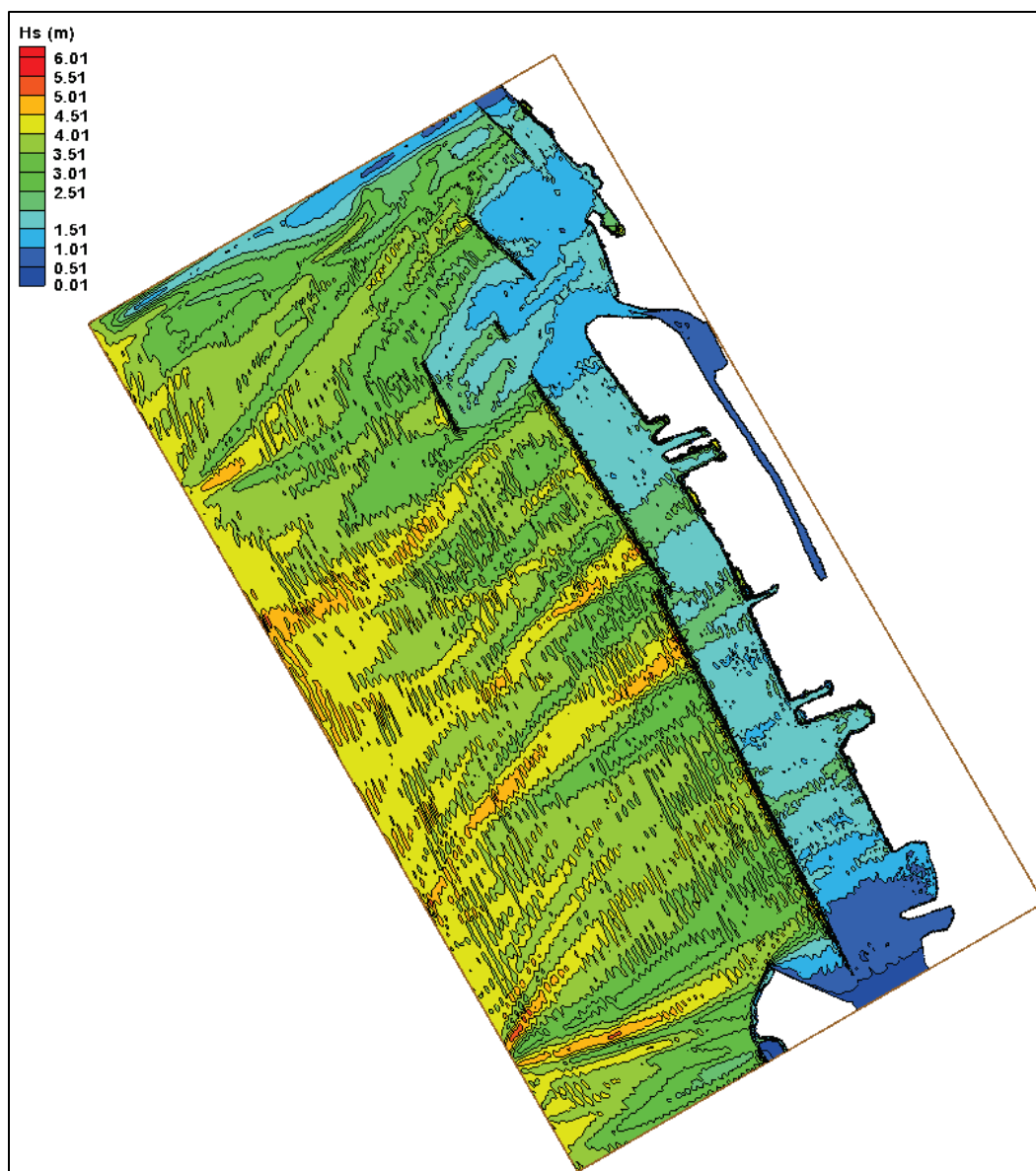
4.7.4 Variation of wave height along transects

The variation of wave heights along 10 transects T1 to T10 for three incident wave directions is shown in Figures 4-21 through 4-30. As shown in Figure 4-2, transects T1 to T7 were positioned in front of breakwaters paralleling each from north to south. Transects T8 to T10 were perpendicular to the SB in the repair area as shown in Figure 4-17. For T1 to T7, the distance along transects is from north end to south end of transects while for T8 to T10, the distance along transects is from west (lakeside) to east ends (harbor side) of transects. There is minimum variability in the water depth in front of the structure, and there is no

smoothing in Figures 4-21 through 4-30. There is a large variability in wave height along transects T1 to T7, and the structure damage occurred quite unevenly in different segments, indicating strong dependence on incident wave direction in these plots.

Although for repairs (Alt1 and Alt2), wave estimates from the cross-shore transects (T8 to T10) would be more appropriate for design calculations, note that these profiles may miss larger wave heights that can occur over the entire footprint of the proposed repair berm and beyond its north and south edges (Figures 4-5 to 4-7). Waves over the entire berm, including its ends where the greatest local focusing occurs, must be checked for design wave height selection in types of engineering applications. The LRB team used this approach to determine the most appropriate design wave to use in its engineering calculations.

Figure 4-21. Wave height variation along T1 for three incident wave directions, showing strong nonlinear wave effects in front of the structure.
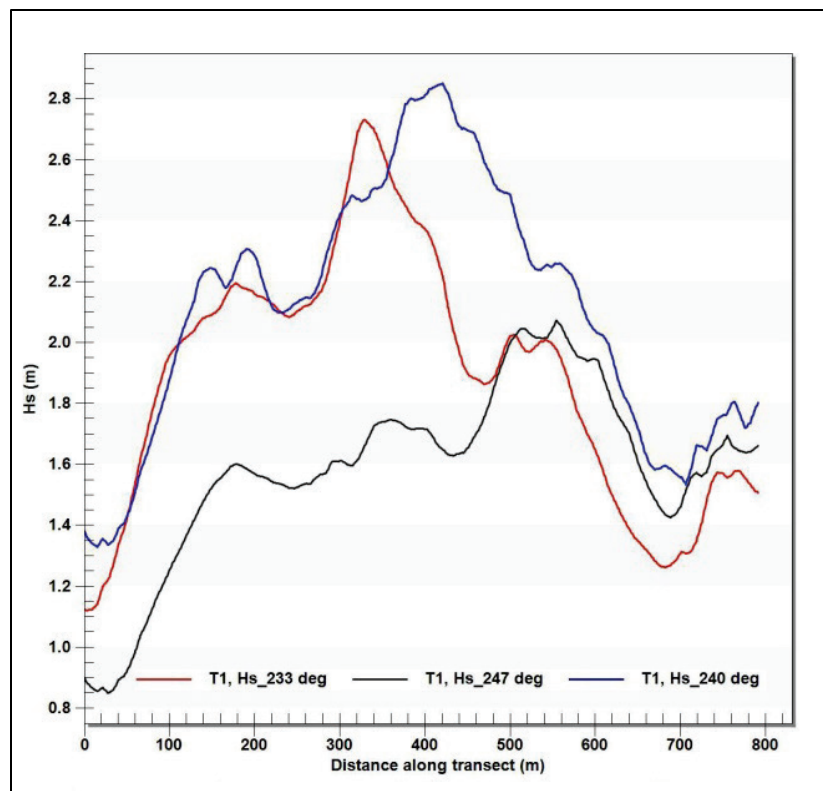
Figure 4-22. Wave height variation along T2 for three incident wave directions.
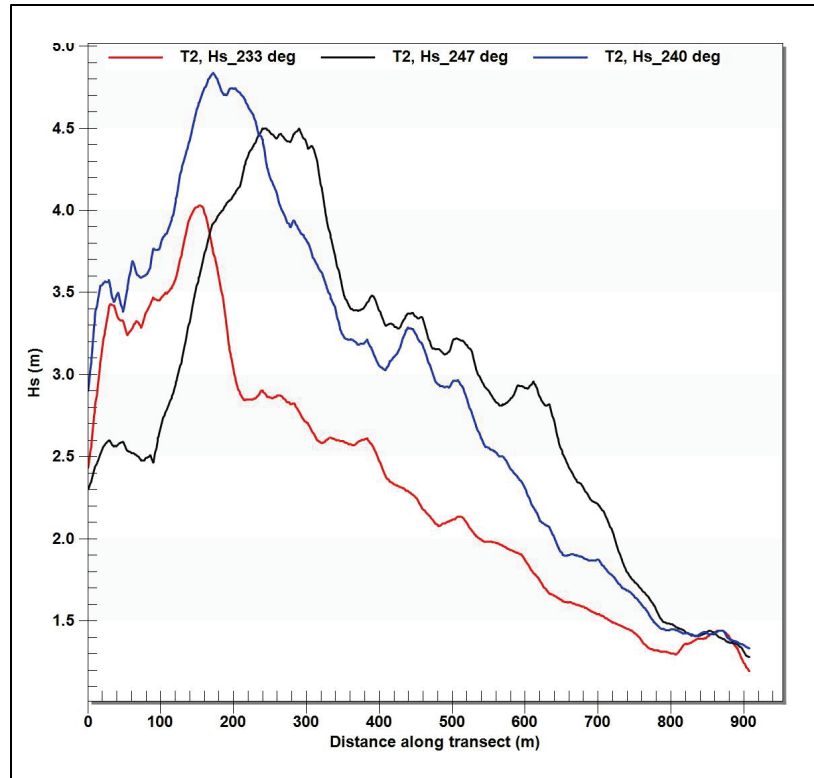
Figure 4-23. Wave height variation along T3 for three incident wave directions.
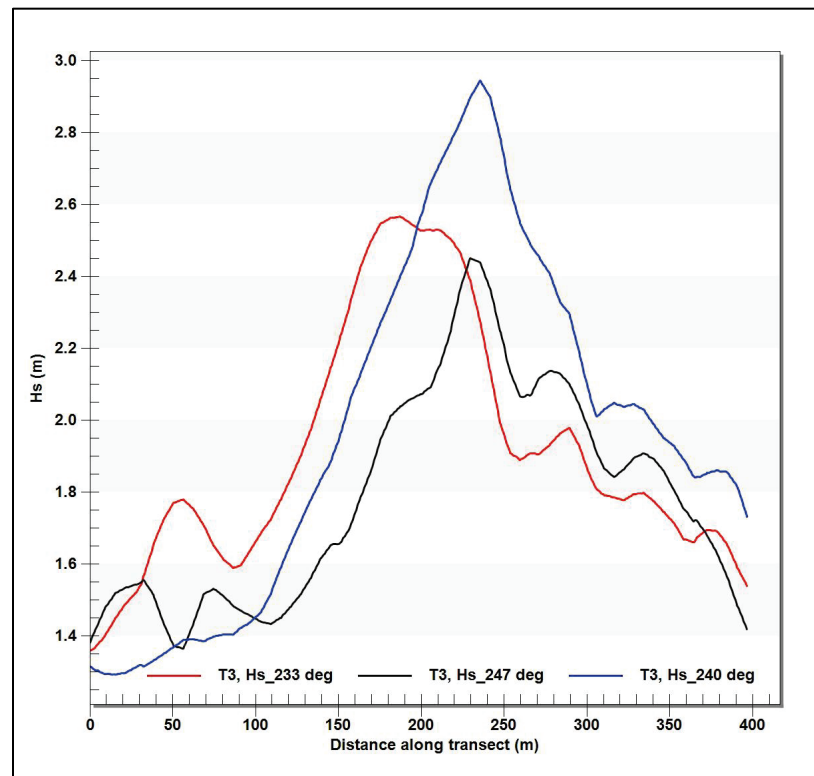
Figure 4-24. Wave height variation along T4 for three incident wave directions.
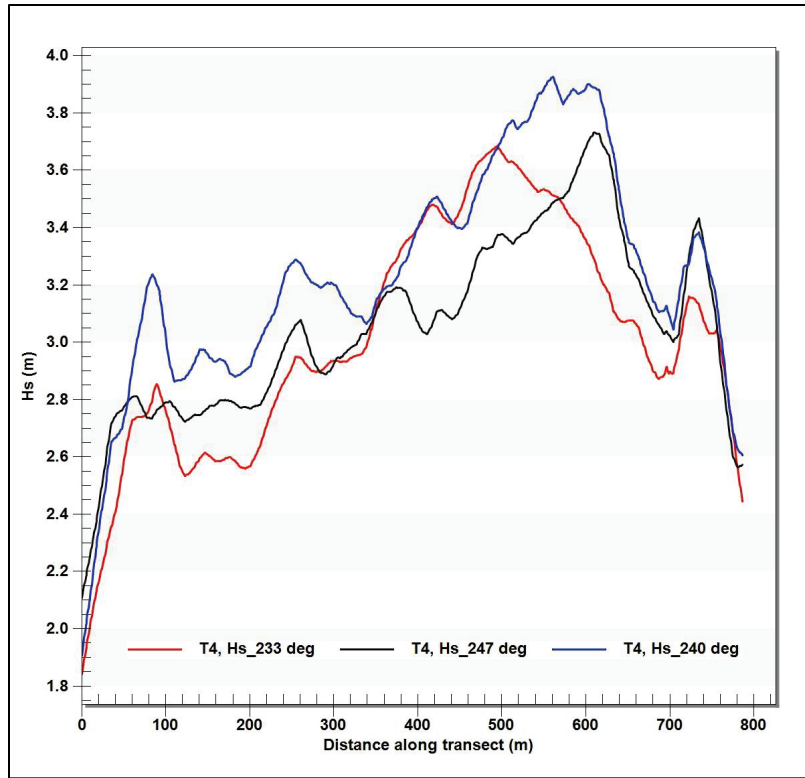
Figure 4-25. Wave height variation along T5 for three incident wave directions.
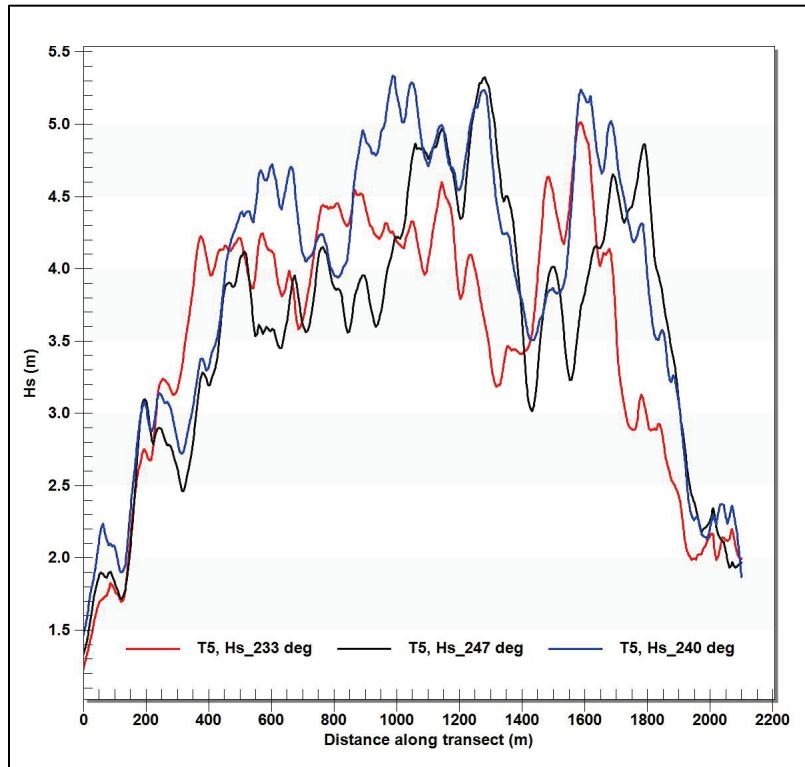
Figure 4-26. Wave height variation along T6 for three incident wave directions.
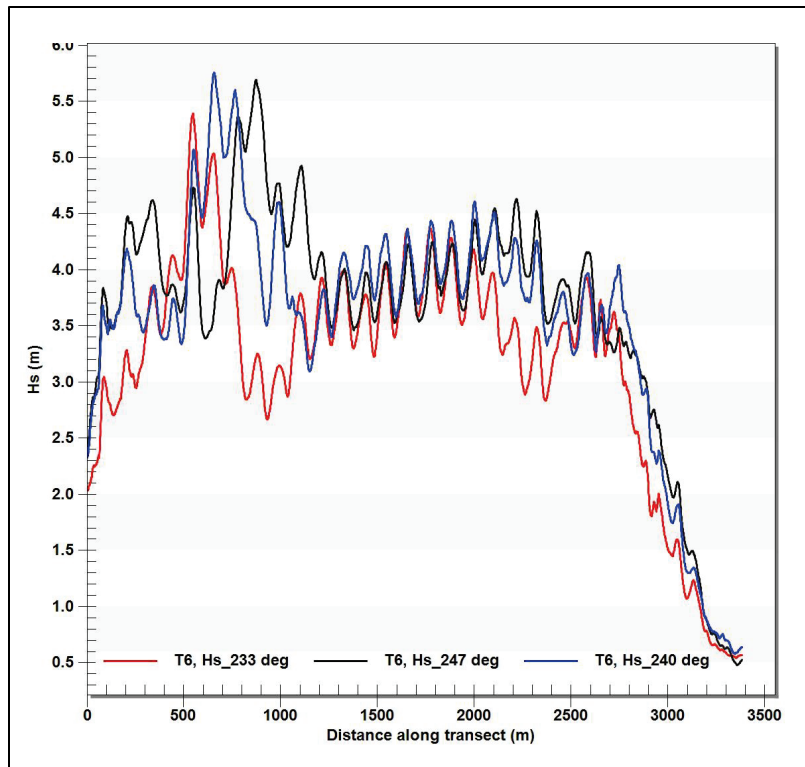
Figure 4-27. Wave height variation along T7 for three incident wave directions.
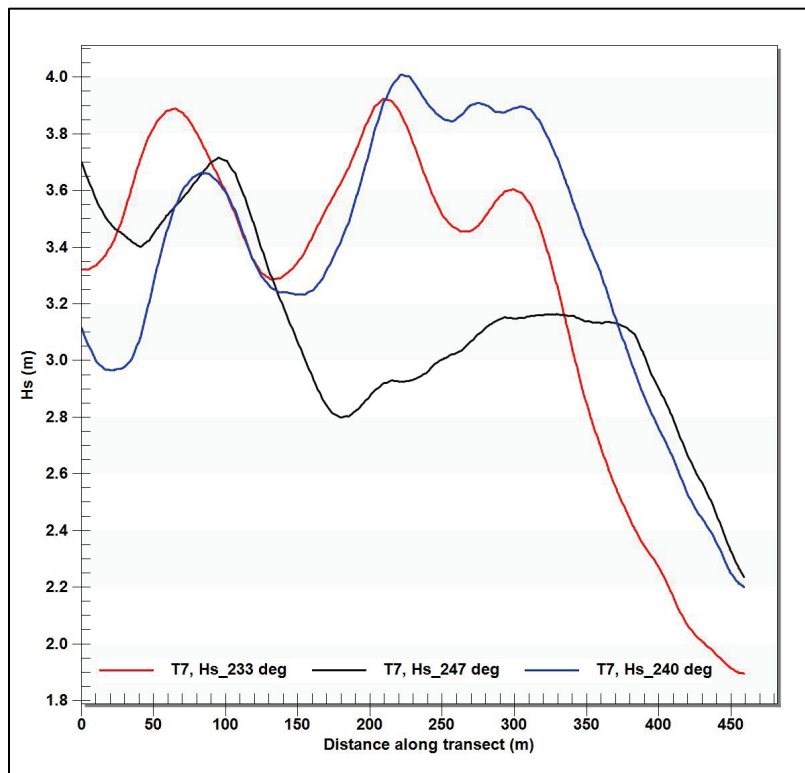
Figure 4-28. Wave height variation along T8 for three incident wave directions. Breakwater located at Distance = 120 m (394 ft).
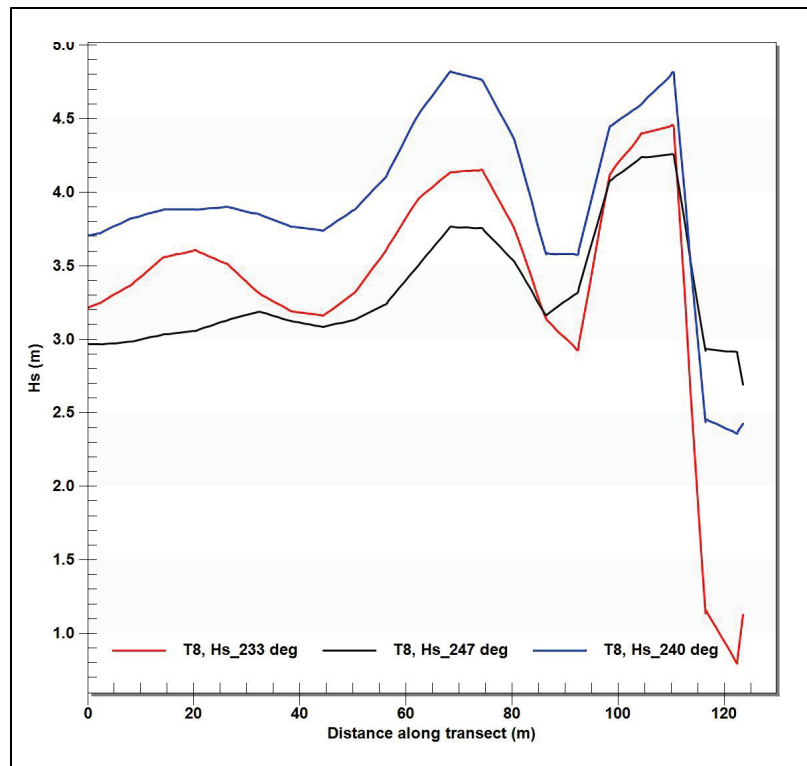
Figure 4-29. Wave height variation along T9 for three incident wave directions. Breakwater located at Distance = 120 m (394 ft).
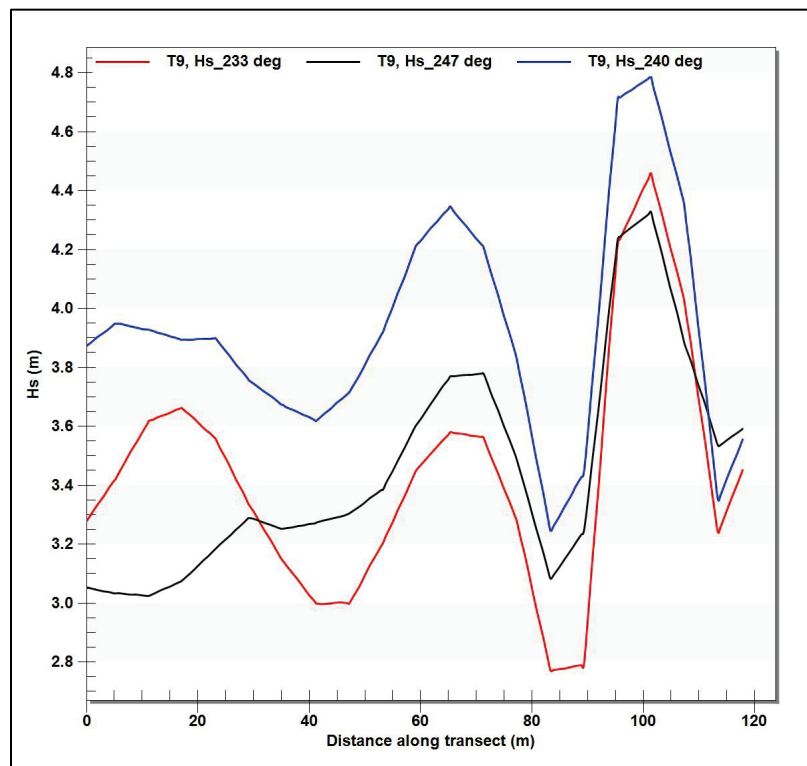
Figure 4-30. Wave height variation along T10 for three incident wave directions. Breakwater located at Distance = 120 m (394 ft).
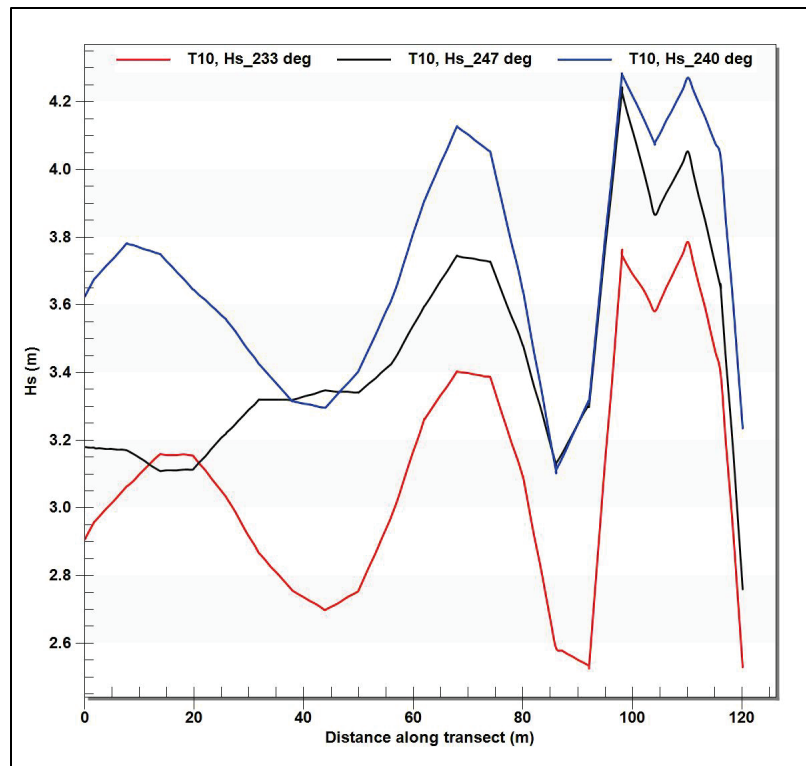
In addition to showing the variation in wave height, Figures 4-21 to 4-30 also provide values of the maximum wave height extracted along each transect. This information is useful in engineering design calculations, risk studies, and port operations but is not sufficient for selection of design estimates. For example, it was emphasized earlier that in the wave convergence zone passing over or near the damaged section of the SB, the largest wave height does not occur over the berm used in the Alt1 and Alt2 repairs. Consequently, maximum wave heights required for engineering calculations were extracted along the cross-shore transects T8 to T10 (Figures 4-28 to 4-30). If transects T8 to T10 were repositioned in different locations across the berm, or moved off to the north or south sides of the berm, different maximum wave heights could be obtained. With or without presence of berm, different values of design wave height would be obtained for different scenarios mentioned. With a berm, the location of design waves may change by shifting from a location on the top of berm to north or south edges of the berm.

To further test this hypothesis, model results were examined in detail using the SMS. The maximum significant wave height of 5.6 m (18.4 ft) was detected at an area close to the north edge of the berm. Results of this

analysis are displayed in Figures 4-31 to 4-33. A similar analysis was conducted by the LRB team that confirmed this finding. Figures 4-34 to 4-36 depict the LRB analysis results. These two independent analyses demonstrate that the selected profiles (transects) may miss larger wave heights occurring in adjacent areas to the berm.

Figure 4-31. Local wave height at and around the berm for θ = 233 deg.
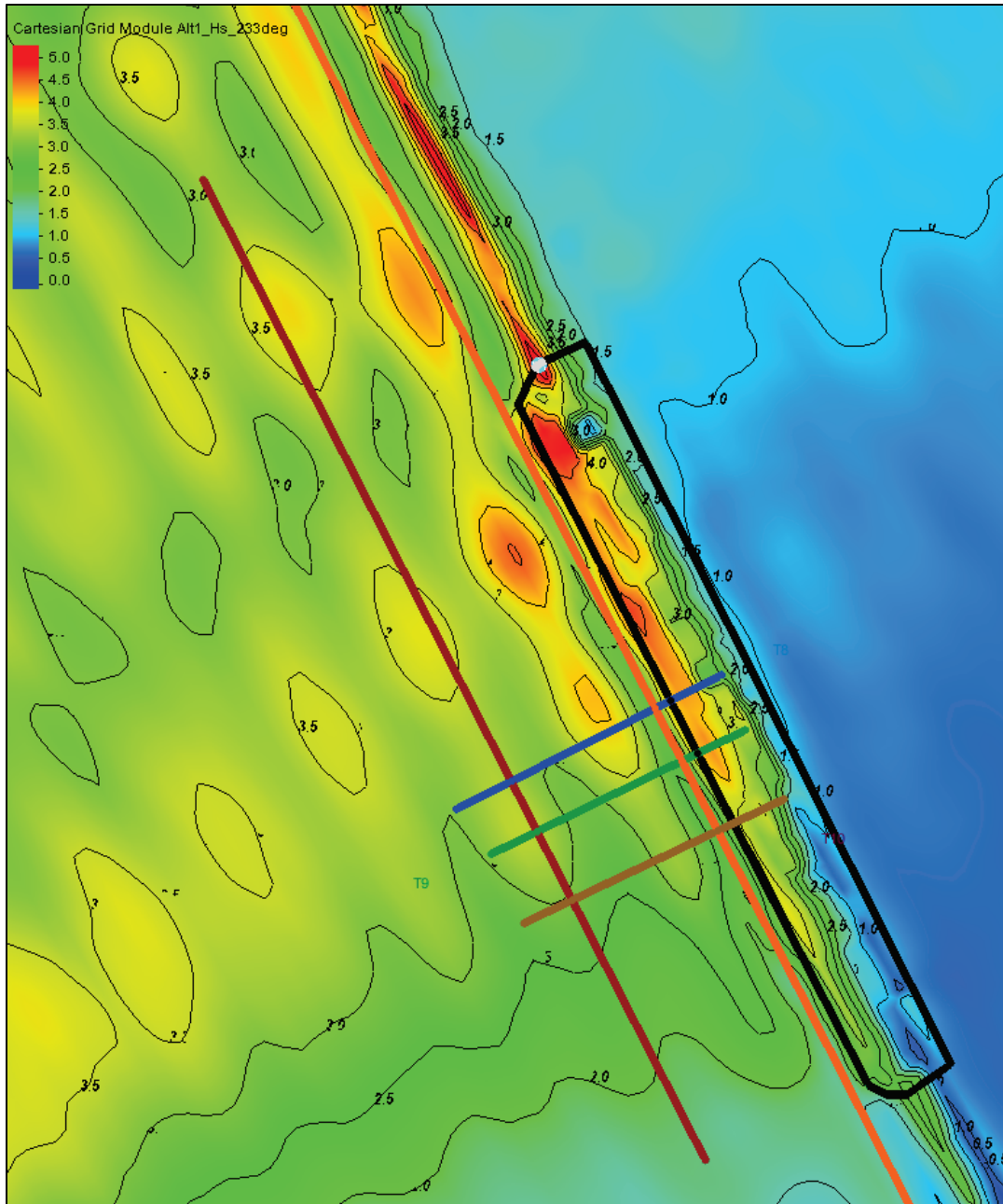
Figure 4-32. Local wave height at and around the berm for θ = 240 deg.
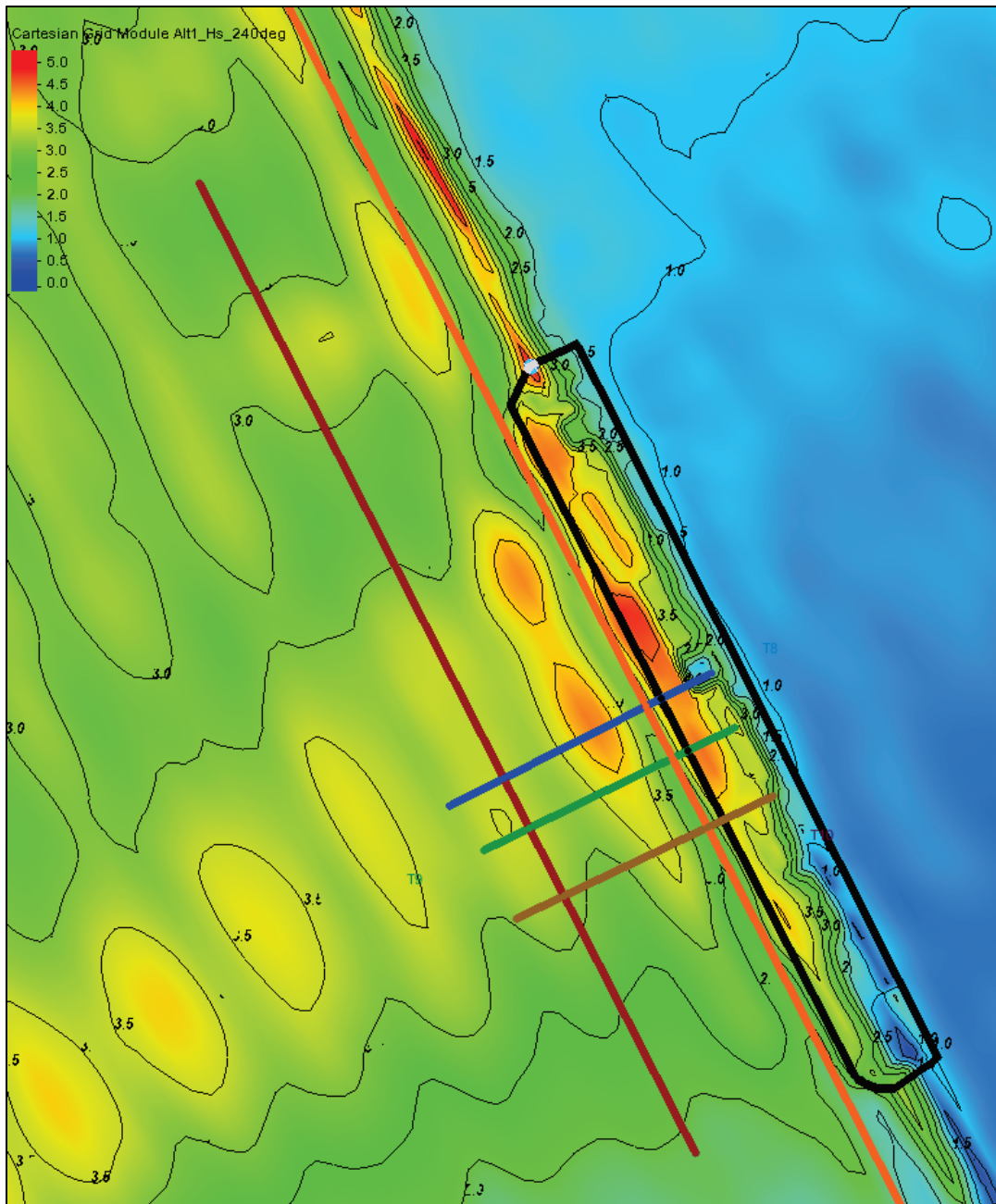
Figure 4-33. Local wave height at and around the berm for θ = 247 deg.
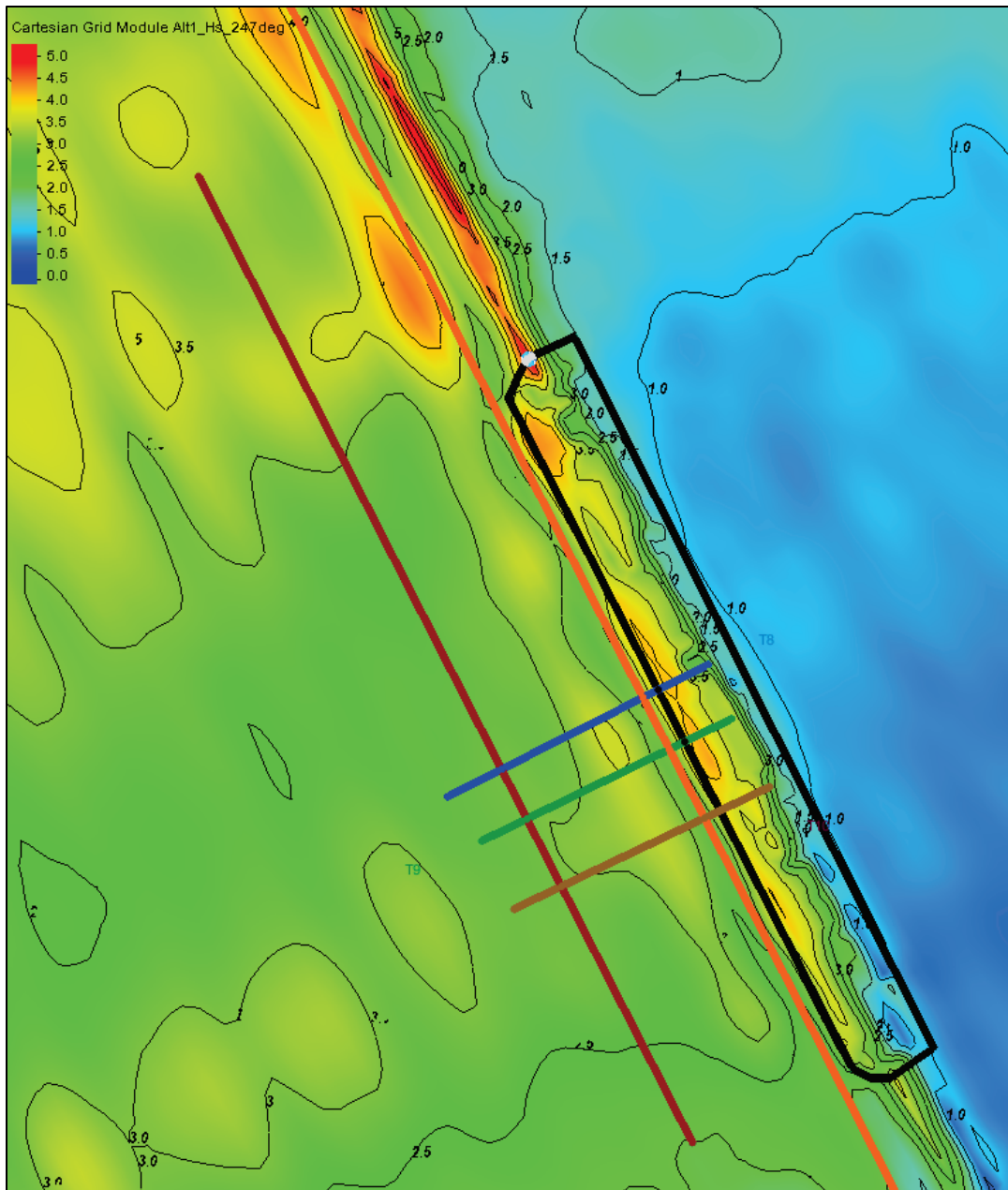
Figure 4-34. LRB wave height analysis of north portion of berm for θ = 233 deg.
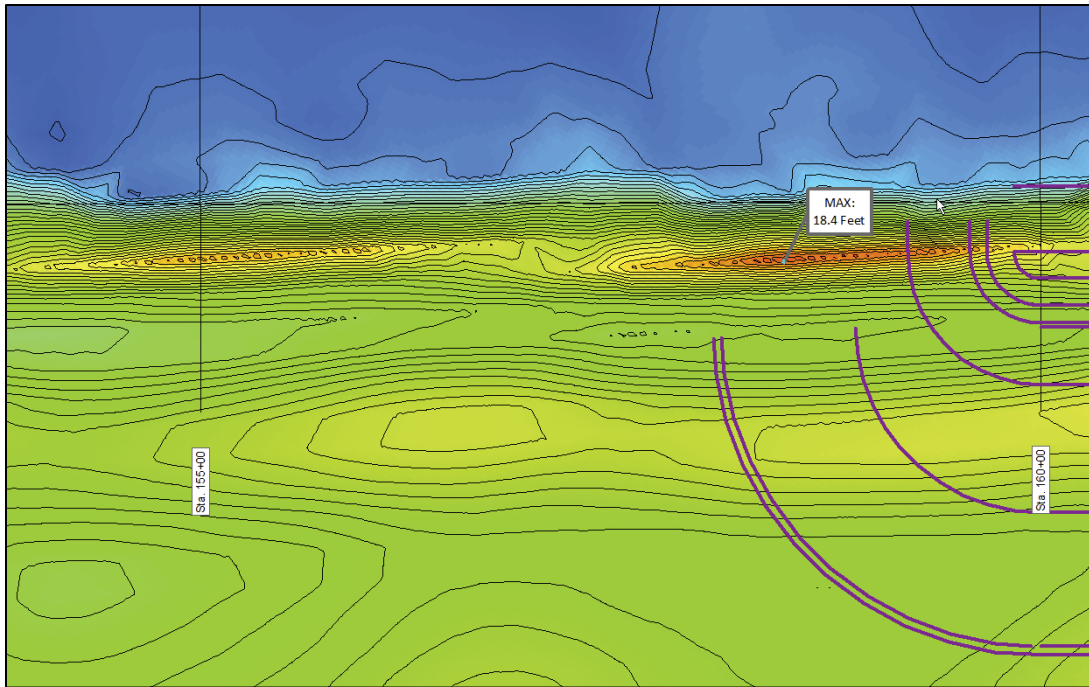
Figure 4-35. LRB wave height analysis of north portion of berm for θ = 240 deg.
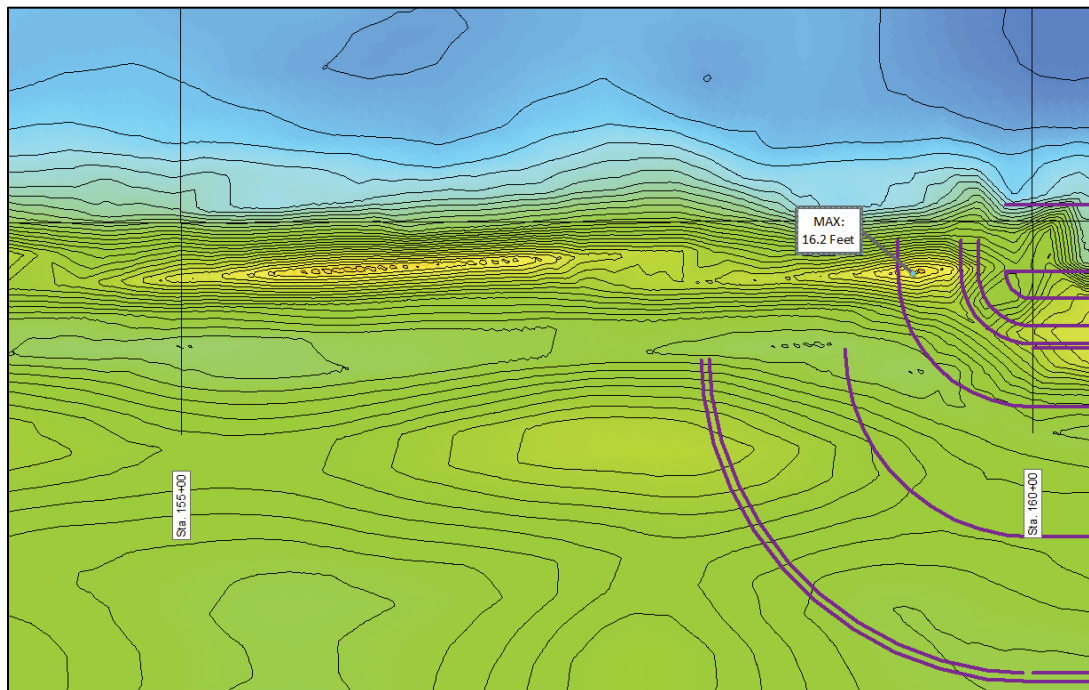
Figure 4-36. LRB wave height analysis of north portion of berm for θ = 247 deg.
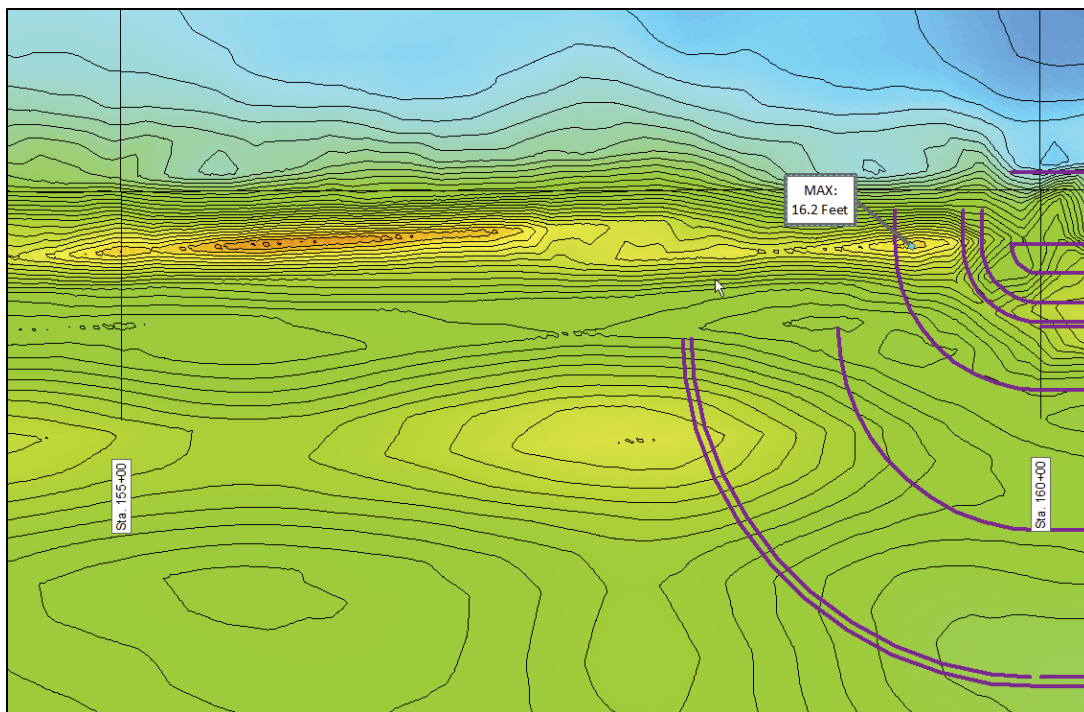
The neighboring areas impacted by the submerged berm were considered in determining the largest design wave height for repairs of the damaged area of the SB structure at and around the berm. Figures 4-31 to 4-36 provide details of the interaction between converging waves with berm-SB system. These showed the influence of interaction on local wave field on the adjacent segments of the SB connecting to the berm. The approach outlined in the next paragraph for finding a maximum design wave from B2D solutions is applicable to future repairs of damaged sections of other breakwaters in BH.

In the search for the maximum design wave estimate, a polygon (in black) was used to define the extent of berm footprint (Figure 4-31). Three cross-shore transects (T8, T9, and T10) perpendicular to the berm and SB are in blue, green, and brown colors. A white dot near the north edge of the berm points to the location of maximum wave height detected from the SMS analysis of wave height fields. Results for three incident wave directions showed comparatively larger wave heights occurring in north side of the berm than wave heights either over the berm itself or its south section. Analysis of the maximum wave heights in the north and south sides of the berm for three incident wave directions is summarized in Table 4-2.

Table 4-2. Summary of wave height estimate at and around the berm for Alt1 and Alt2.

Incident Wave Direction	H$_{smax}$ in North Side of Berm	H$_{smax}$ in South Side of Berm	Design Wave Height	Design Water Level
233 deg	5.6 m (18.4 ft)	2.8 m (9.2 ft)		
240 deg	5 m (16.4 ft)	3.3 m (10.8 ft)	5.6 m (18.4 ft) 3 m (9.8 ft)	
247 deg	5.1 m (16.6 ft)	3.6 m (11.2 ft)		

The above values were extracted from two points located close to the north and south edges of the black polygon in Figure 4-31. The largest wave height obtained from three incident directions and 3 m (9.8 ft) water level was used by the LRB for in-house engineering design calculations.

4.7.5 Three-dimensional (3D) images of instantaneous wave overtopping

There are gaps and low spots throughout the existing breakwater structures located in the BH. Such features might be part of the original design and construction specifications or resulted from damages and aging of structures. Model simulations showed wave overtopping occurring at or near these locations. Results indicate overtopping positions move (do not remain fixed) as water level and wave height change along the front face of the breakwaters. In general, breakwater segments (legs) experiencing the strongest wave focusing had the most severe overtopping. Model simulations indicated wave overtopping increased with larger wave height caused by wave focusing described in previous sections (i.e., greater overtopping occurs for larger local waves). The images of instantaneous water surface elevation described in this section help to determine which portions of breakwaters are experiencing wave overtopping.

Figure 4-37 through Figure 4-47 are the snapshots of wave fields displaying temporal and spatial details of waves in the lake side along the front face of breakwaters. These zoomed images are time-varying instantaneous snapshots for viewing wave runup and overtopping of structures. The instants of wave overtopping were captured from the three B2D simulations near the breakwaters. This was done by magnifying the vertical scale in the B2D animations in an attempt to show details of wave-structure interactions. The 3D displays provide additional information about spatial variability, location, and intensity of the water surface outside and in the interior of harbor and in/around the breakwaters. The images show change in the locations of overtopping along the breakwaters

with changing incident wave direction. These images indicate there is persistent overtopping of certain segments of breakwaters but no evidence of wave overtopping over other portions of breakwaters. These details gleaned about waves in and around the BH breakwaters are different from the wave height variation along breakwaters. These plots of sea surface elevation animation represent the condition of the sea state at different instants of time in selected parts of the BH grid, presenting frames of instantaneous spatial variation of waves outside and inside the harbor.

In structural design and repair work, it is desired to know the thickness of the water layer that is passing over the crest of the structure. By placing wave probes on top of the structure, it is possible to record a time series of the water column. By time-domain analysis of these overtopping probe results, it is possible to calculate the volume of fluid passing over the structure at that location, thickness time history, velocity, and resulting wave loads needed to displace structure stone. Along the structure, there will be sections with low and high crest elevations. This model (B2D) will identify those segments that have been damaged or that should be elevated to prevent damage.

Figure 4-37. Snapshot of water surface elevation at SB repair site (θ = 247 deg).
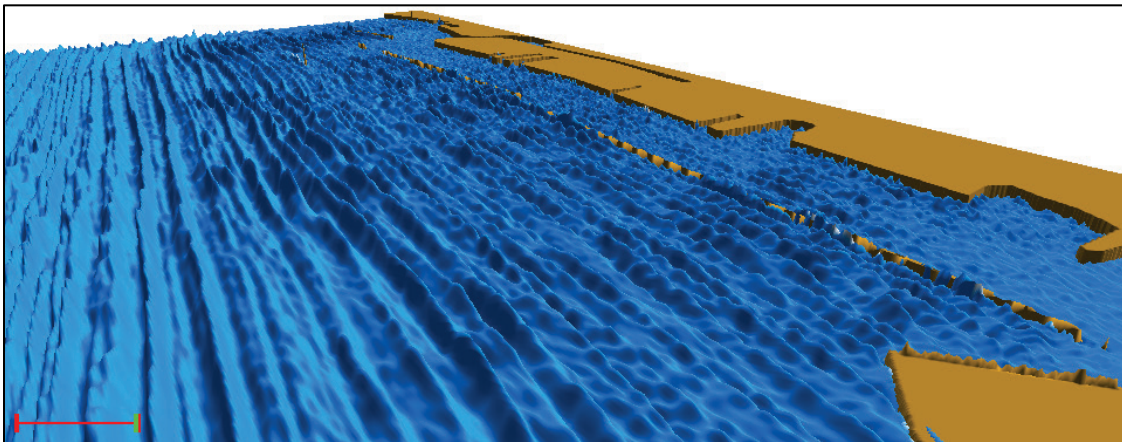
Figure 4-38. Zoomed image of water surface elevation at SB repair site (θ = 247 deg).
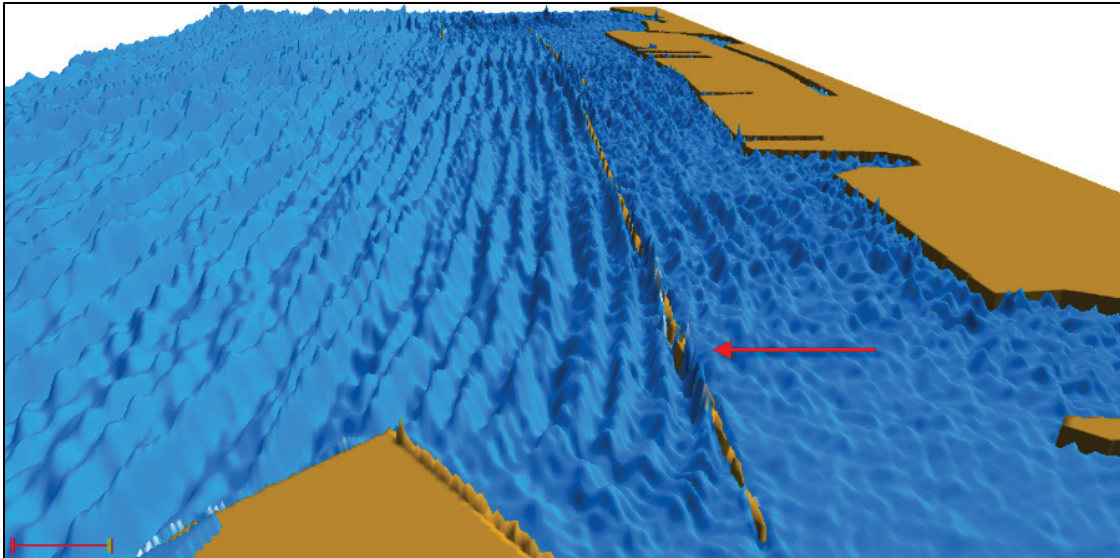
Figure 4-39. Zoomed image of water surface elevation at SB repair site (θ = 240 deg).
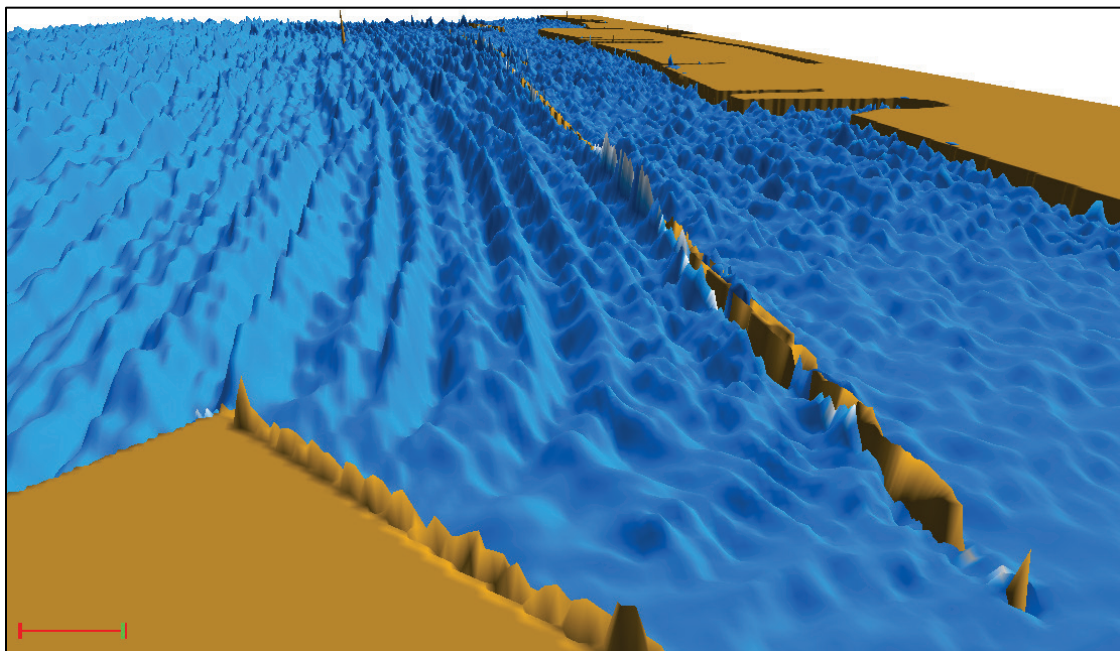
Figure 4-40. Zoomed image of water surface elevation at SB repair site (θ = 233 deg).
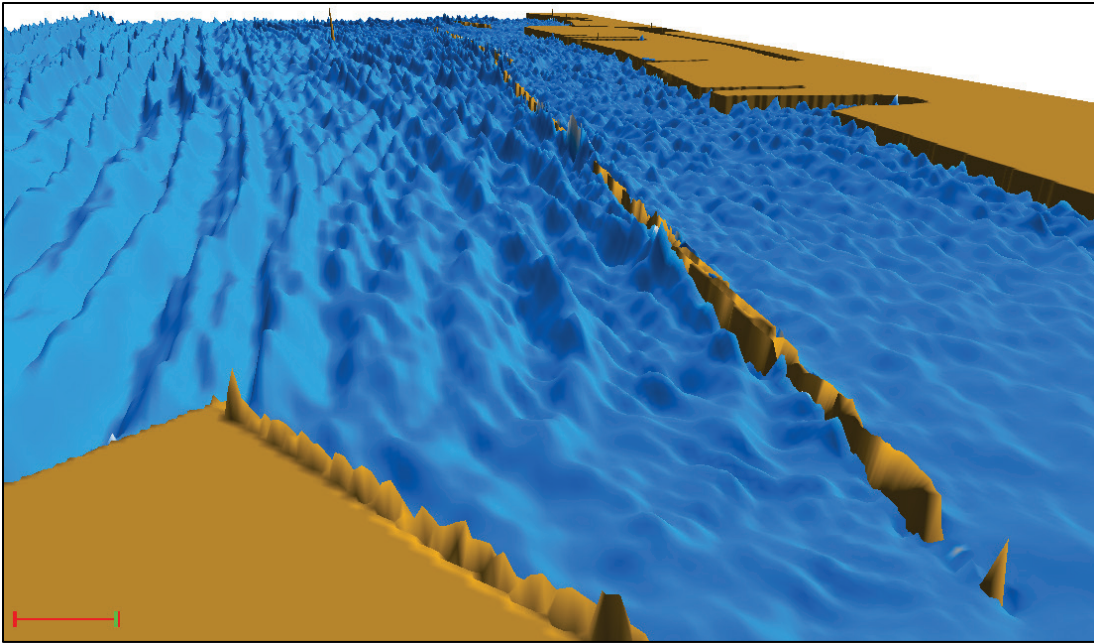
Figure 4-41. Variation of water surface elevation along OB and SB (θ = 233 deg).
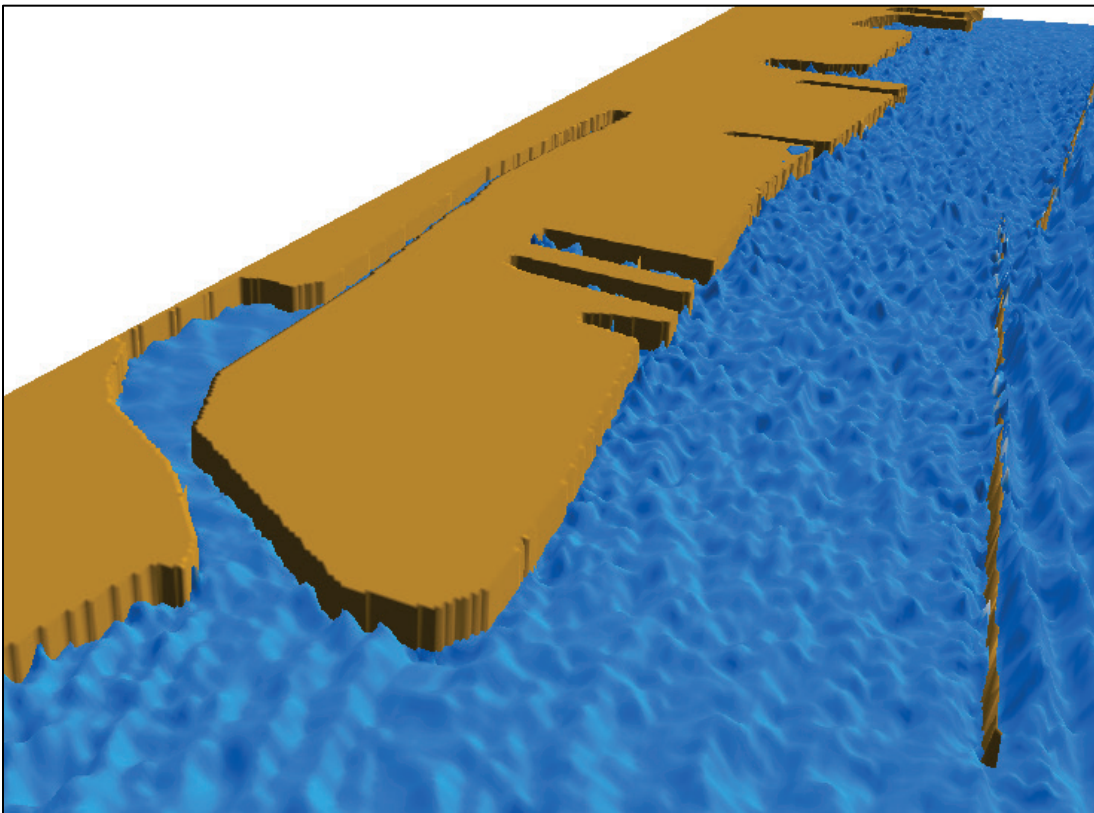
Figure 4-42. Zoomed image of water surface elevation along OB and SB (θ = 233 deg).
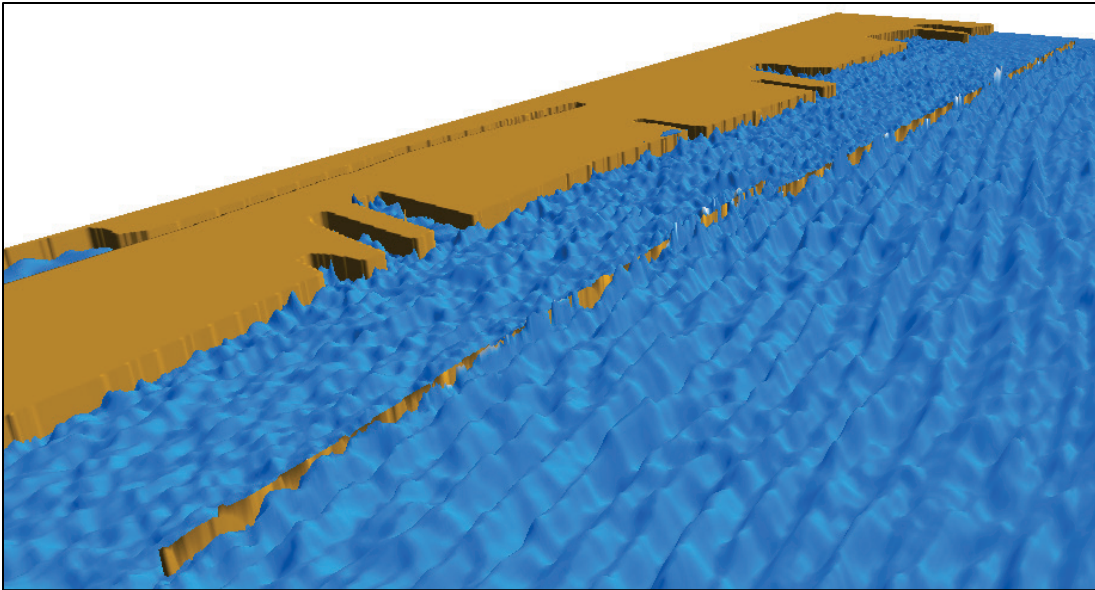
Figure 4-43. Variation of water surface elevation along OB and SB (θ = 240 deg).
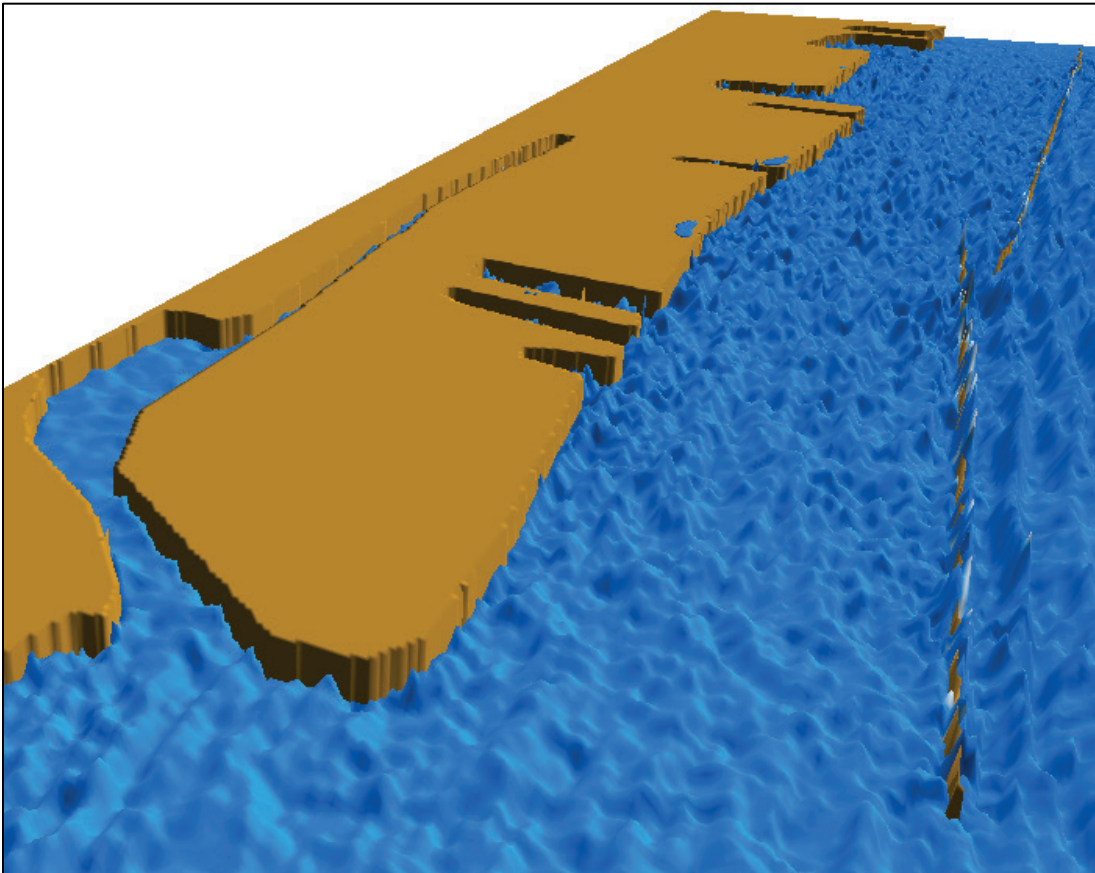
Figure 4-44. Zoomed image of water surface elevation showing overtopping of NB, OB, OBNL, and SB (θ = 240 deg).
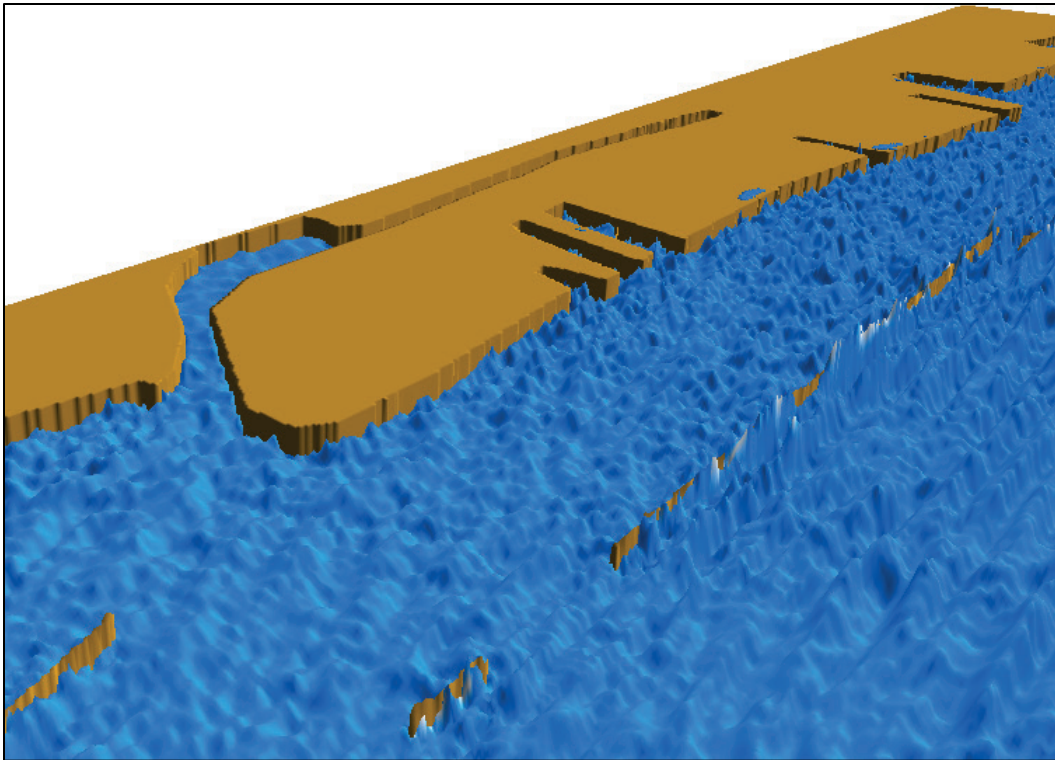
Figure 4-45. Water surface elevation field along NB, OB, OBNL, and WB (θ = 240 deg).
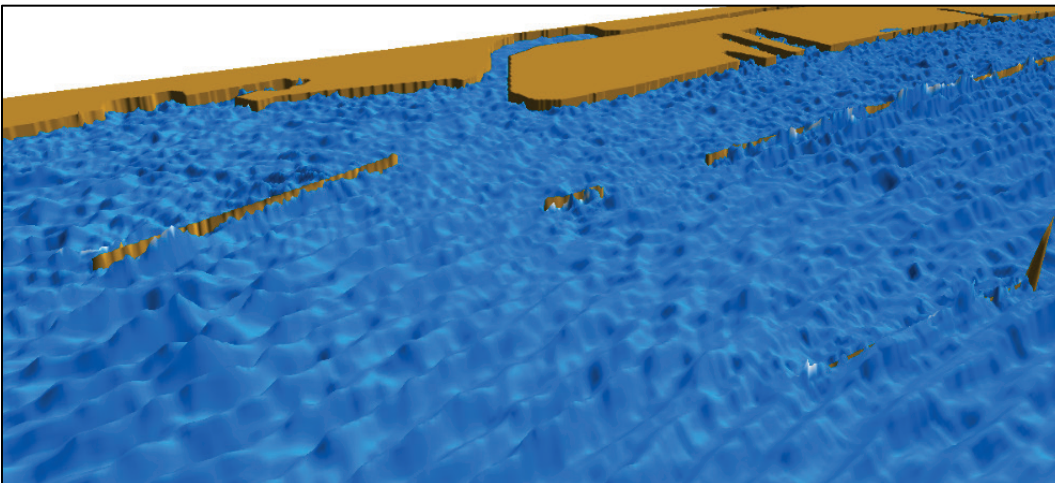
Figure 4-46. Water surface elevation field along NB and OBNL (θ = 233 deg).
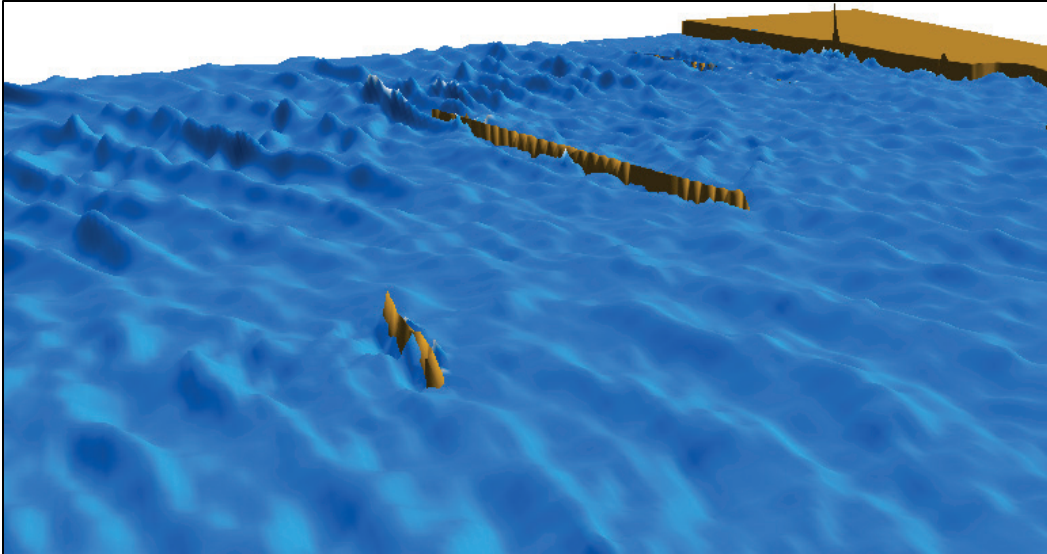
Figure 4-47. Zoomed water surface elevation around NB, OB, OBNL, and WB (θ = 233 deg).
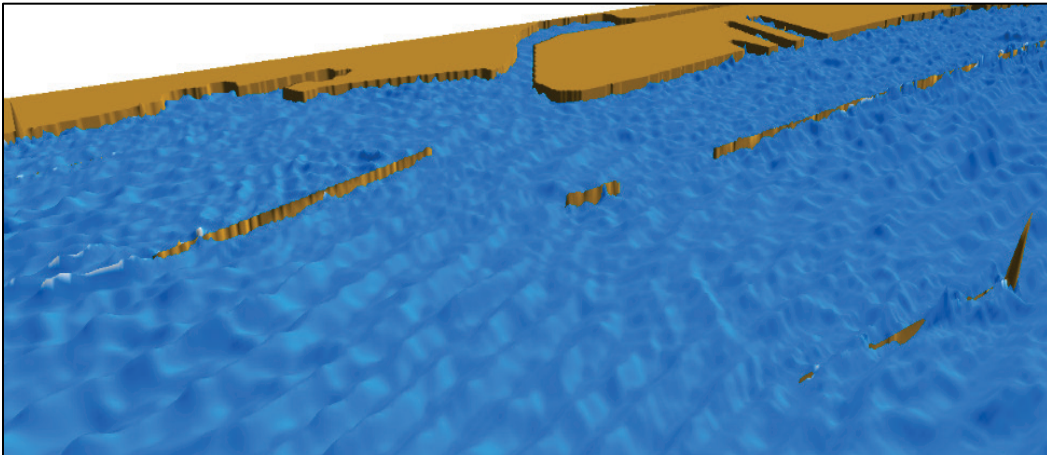
The B2D calculated water surface elevations were saved at each grid cell as time series similar to wave gauges deployed in prototype and laboratory field data collection studies. The plots of water surface elevation in Figures 4-37 to 4-47 show detailed information about wave overtopping for three incident wave directions.

4.7.6 Results for LaSalle Park (LP) seawall

A new set of transects were used for the LP seawall modeling. These are shown in Figures 4-48 and 4-49 with shore perpendicular transects (T1-T5) and shore parallel transects (T6-T9).

Figure 4-48. Transects T1 to T9 used in the LP seawall study.
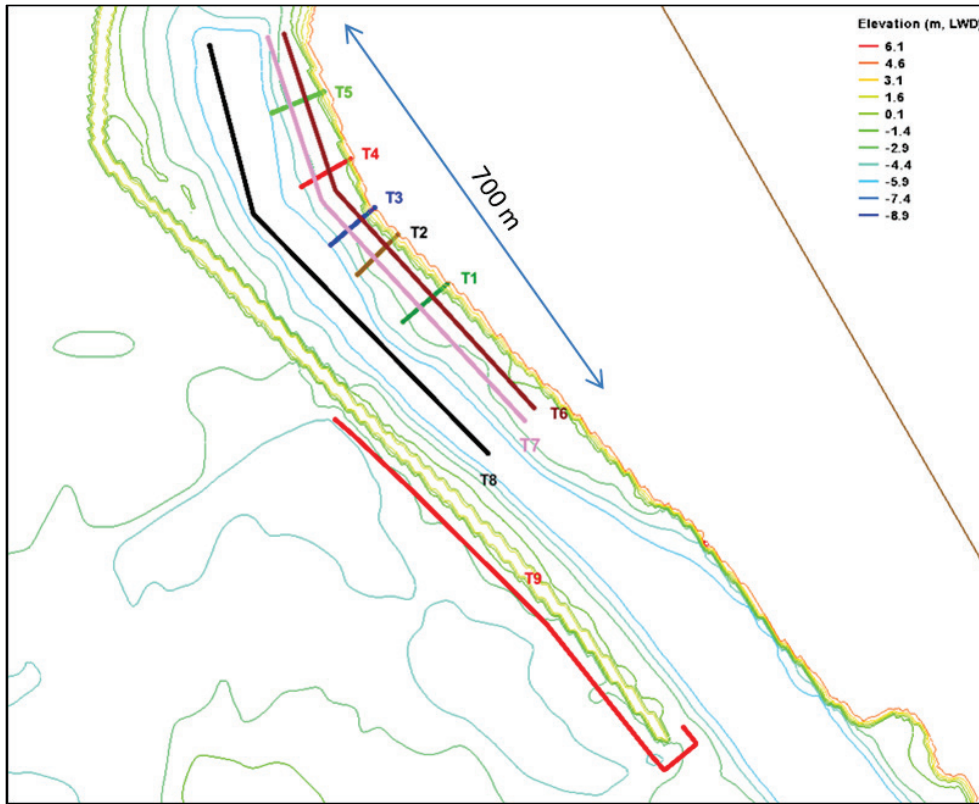
Figure 4-49. LP grid bathymetry and transects T1-T9.
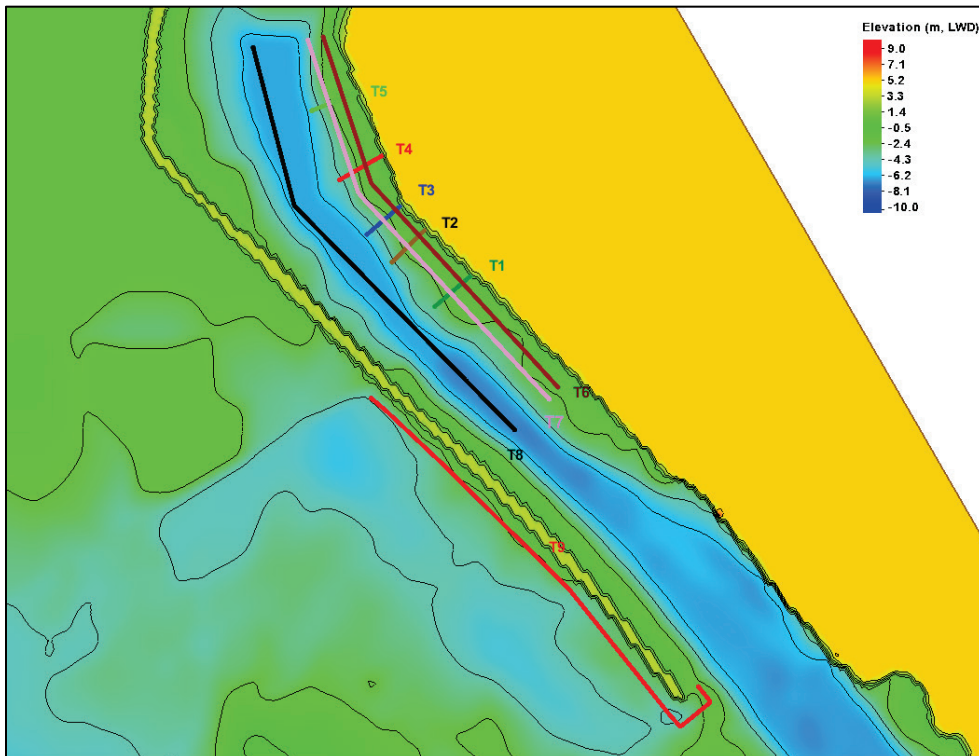
The 2D wave height fields are provided in Figures 4-50, 4-51, and 4-52 for three incident wave directions (θ = 233, 240, and 247 deg). These show the spatial variation of waves in the LP area in the north side of BH. Incident waves penetrating into the Black Rock Canal (Figure 1-6) where vessel traffic occurs, and also waves arriving at the Bird Island Pier (Figure 1-6) on the west side that protects this canal from incident waves, are depicted in these figures. These figures also show waves affecting the entire shore-side of the canal where the LP seawall is situated. Model results are displayed in these figures farther south down to the Seaplane Ramp shown in Figure 1-7.

Figure 4-50. Wave height field at LP seawall area for incident wave from θ = 233 deg.
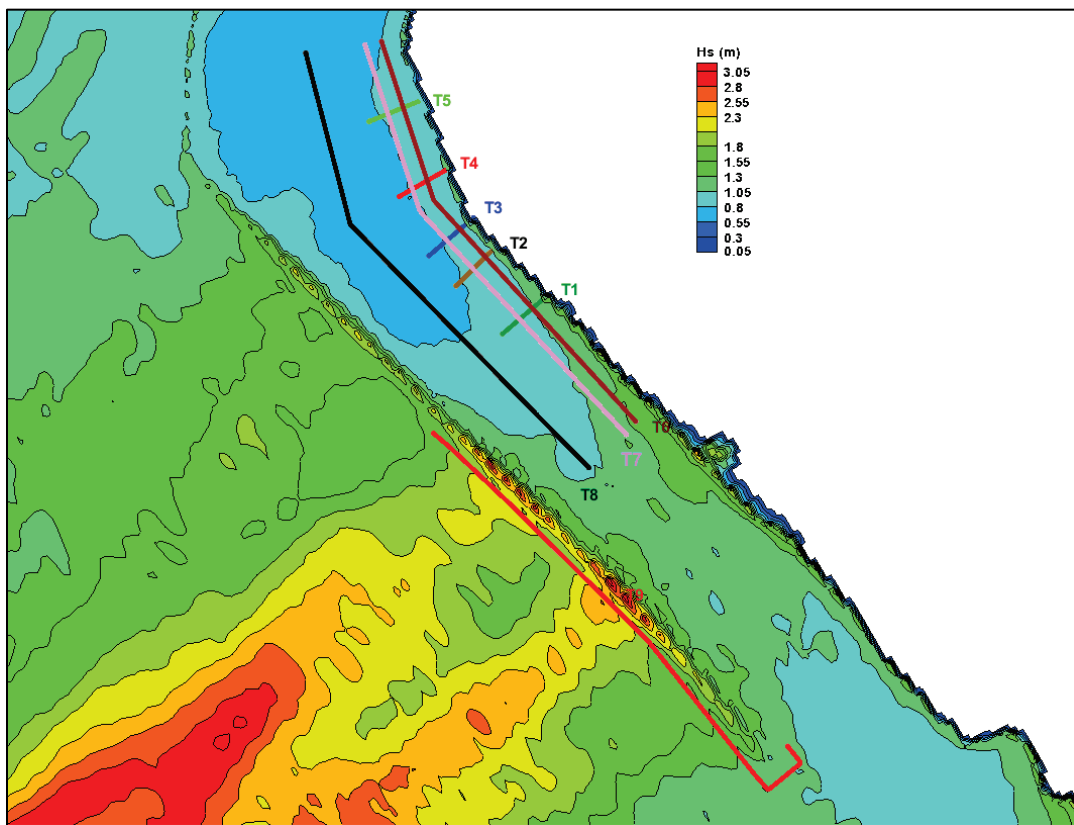
Figure 4-51. Wave height field at LP seawall area for incident wave from θ = 240 deg.
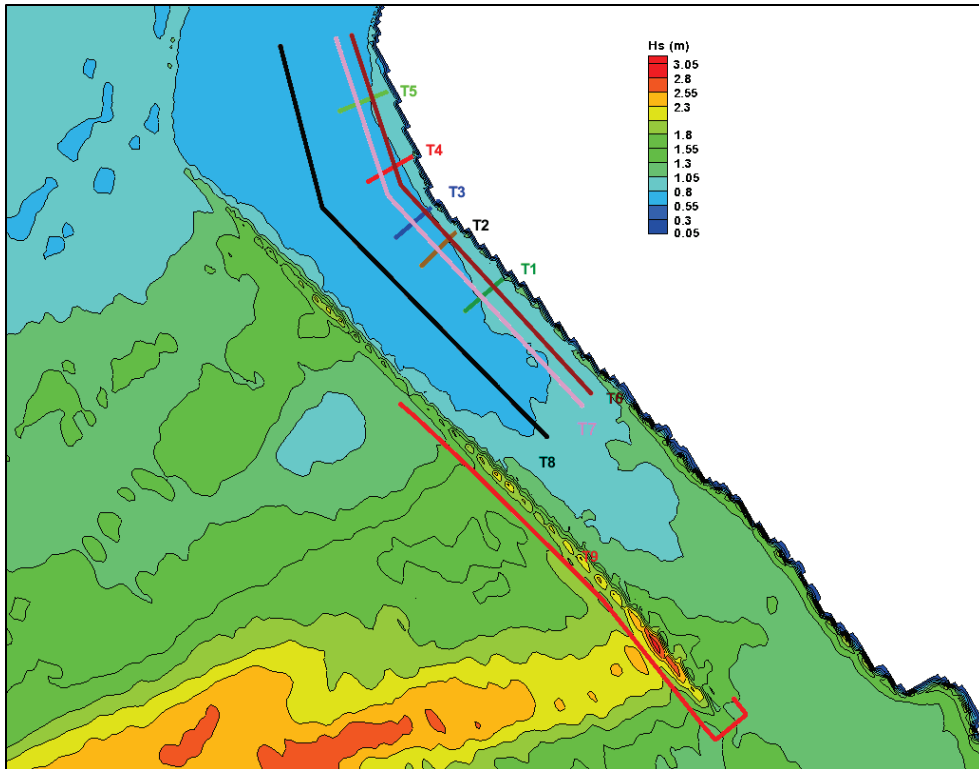
Figure 4-52. Wave height field at LP seawall area for incident wave from θ = 247 deg.
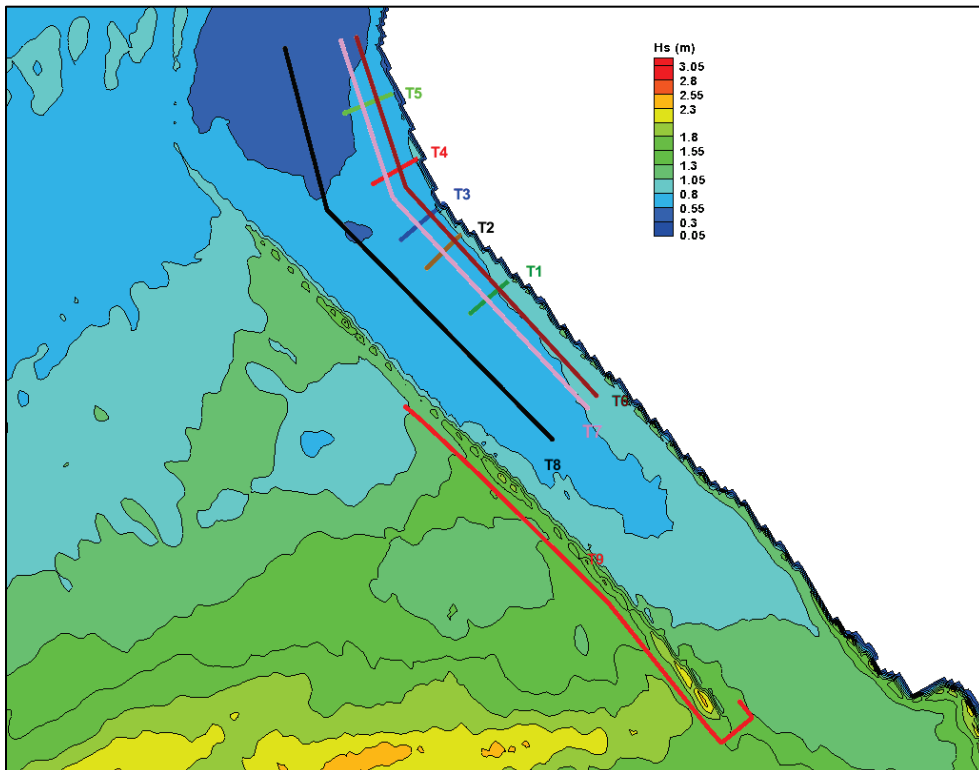
Examination of these 2D fields indicates the largest wave heights in these areas of interest are caused by incident waves from 233 deg as a result of combined wave refraction, diffraction, and reflection. Incident waves from this direction converge due to bathymetry into the northern portion of BH, especially at LP and vicinity from the Seaplane Ramp and in the north reaching the marina at the Porter Ave (Figure 1-7). Incident waves from 240 deg also affect these areas, but less. Smaller wave heights were produced by incident waves from 247 deg in these areas. Wave heights extracted along the local transects T1 to T9 specific to the LP study are shown in Figure 4-53 to Figure 4-61. Larger wave heights are obtained along the south ends of shore-parallel transects (T6 to T9) and on the east ends of the cross-shore transects (T1 to T5). Wave height increases near seawall as a result of wave shoaling and reflection. As expected, the largest wave heights are along T9 approaching 2.5 m (8.2 ft) due to the open lake exposure, followed by wave heights of up to 1.4 m (4.6 ft) over the south portions of T6, T7, and T8. Figures 4-62 and 4-63 are the snapshots that show partial wave overtopping occurring over the south portion of the Bird Island Pier dike.

Figure 4-53. Variation of wave height along T1 for LP seawall study.
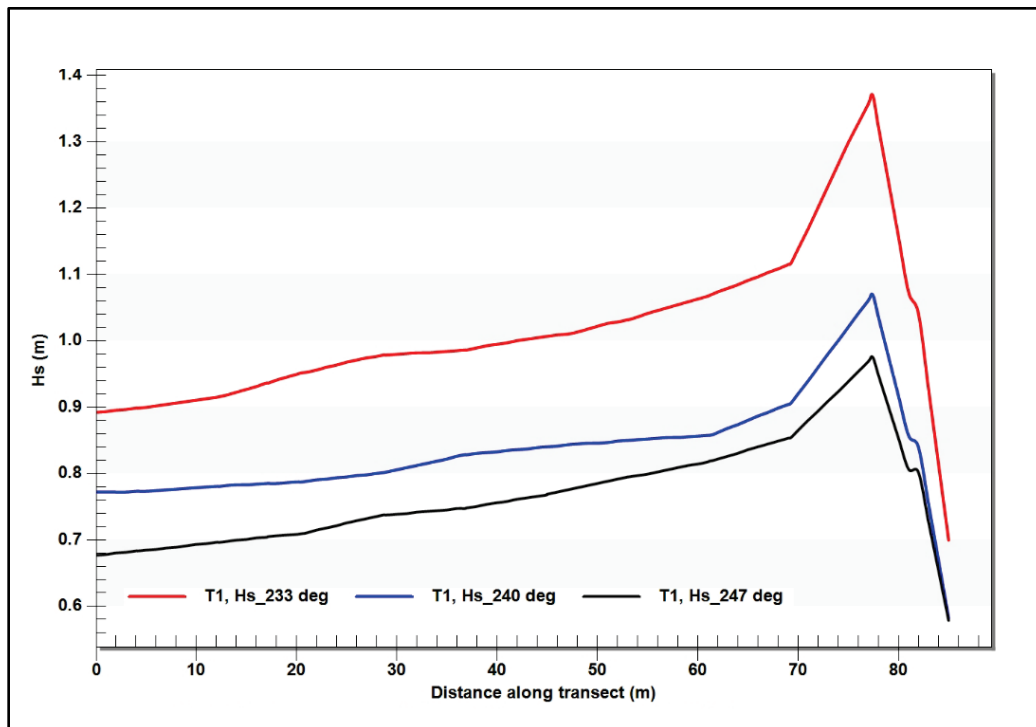
Figure 4-54. Variation of wave height along T2 for LP seawall study.
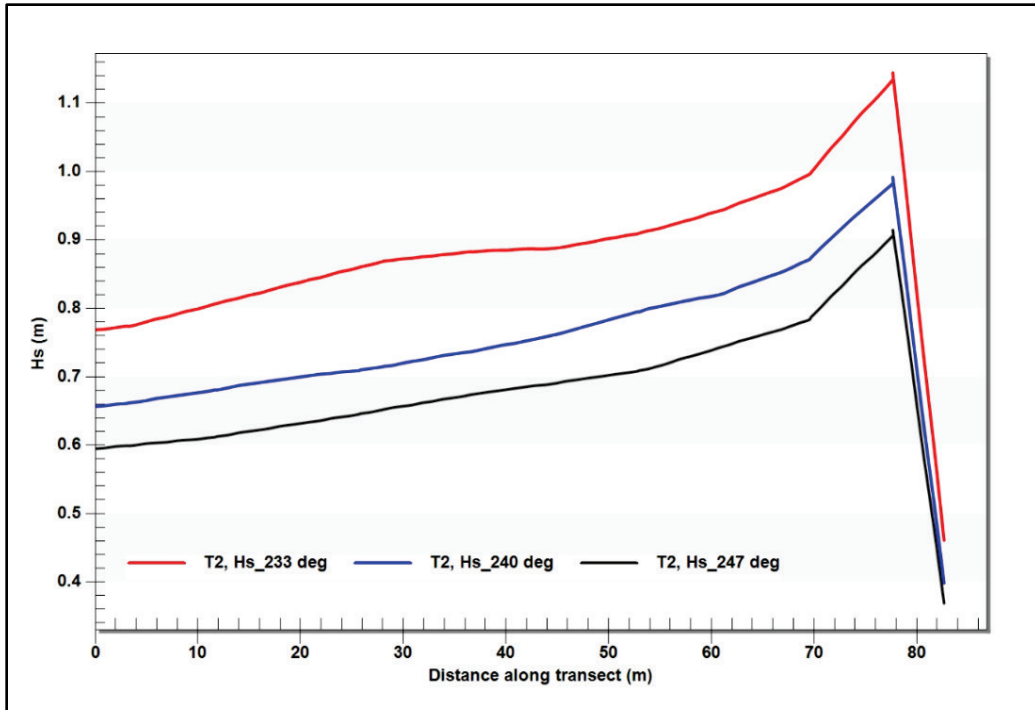
Figure 4-55. Wave height variation along T3 for LP seawall study.
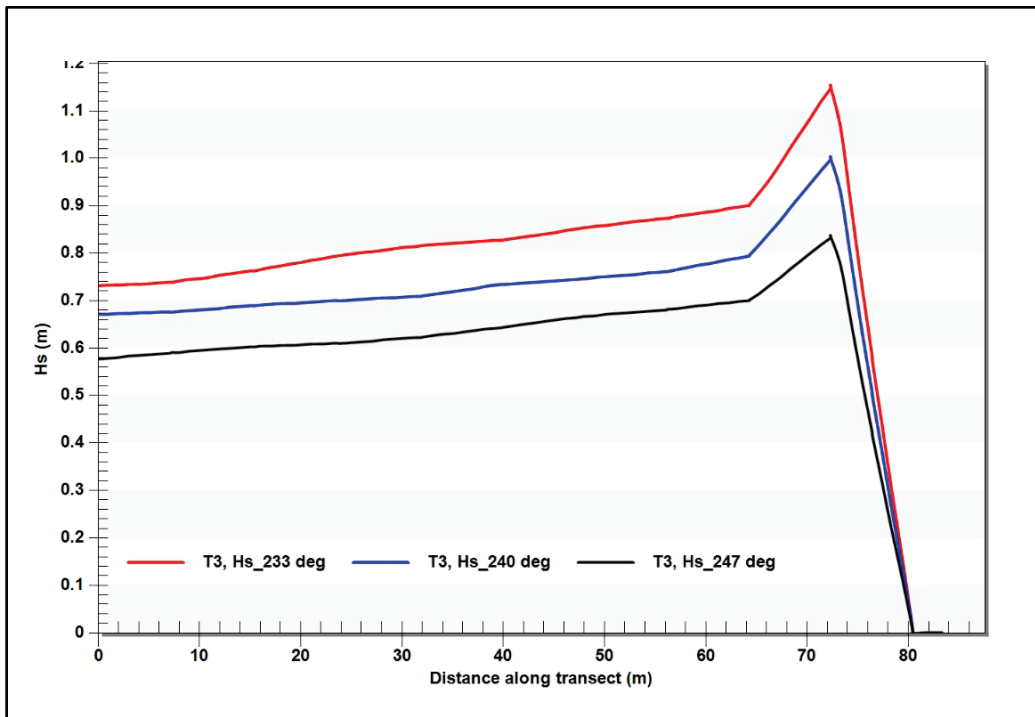
Figure 4-56. Wave height variation along T4 for LP seawall study.
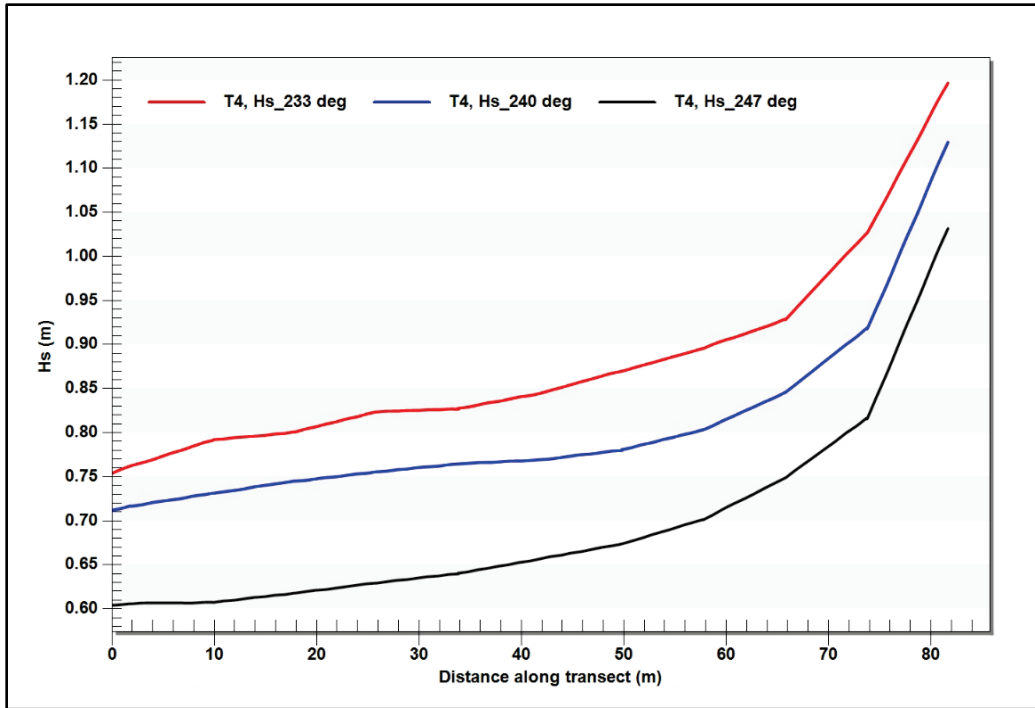
Figure 4-57. Wave height variation along T5 for LP seawall study.
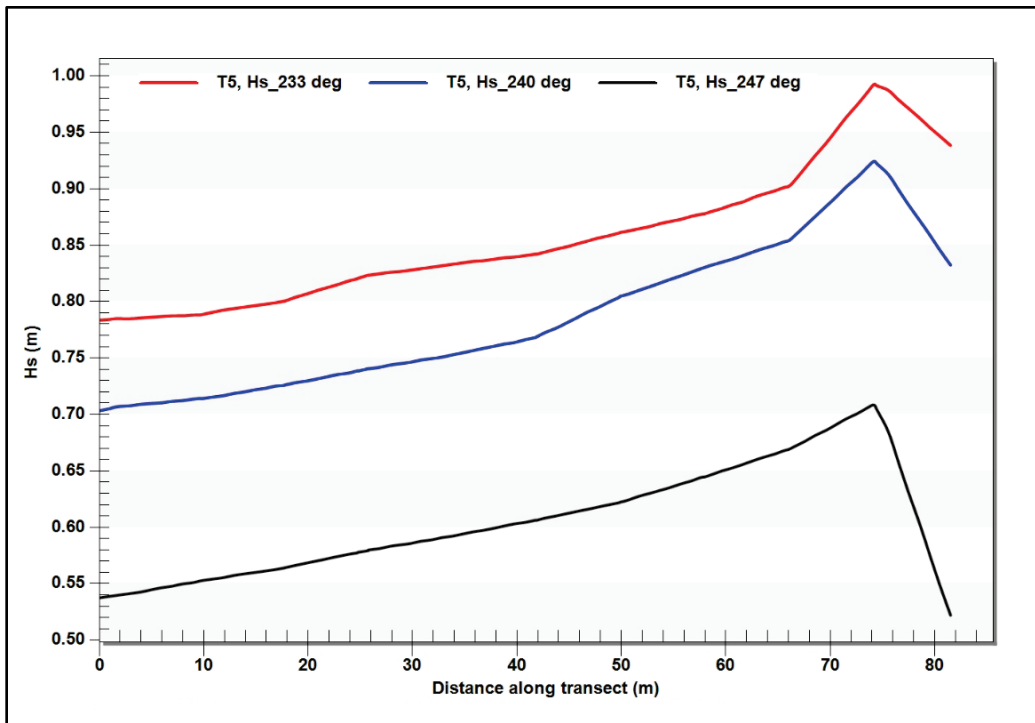
Figure 4-58. Wave height variation along T6 for LP seawall study.
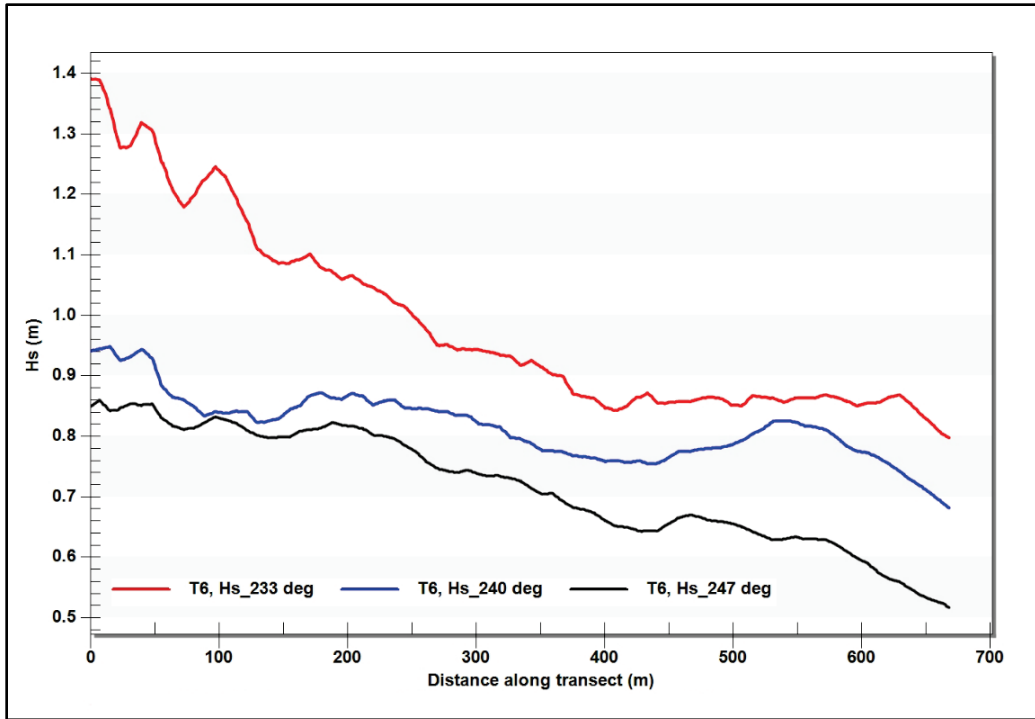
Figure 4-59. Wave height variation along T7 for LP seawall study.
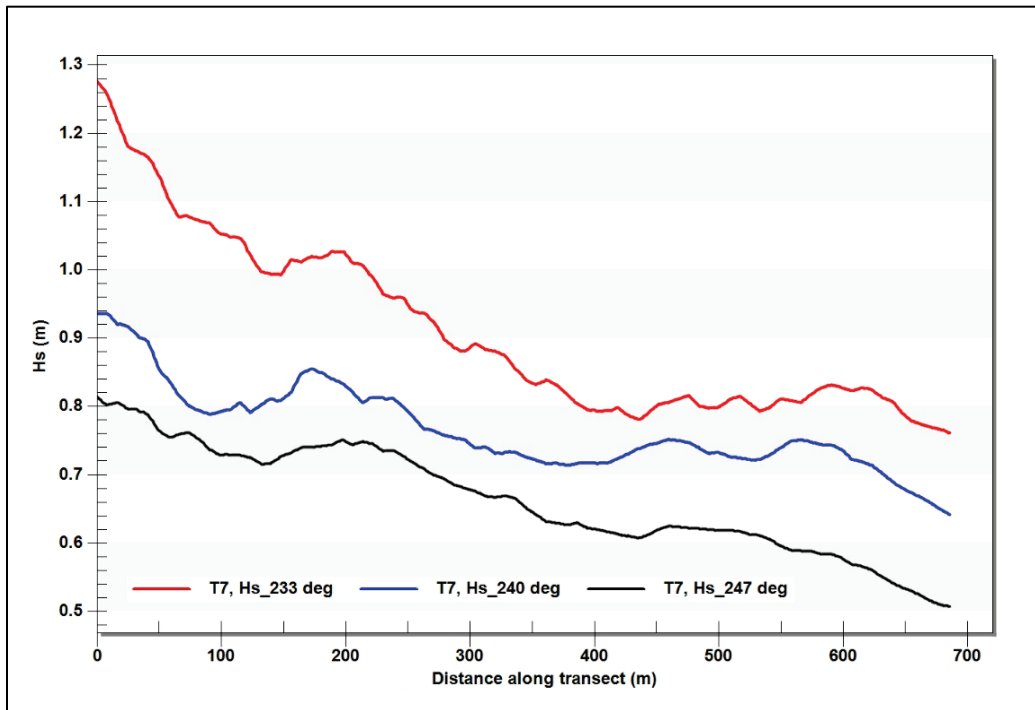
Figure 4-60. Wave height variation along T8 for LP seawall study.
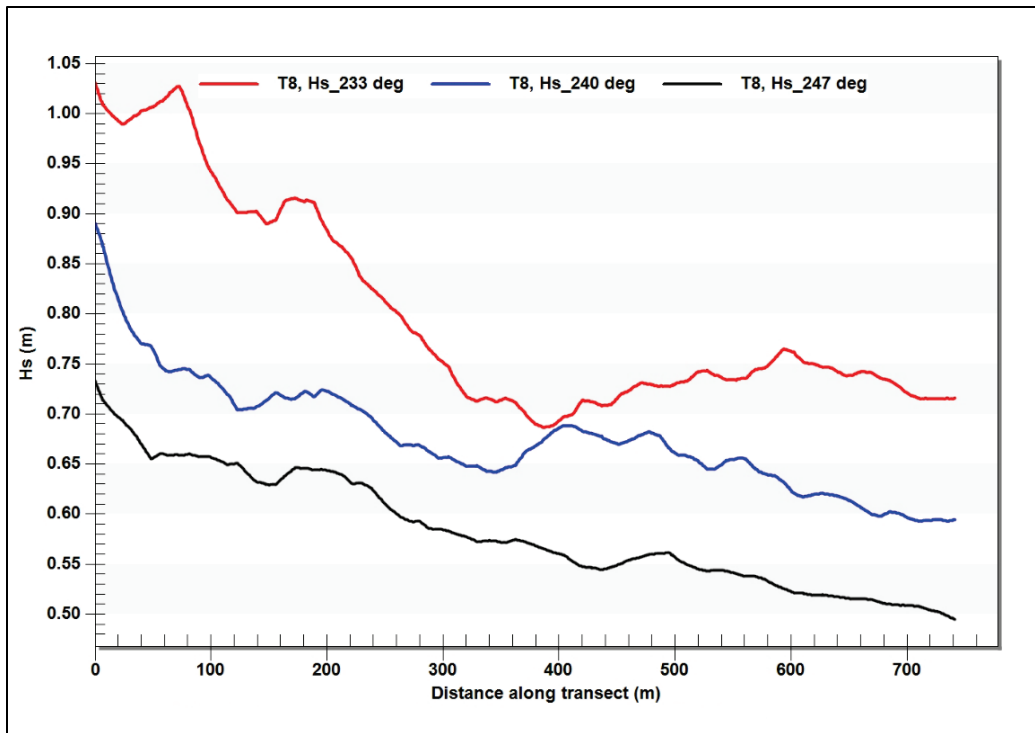
Figure 4-61. Wave height variation along T9 for LP seawall study.
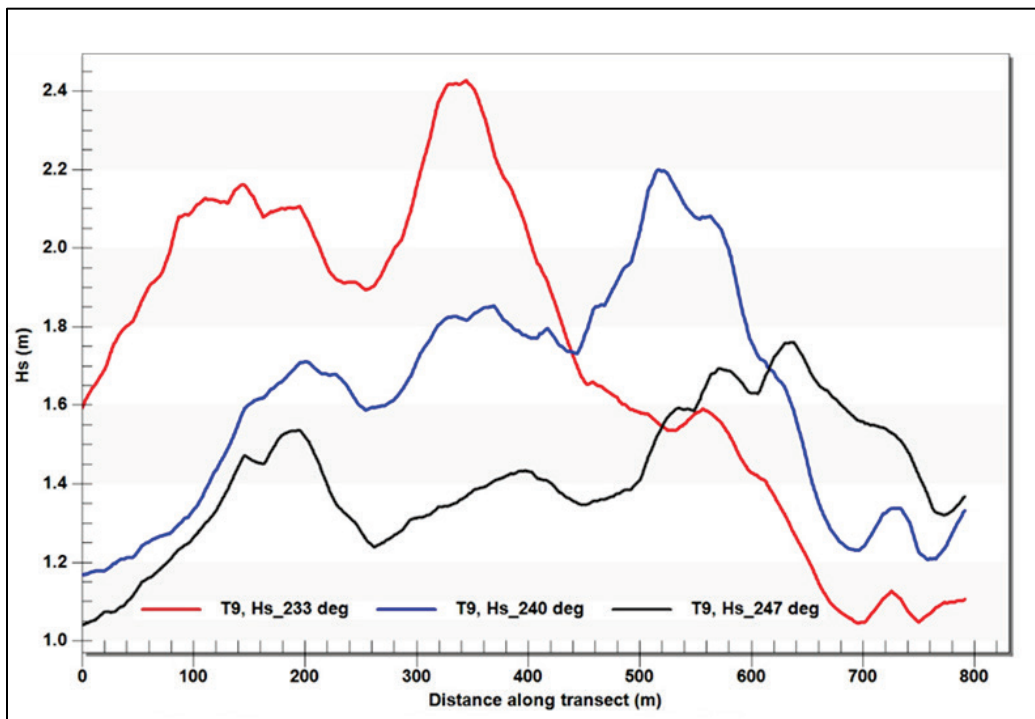
Figure 4-62. Water surface elevation field in the LP area of interest (θ = 233 deg).
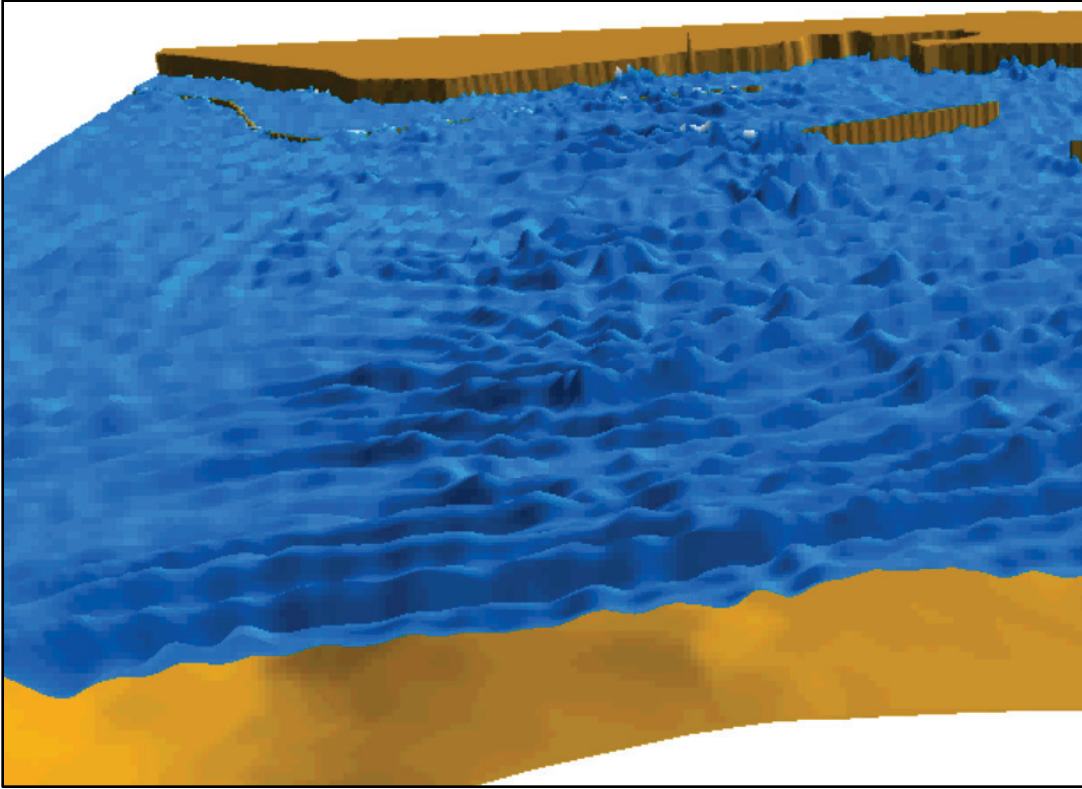
Figure 4-63. Snapshot of wave overtopping in the LP area (θ = 240 deg).
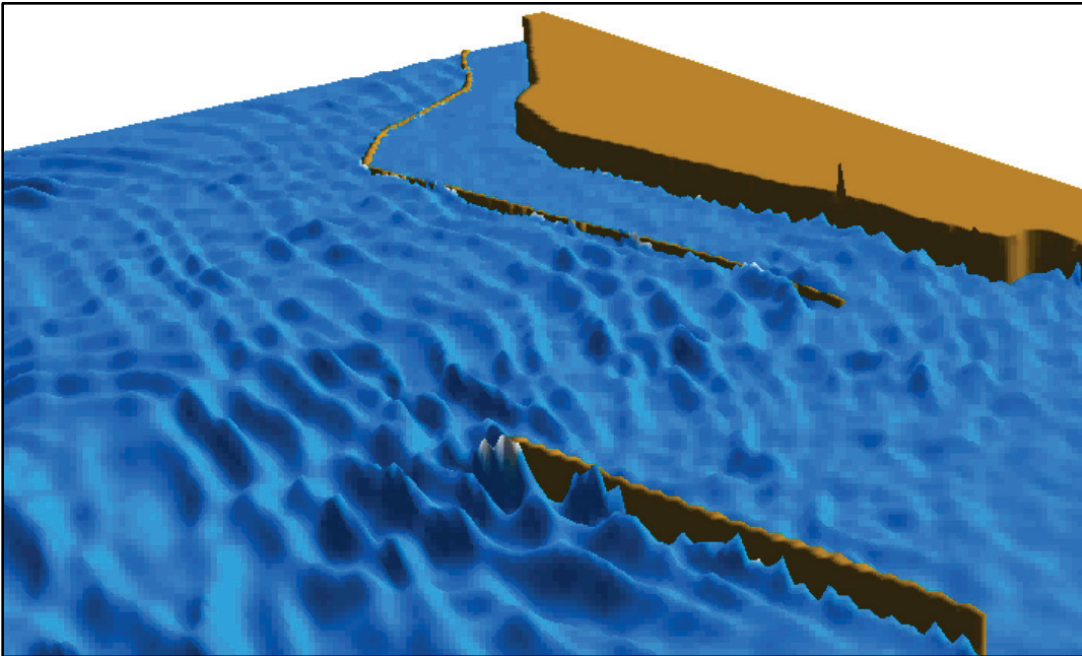
5   Summary and Conclusions

Design waves and water levels were estimated in this study for repairs of (1) the existing Buffalo Harbor SB and its two repair alternatives, and the existing Buffalo Harbor NB, and (2) the LP seawall along the northeast shore of the harbor that connects to the Niagara River canal. Modeling wave processes in the exterior and interior areas of BH was performed to develop wave estimates at and around breakwaters and the seawall. This required the use of two different classes of wave models: (1) CMS-Wave, a spectral wind-wave generation, growth, and transformation model, and (2) a nonlinear Boussinesq-type wave model BOUSS-2D (B2D). The spectral wave model CMS-Wave was coupled with CMS-Flow to calculate nearshore waves and water levels as input conditions for B2D wave modeling of the breakwaters and seawall. B2D is a time-domain, nonlinear wave model designed specifically for wave-structure interactions and for modeling waves in ports and harbors. This small-domain nearshore wave model provided waves for structural repairs. Details of CMS-Wave and B2D modeling are described in Chapter 3 and Chapter 4, respectively.

The focus of this present modeling investigation was development of design wave parameters for repair of (1) the Buffalo Harbor SB and NB and (2) the LP seawall of the harbor. Both of these evaluations required modeling wave overtopping of structures designed to shelter the BH interior from the metocean forcing in Lake Erie. CMS simulations were performed with the parent and child grids for three design storm conditions (Demirbilek et al. 2017). Wave results from the CMS were used as input in the B2D simulations. The inputs were prepared at the B2D's open boundary in the lake at approximately a 14 m (45.9 ft) water depth. Calculated wave heights by B2D for each of three selected incident wave directions lakeward of the breakwaters exhibited a similar pattern with a noticeable wave focusing zone outside in the lake and along the front face of breakwaters. Patterns were similar for different wave heights by direction but varied significantly for the three different directions.

The incident wave height of 4.15 m (13.6 ft) at the B2D offshore boundary for three storms reached 5.6 m (18.4 ft) in the wave focusing areas along a segment of the SB in the south side. This increase of wave height was caused by strong wave-structure interaction, including wave reflection and diffraction by the dike and water levels associated with each storm. Large wave heights arriving at the breakwaters reduced significantly after

overtopping the structures. Wave heights on the sheltered sides of breakwaters were much less (50% lower) than the heights in the front lake face of each structure. The B2D modeling revealed far more insight into the spatial and temporal changes in the wave runup and overtopping rate along 10 transects for the SB and NB structures and along 9 additional transects for the LP study area.

Based on results from the two types of numerical wave models (CMS-Wave and B2D) applied and performed in this study, design wave height of 5.6 m (18.5 ft) and water level of 3 m (9.8 ft) LWD were recommended for the two repairs of the existing SB on the south side of this structure. For future repairs of other segments of the SB or future repairs to other breakwaters (NB and OB), the B2D model results should be analyzed for each breakwater to determine appropriate design wave estimates. For the LP seawall, design wave height of 2.5 m (8.2 ft) would be appropriate for engineering works on the south side of the LP shoreline. For the middle and north areas of the LP shore, model results indicated a 1.5 m (4.9 ft) and 1.0 m (3.3 ft) design wave height, respectively, with wave period of 10 sec and water level of 3 m (9.8 ft). Individual sites within the LP study area would require a reanalysis utilizing B2D to deduce applicable design wave estimates for future studies.

The purpose of this B2D modeling of the Buffalo Harbor NB and SB was to identify segments of the breakwaters with low crest elevations or gaps that experience overtopping, and which may require repair presently or at some future date. If the structure is not being overtopped, then wave runup is not an engineering concern.

This model study time series was not of sufficient length to detect IG waves. This does not imply that IG waves may not exist in BH. Generally, IG waves are present in most confined harbors, but their intensity varies depending on other factors besides the geometry of the harbor. BH is not a confined harbor, and weak IG waves might develop in some shallow areas of the harbor. Because BH is largely an open harbor as part of Lake Erie, the presence of strong persistent IG waves is not expected in BH.

References

Demirbilek, Z., L. Lin, O. G. Nwogu, M. C. Mohr, S. Chader, and G. K. Hintz. 2017. *Numerical Modeling of Wave Overtopping of Buffalo Harbor Confined Disposal Facility (CDF4)*. ERDC/CHL TR-17-18. Vicksburg, MS: U.S. Army Engineer Research and Development Center.

Demirbilek, Z., L. Lin, T. D. Laczo, and A. A. Clark. 2016a. *Hydrodynamic Modeling for Channel and Shoreline Stabilization at Rhodes Point, Smith Island, Maryland*. ERDC/CHL TR-16-17. Vicksburg, MS: U.S. Army Engineer Research and Development Center.

Demirbilek, Z., L. Lin, O. G. Nwogu, K. K. Hathaway, W. C. Butler, J. H. Podoski, and T. D. Smith. 2016b. *Assessment of Modifications for Improving Navigation at Hilo Harbor, Hawaii*. ERDC/CHL TR-16-9. Vicksburg, MS: U.S. Army Engineer Research and Development Center.

Demirbilek, Z., L. Lin, O. G. Nwogu, W. C. Butler, K. K. Hathaway, and T. D. Smith. 2015a. *Kikiaola Light Draft Harbor Monitoring Plan Part 2: Numerical Wave Modeling for Evaluation of Structural Alternatives*. ERDC/CHL TR-14-9. Vicksburg, MS: U.S. Army Engineer Research and Development Center.

Demirbilek, Z., L. Lin, O. G. Nwogu, J. A. Goo, and T. D. Smith. 2015b. *Faleasao Harbor, American Samoa: Investigation of Modifications for Improving Navigation*. ERDC/CHL TR-15-15. Vicksburg, MS: U.S. Army Engineer Research and Development Center.

Demirbilek, Z., L. Lin, D. L. Ward, and D. B. King. 2015c. *Modeling Study for Tangier Island Jetties, Tangier Island, Virginia*. ERDC/CHL TR-14-8. Vicksburg, MS: U.S. Army Engineer Research and Development Center.

Demirbilek, Z., L. Lin, E. Hayter, C. O'Connell, M. M. Mohr, S. Chader, and C. Forgette. 2015d. *Modeling of Waves, Hydrodynamics and Sediment Transport for Protection of Wetlands at Braddock Bay, New York*. ERDC TR-14-8. Vicksburg, MS: U.S. Army Engineer Research and Development Center.

Demirbilek, Z., and C. L. Vincent. 2015. "Water Wave Mechanics." Chapter 1. EM 1110-2-1100, Part 2. *Coastal Engineering Manual*. Vicksburg, MS: U.S. Army Engineer Research and Development Center.

Demirbilek, Z., and J. Rosati. 2011. *Verification and Validation of the Coastal Modeling System, Report 1: Summary Report*. ERDC/CHL TR-11-10. Vicksburg, MS: U.S. Army Engineer Research and Development Center.

Demirbilek, Z., O. G. Nwogu, D. L. Ward, and A. Sanchez. 2009. *Wave Transformation over Reefs: Evaluation of One-Dimensional Numerical Models*. ERDC/CHL TR-09-1. Vicksburg, MS: U.S. Army Engineer Research and Development Center.

Demirbilek, Z., L. Lin, and O. G. Nwogu. 2008. *Wave Modeling for Jetty Rehabilitation at the Mouth of the Columbia River, Washington/Oregon, USA*. ERDC/CHL TR-08-3. Vicksburg, MS: U.S. Army Engineer Research and Development Center.

Demirbilek, Z., and O. G. Nwogu. 2007. *Boussinesq Modeling of Wave Propagation and Runup over Fringing Coral Reefs, Model Evaluation Report*. ERDC/CHL TR-07-12. Vicksburg, MS: U.S. Army Engineer Research and Development Center.

Demirbilek, Z., O. G. Nwogu, and A. K. Zundel. 2007a. *Infra-Gravity Wave Input Toolbox (IGWT): User's Guide*. ERDC/CHL CHETN-I-73. Vicksburg, MS: U.S. Army Engineer Research and Development Center.

Demirbilek, Z., O. G. Nwogu, D. L. Ward. 2007b. *Laboratory Study of Wind Effect on Runup over Fringing Reefs. Report 1: Data Report*. ERDC/CHL TR 07-4. Vicksburg, MS: U.S. Army Engineer Research and Development Center.

Demirbilek, Z., L. Lin, and A. Zundel. 2007c. *WABED Model in the SMS: Part 2. Graphical Interface*. ERDC/CHL CHETN-I-74. Vicksburg, MS: U.S. Army Engineer Research and Development Center.

Demirbilek, Z., A. Zundel, and O. Nwogu. 2005a. *BOUSS-2D Wave Model in SMS: I. Graphical Interface*. ERDC/CHL CHETN-I-69. Vicksburg, MS: U.S. Army Engineer Research and Development Center.

Demirbilek, Z., A. Zundel, and O. Nwogu. 2005b. *BOUSS-2D Wave Model in SMS: II. Tutorial with Examples*. ERDC/CHL CHETN-I-70. Vicksburg, MS: U.S. Army Engineer Research and Development Center.

Irvine, K.N., G.P. Stein, and J.K. Singer. 1991. *An Environmental Guide Book to the Buffalo River*. Center for Environmental Research and Education, SUNY College at Buffalo.

Lin, L., and Z. Demirbilek. 2005. "Evaluation of Two Numerical Wave Models with Inlet Physical Model." *Journal of Waterway, Port, Coastal, and Ocean Engineering ASCE* 131(4): 149–161.

Lin, L., and Z. Demirbilek. 2012. *Coupled BOUSS-2D and CMS-Wave Modeling Approach for Harbor Projects*. ERDC/CHL CHETN-IV-84. Vicksburg, MS: U.S. Army Engineer Research and Development Center.

Lin, L., Z. Demirbilek, H. Mase, and F. Yamada. 2008. *CMS-Wave: A Nearshore Spectral Wave Processes Model for Coastal Inlets and Navigation Projects*. ERDC/CHL TR-08-13. Vicksburg, MS: U.S. Army Engineer Research and Development Center.

Lin, L., Z. Demirbilek, and H. Mase. 2011a. "Recent Capabilities of CMS-Wave: A Coastal Wave Model for Inlets and Navigation Projects." In "Proceedings, Symposium to Honor Dr. Nicholas Kraus." *Journal of Coastal Research* Special Issue 59: 7–14.

Lin, L., Z. Demirbilek, R. Thomas, and J. Rosati. 2011b. *Verification and Validation of the Coastal Modeling System, Report 2: CMS-Wave*. ERDC/CHL TR-11-10. Vicksburg, MS: U.S. Army Engineer Research and Development Center.

Nwogu, O., and Z. Demirbilek. 2010. "Infragravity Wave Motions and Runup over Shallow Fringing Reefs." *ASCE Journal of Waterway, Port, Coastal, and Ocean Engineering*. http://dx.doi.org/10.1061/(ASCE)WW.1943-5460.0000050)

Nwogu, O., and Z. Demirbilek. 2006. "Nonlinear Wave Interaction with Submerged and Surface-Piercing Porous Structures." In *Proceedings, 30th International Conference on Coastal Engineering, San Diego, CA*, 287–299.

Nwogu, O., and Z. Demirbilek. 2008. "Nonlinear Wave Transformation and Runup over Fringing Coral Reefs." In *Proceedings, 31st International Conference on Coastal Engineering, Hamburg, Germany.*

Nwogu, O. 2006. "Boussinesq Modeling of Landslide-Generated Waves and Tsunami Runup." Edited by P.L.-F Liu, H. Yeh and. C. Synolakis. In *Advanced Numerical Models For Simulating Tsunami Waves and Runup Advances in Coastal and Ocean Engineering* 10: 273–278.

Nwogu, O. G., and Z. Demirbilek. 2001. *BOUSS-2D: A Boussinesq Wave Model for Coastal Regions and Harbors.* ERDC/CHL TR-01-25. Vicksburg, MS: U.S. Army Engineer Research and Development Center.

Nwogu, O. 1994. "Nonlinear Evolution of Directional Wave Spectra in Shallow Water." In *Proceedings, 24th International Conference on Coastal Engineering, Kobe, Japan*, Vol. 1, 467–481.

Nwogu, O. 1993. "Alternative Form of Boussinesq Equations for Nearshore Wave Propagation." *Journal of Waterway, Port, Coastal and Ocean Engineering, ASCE* 119(6): 618–638.

Sanchez, A., W. Wu, T. M. Beck, H. Li, J. D. Rosati, Z. Demirbilek, and M. Brown. 2011a. *Verification and Validation of the Coastal Modeling System, Report 4: Sediment Transport and Morphology Change.* ERDC/CHL TR-11-10. Vicksburg, MS: U.S. Army Engineer Research and Development Center.

Sanchez, A., W. Wu, T. M. Beck, H. Li, J. Rosati III, R. Thomas, J. D. Rosati, Z. Demirbilek, M. Brown, and C. Reed. 2011b.*Verification and Validation of the Coastal Modeling System, Report 3: Hydrodynamics.* ERDC/CHL TR-1-10. Vicksburg, MS: U.S. Army Engineer Research and Development Center.

Appendix A: Description of the Coastal Modeling System (CMS)

The CMS was used in this study to provide estimates of waves and water levels in Buffalo Harbor for studies involving repairs of breakwaters and a seawall. A brief description of the CMS is provided here for completeness. Figure A-1 shows the modular framework of the CMS and its components. CMS consists of numerical models for waves, flows, and sediment transport and morphology change in coastal areas. This modeling system includes representation of relevant nearshore processes for practical applications of navigation channel performance and sediment management at coastal inlets and adjacent beaches. The development and enhancement of CMS capabilities continues to evolve as a research and engineering tool for desktop computers. CMS uses the SMS interface for grid generation and model setup as well as plotting and post-processing. Additional information about CMS is available (Demirbilek and Rosati 2011; Demirbilek et al. 2007a,b,c; Lin and Demirbilek 2012, 2005; Lin et al. 2011a,b, 2008).

Figure A-1. The CMS framework and its components.
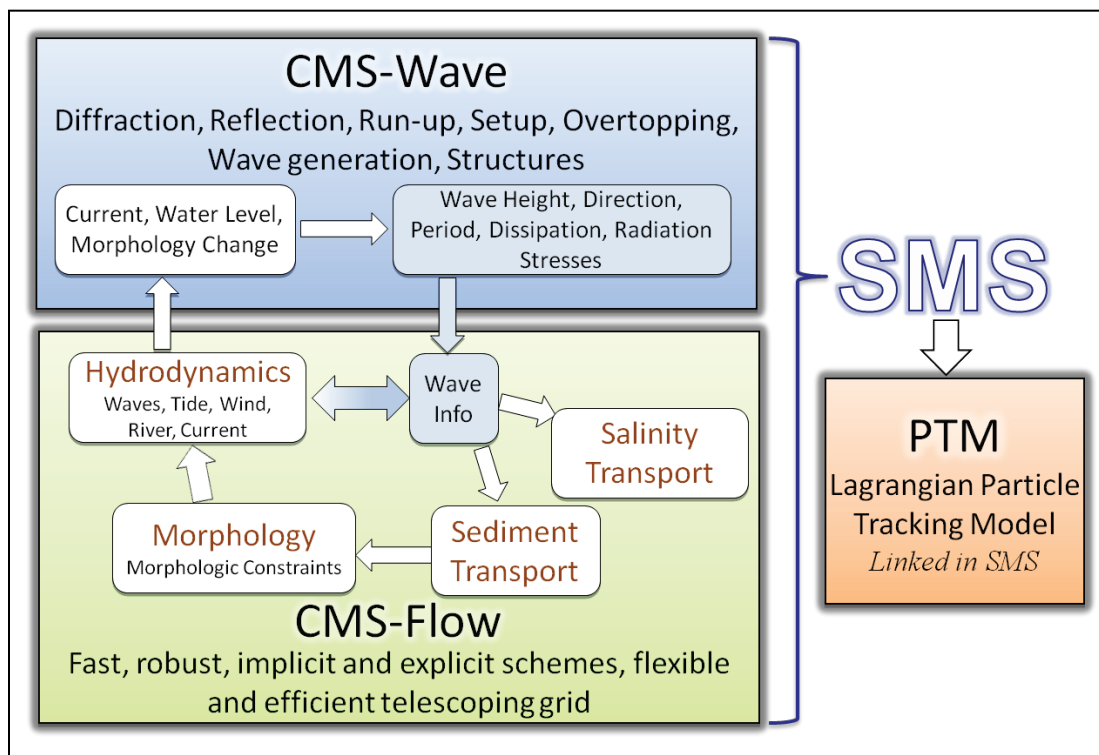
CMS uses the SMS interface for grid generation and model setup, as well as plotting and post-processing. The Verification and Validation (V&V) Report 1 (Demirbilek and Rosati 2011) and Report 2 (Lin et al. 2011) have detailed information about the CMS-Wave features and evaluation of model's performance skills in a variety of applications. Report 3 and Report 4 by Sanchez et al. (2011a and 2011b) describe coupling of wave-flow models and hydrodynamic and sediment transport and morphology change aspects of CMS-Flow. The performance of the CMS for a number of applications is summarized in Report 1, and details are described in the three companion V&V Reports 2, 3, and 4.

The CMS-Wave is a spectral wave model and was used in this study given the large extent of modeling domain over which wave estimates were required. Details of the wind-wave modeling are described in Chapter 3 of this report. The main wave processes included in the CMS-Wave are wind-wave generation and growth, diffraction, reflection, dissipation due to bottom friction, white-capping and breaking, wave-current interaction, wave runup, wave setup, and wave transmission through structures. The height and direction of waves approaching the Buffalo Harbor change due to wave shoaling, refraction, diffraction, reflection, and breaking. Waves propagating toward the breakwaters interact with bathymetry, surrounding land features, and coastal structures. These features affect waves propagating and reaching the protective structures, waves going over these structures and getting into the interior of harbor, which can affect navigation and utilization of harbor.

CMS-Wave model solves the steady-state wave-action balance equation on a non-uniform Cartesian grid to simulate steady-state spectral transformation of directional random waves at and around the breakwaters in Buffalo Harbor. CMS-Wave is designed to simulate wave processes with ambient currents in navigation channels, coastal inlets, and harbors. The model can be used either in half-plane or full-plane mode for spectral wave transformation (Lin et al. 2008; Demirbilek et al. 2007b). The half-plane mode is the default because in this mode CMS-Wave can run more efficiently as waves are transformed primarily from the lakeward boundary toward shore. See Lin et al. (2011, 2008) for features of the model and step-by-step instructions with examples for application of CMS-Wave to a variety of coastal inlets, ports, structures, and other navigation problems. Publications listed in the V&V reports and this report provide additional information about CMS-Wave and its engineering applications. Additional

information about CMS-Wave is available from the CIRP website:
http://cirp.usace.army.mil/wiki/CMS-Wave.

Since the flow model was also used in this study, brief information is provided. The CMS-Flow is a 2D shallow-water wave model for hydrodynamic modeling (calculation of water level and current). The explicit and implicit versions of flow (circulation) model are available to provide estimates of water level and current given the tides, winds, and river flows as boundary conditions. CMS-Flow calculates hydrodynamic (depth-averaged circulation) sediment transport, morphology change, and salinity due to tides, winds, and waves. It was used in this study with CMS-Wave to check water level changes in the harbor caused by winds, waves, and river flows.

The hydrodynamic model solves the conservative form of the shallow-water equations that include terms for the Coriolis force, wind stress, wave stress, bottom stress, vegetation flow drag, bottom friction, wave roller, and turbulent diffusion. Governing equations are solved using the finite volume method on a non-uniform Cartesian grid. Finite-volume methods are a class of discretization schemes, and this formulation is implemented in finite-difference for solving the governing equations of coastal wave, flow, and sediment transport models. See the V&V Reports 3 and 4 by Sanchez et al. (2011a,b) for the preparation of the flow model at coastal inlet applications. Additional information about CMS-Flow is available from the CIRP website: http://cirp.usace.army.mil/wiki/CMS-Flow.

Although hydrodynamic, sediment transport, and morphology change modeling were not considered in this study, it is noted for future reference that there are three sediment transport models available in CMS-Flow: a sediment mass balance model, an equilibrium advection-diffusion model, and a non-equilibrium advection-diffusion model. Depth-averaged salinity transport is simulated with the standard advection-diffusion model and includes evaporation and precipitation. The V&V Reports 1 through 4 describe the integrated wave-flow-sediment transport and morphology change aspects of CMS-Flow. The performance of CMS-Flow is described for a number of applications in the V&V reports.

Appendix B: Description of BOUSS-2D

The Boussinesq wave model BOUSS-2D (abbreviated as B2D) is an advanced modeling approach for nonlinear wave propagation nearshore (Nwogu and Demirbilek 2001). This technology was developed and implemented in the SMS in the 1990s through early 2000 and has since been used by districts and industry for navigation channels, inlets, harbors, coastal structures, moored vessels, floating breakwaters, and wave runup and overtopping on revetments, shorelines, and levees. Recent publications describe different applications of B2D model (Demirbilek et al. 2017, 2016, 2015, 2009, 2008, 2007a,b,c, 2005a,b; Nwogu and Demirbilek 2010, 2008, 2006, 2004; Nwogu 2009, 2007, 2006, 2000, 1996, 1994, 1993a,b). Additional information about B2D is available from these and other related publications in the References section of this report.

B.1 Types of problems for B2D application

The list below shows types of wave problems that can be simulated using Boussinesq wave models:

- harbor/port/marina problems: harbor resonance, harbor and marina infrastructure modifications
- generation of wave sub- and super-harmonics
- wave dissipation over porous media
- wave reflection and diffraction from structures, shorelines, and variable surfaces
- wave-wave interactions in shallow water
- channel deepening/widening/realignment
- wave-structure interactions: levees, flood walls, barriers, revetments, seawalls, groins, and breakwaters design and repair (coastal and inland)

  o wave runup/overtopping
  o structure loading (wave forces)
  o structure freeboard requirements
  o frictional dissipation (i.e., waves on vegetated surfaces)
  o wave interaction with an array of structure types
  o embankment stability
  o wave interaction with complex geometries of levees, navigation channels and canals, ports/harbors, etc.

- inundation mapping: overland propagation and runup
- bore propagation through rivers and canals
- transient waves (tsunamis, sneaker waves)
- vessel-generated waves and ship wakes

  o vessel-generated waves and effect on shorelines
  o vessel-generated bed velocities and shear stresses
  o vessel interactions with other vessels and with locks and dams.

Some images from example applications of B2D are shown at the end of Appendix B.

B.2 Background

The B2D model was used for numerical modeling of waves in Buffalo, NY, to provide design wave estimates for repairs of breakwaters and a seawall. B2D was used in this study for investigation of waves with structures in the harbor, including wave reflection, diffraction, runup, and overtopping. The study plan in Chapter 1 describes the overall purpose of numerical modeling study and tasks. The implementation details for wave modeling are described in Chapters 3 and 4 of this report. Only a brief description of the B2D features is provided here for completeness because details of model's theory, numerical computational schemes, and examples are available from the listed references.

Boussinesq models are essentially shallow-water models with extra dispersive and nonlinear terms and are applicable to both short and long period large and/or long waves in shallow depths. Processes modeled well by Boussinesq models include nearshore wind-wave propagation, harbor resonance, nonlinear shoaling, runup and inundation, nearshore circulation, and tsunamis. Because Navier-Stokes models are not practical for field-scale problems, Boussinesq models presently are the computational tools of choice for calculating runup and overtopping of sloping structures, walls or impulsive forces on structures. Boussinesq models can propagate vessel-generated waves if a source term is added for generation (i.e., moving pressure source or internal boundary). Boussinesq models are much better at this than shallow-water models because they include both short and long waves whereas shallow water wave equations (SWWEs) can only represent the long-wave component of the vessel-induced disturbances.

The B2D computes changes to waves caused by shoaling and refraction over variable bathymetry, reflection and diffraction from shorelines and structures, and nonlinear wave-current and wave-wave interactions. The internal Boussinesq equations defining the B2D do not contain adjustable parameters. Potential errors are introduced in numerical discretization of mathematical equations, imperfect boundary conditions, and physical processes that contain process-specific parameters, such as wave turbulence, dissipation, bottom friction, and boundary reflectivity. The B2D needs field data to calibrate the model parameters as it can simulate processes that cannot be estimated well in physical models (i.e., laboratory experiments) due to scaling effects. In the absence of field data, physical model data if available could be used in B2D for validation and calibration of boundary conditions, material parameters, and numerical algorithms. Generally, errors in the nearshore wave estimates come from two sources: input to the model and the model itself, including errors in the incident wave conditions, bathymetry, and boundary specifications. The largest errors are associated with the specification of incident wave parameters and the simplification of wave breaking, dissipation processes, and contamination from model boundaries.

The B2D provides spatially and temporally varying wave, current, and water level parameter estimates for engineering problems. Estimates include significant wave height, peak period and direction, wave spectrum, time series of surface elevation, velocity and pressure, and wave-induced circulation. B2D model interface is operational in the SMS for grid generation and visualization of model results. The custom-built SMS interface of B2D allows users to set up and run the model in an intuitive manner, with built-in safeguards (Demirbilek et al. 2005a,b). The B2D can be run on PCs, workstations, and super-computers.

The B2D consists of a set of comprehensive numerical modeling systems based on a time-domain solution of Boussinesq-type equations for simulating waves (wind-waves and vessel-generated waves) and their propagation in coastal regions, harbors, and waterways. The B2D represents most of wave phenomena of interest in the nearshore zone for navigation projects, inlets, harbors, levees, structures, reefs, wetlands, ship wakes, wave-ship-bank interactions, and wave-current-structure interactions. The B2D-based engineering analysis systems may be used in navigation infrastructure design with a risk-based probabilistic design approach to evaluate life-cycle cost of alternatives, operation, and maintenance of

coupled systems in deciding the benefit or negative consequences of structures in projects. The B2D has capability of replacing considerably more expensive physical models, with flexibility and generality for extension to sediment transport and morphology change, channel infilling, and water-quality issues. It is expected that the USACE Operation and Maintenance budget for dredging navigation channels and expansion of ports/harbor economic capacity will continue to experience an increasing number of calls for deepening and widening channels and harbors to accommodate future fleets having larger, deeper draft, and faster vessels. Vessel-to-vessel and vessel-to-bank interactions and risk of accidents will also increase with these demands. Aging and natural deterioration of navigation structures increases vessel transit and maneuvering risks along the high-traffic shipping routes, channels, and ports.

Numerical models that solve Boussinesq-type water-wave evolution equations are commonly used to investigate surface wave propagation and transformation in coastal regions. Most of the models use finite difference schemes to discretize the equations over uniformly spaced rectangular grids (Nwogu and Demirbilek 2001). The popularity of finite difference schemes is largely based on their simplicity and ease of implementation. However, the use of structured grids can severely restrict the potential application of such models to complex boundary problems such as coastal flooding over complex topography, wave propagation in curved channels, wave interaction with coastal structures of arbitrary shape, and wave agitation in harbors of arbitrary shape. Because unstructured grids provide users the flexibility of modeling complex geometries and the grid resolution can be refined where needed such as near structures or in shallow regions, it was therefore highly desirable to develop an unstructured-grid version of the finite-difference B2D model used in civil and military works. The development of an unstructured-grid, finite-volume version of B2D has been completed. This new model is being tested on super-computers, and its interface in SMS is under development.

The B2D is designed to simulate wave processes with ambient currents at coastal inlets and in navigation channels. The model can be used for spectral wave transformation. See Lin and Demirbilek (2012) for step-by-step instructions for examples of coupled B2D and CMS-Wave modeling approach to harbor projects and other applications to coastal inlets, ports, structures, and other navigation problems. See Nwogu and Demirbilek (2001), Demirbilek et al. (2005a,b), and other publications listed in the

References section for further information about the B2D and its engineering applications. Additional information about CMS-Wave is also available from these websites: http://cirp.usace.army.mil/wiki/BOUSS-2D and http://www.xmswiki.com/xms/SMS:BOUSS-2D.

In this study, B2D model was used for nearshore wave modeling to investigate estimates of waves at the breakwaters and seawall, including wave runup/overtopping. Details of B2D modeling are described in Chapter 4 of this report.

B.3   Example applications

The images in Figures B-1 through B-10 show some recent examples of B2D model applications. See References for other types of applications.

Figure B-1. BOUSS-2D calculated wave-induced current field for Pillar Point Harbor, California.
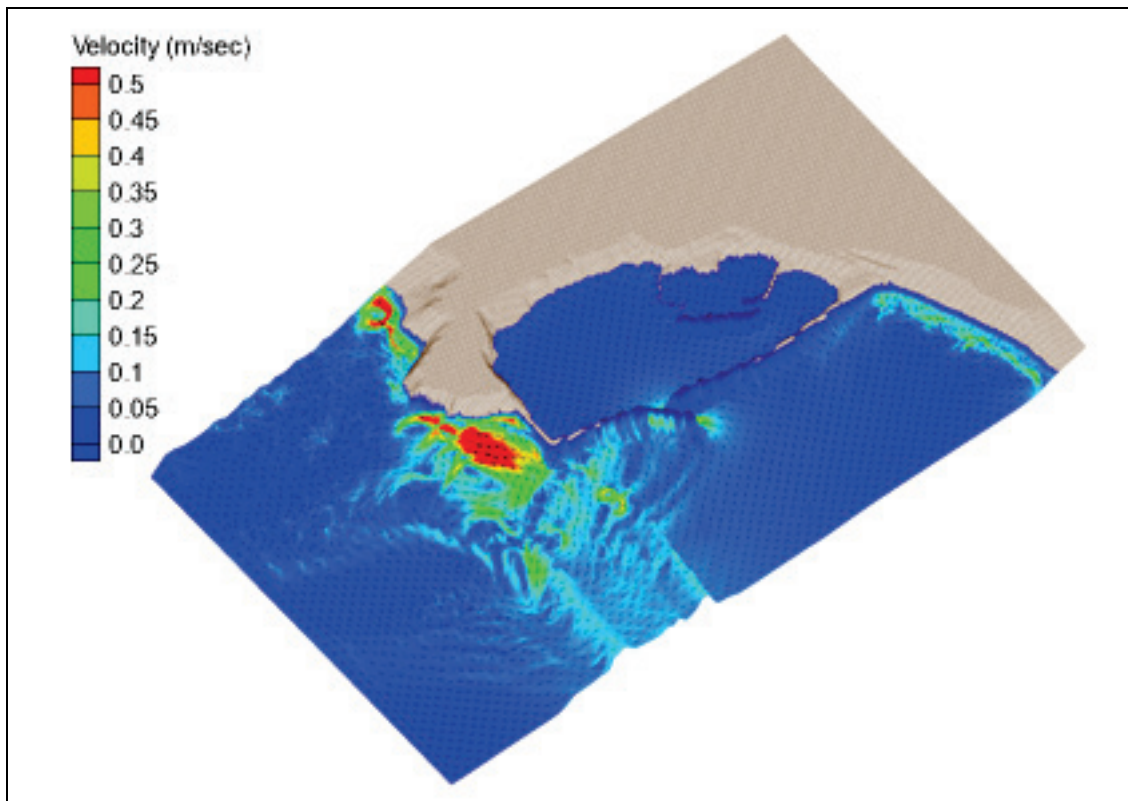
Figure B-2. Calculated wave fields by (a) BOUSS-2D, and (b) CMS-Wave
at Point Judith Harbor, Rhode Island, for incident wave from SSE.
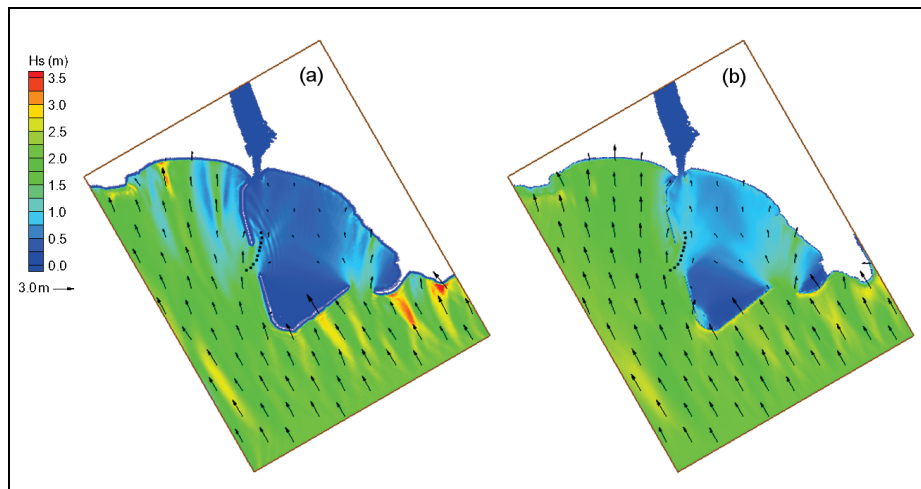
Figure B-3. Wave propagation inside a bay.
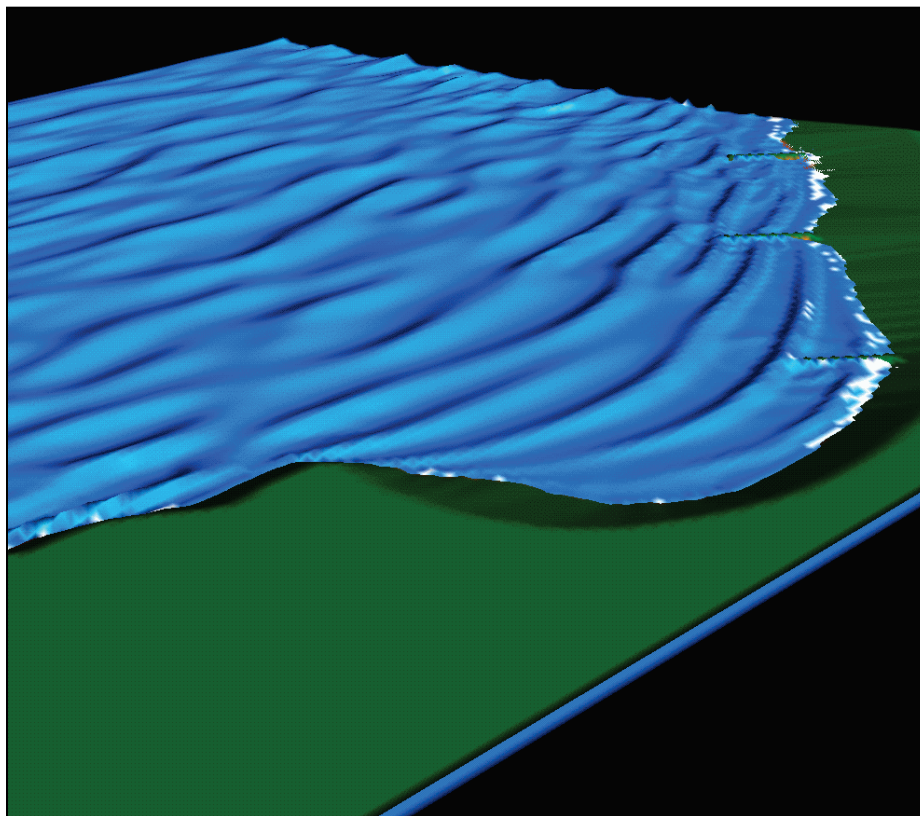
Figure B-4. Wave field around a detached breakwater.
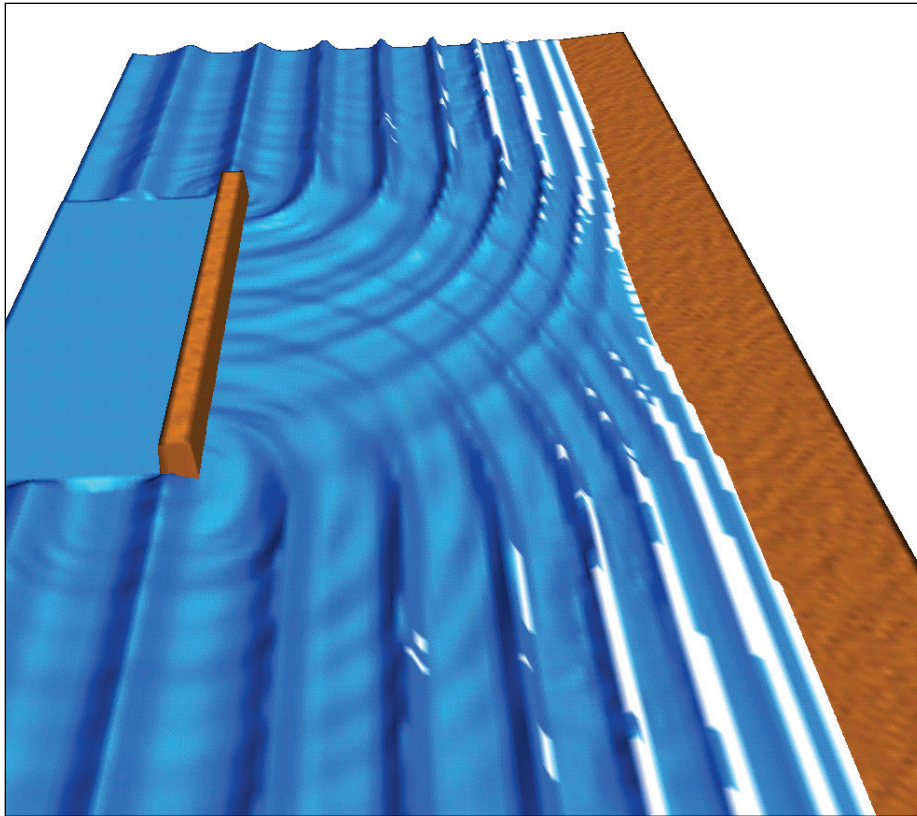
Figure B-5. Waves, wave-induced current, and circulation near a reflective jetty of an inlet.
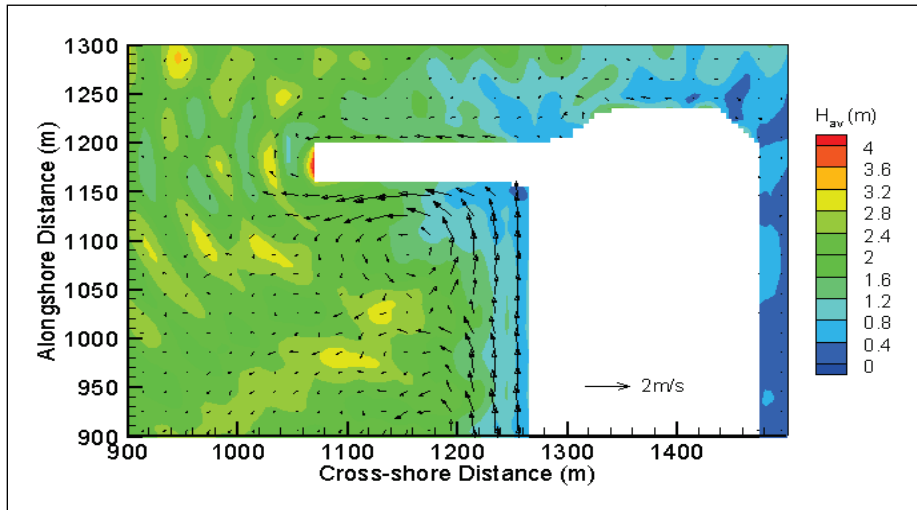
Figure B-6. Wave-induced current field developed between two groins placed on a beach.
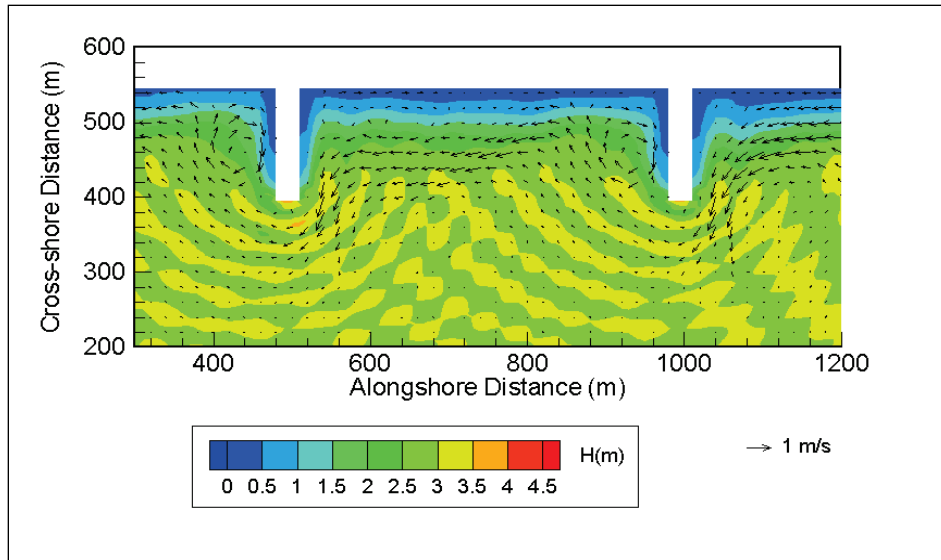
Figure B-7. Multiple ships moving (in transit) in a harbor.
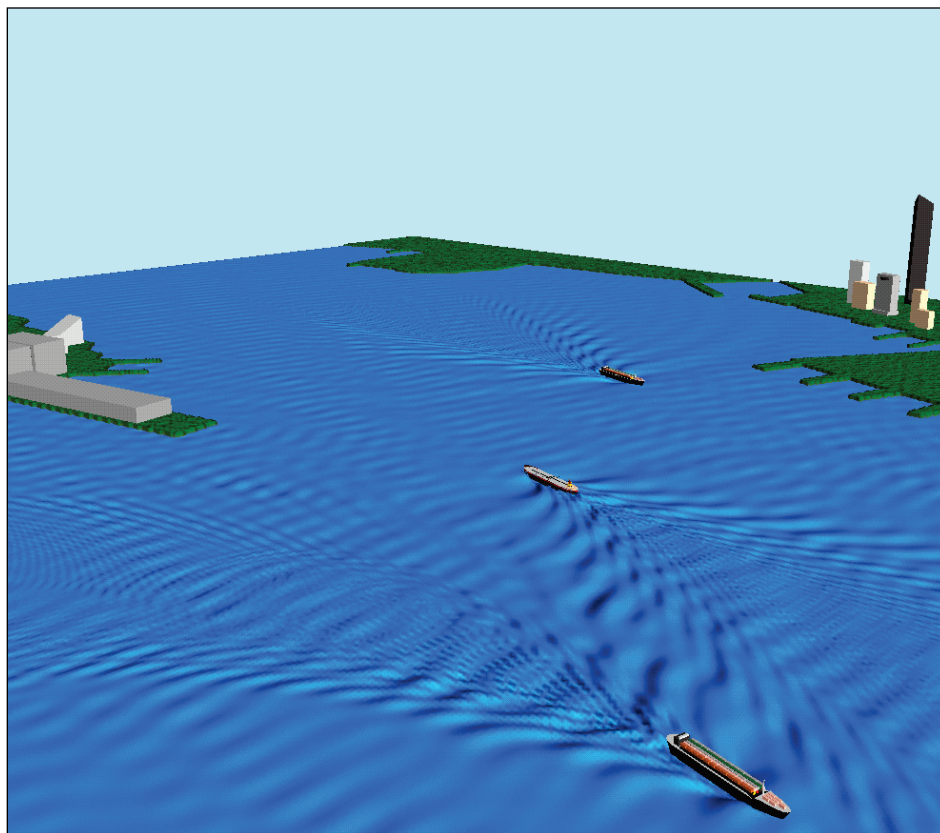
Figure B-8. B2D domain for the Oyster Point Marina, California, entrance and east marina.
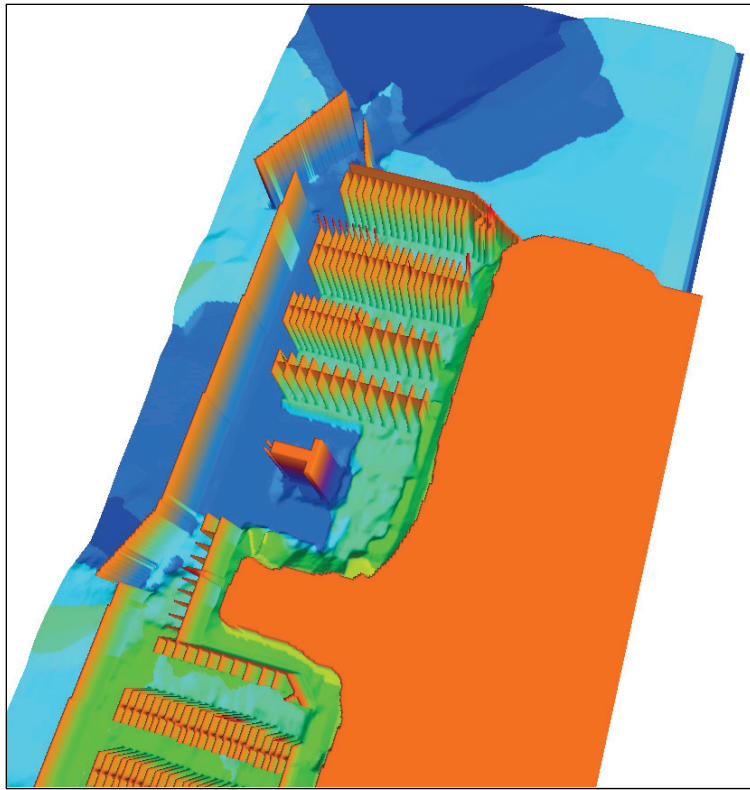
Figure B-9. B2D grid for changes to entrance of Diversey Harbor, Michigan.
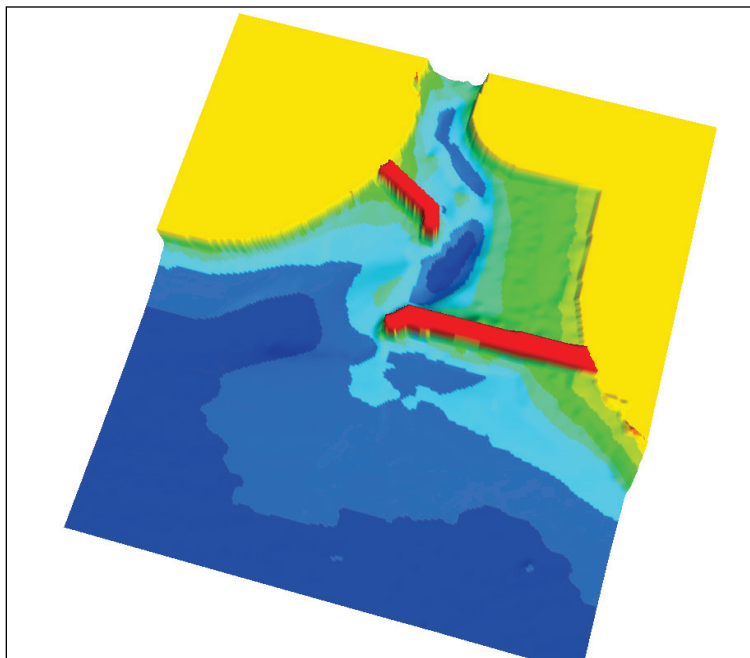
Figure B-10. B2D runup/overtopping toolbox in SMS for a fringing reef application.
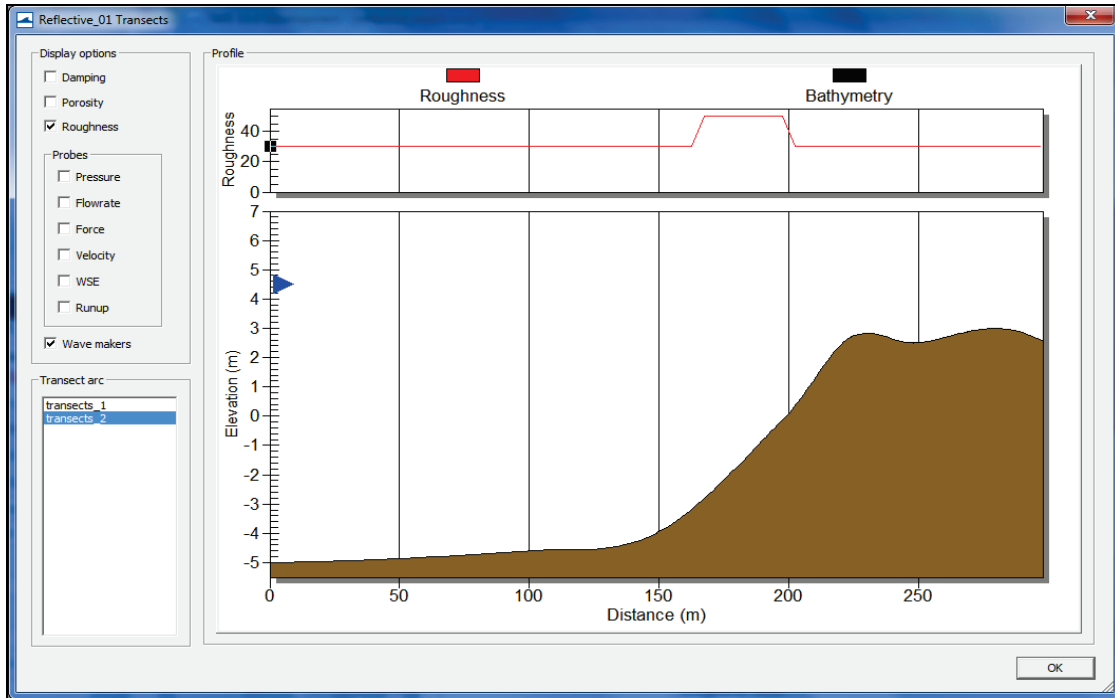
Appendix C: Details of Metocean Data for BH

Chapter 2 provides a summary of data used in this modeling study. This section of the report provides additional information about procedures used by LRB and ERDC in a previous CDF4 study (Demirbilek et al. 2017) for developing meteorological and oceanographic (metocean) data for this numerical modeling study. The purpose of Appendix C is to provide additional information about the sources of metocean data and types of analyses used in the CDF4, which are also used in the present study. For details, the CDF4 study report should be consulted for future studies in Buffalo and other areas in Lake Erie.

C.1 Storm data for modeling

In Chapter 2 of the CDF4 study report and present report, three storms were selected for modeling waves in Buffalo, NY. These included one hypothetical storm representing the 2-year wave and 2-year water level (Storm Condition 1), one hypothetical design storm representing the 20-year wave and 10-year water level (Storm Condition 2), and one actual storm (Storm Condition 3). The methodology and data used to identify, create, and assemble these three storms' data follow. For each storm, hourly data of the deepwater wave height, wave period, and wave direction, the wind speed and wind direction, and the water level are described.

C.1.1 Data sources

The wave and wind data offshore of the site are available from two sources. The WIS hourly wave hindcast conditions are available at 243 locations within Lake Erie for the 34-year period (1979–2012). The GLCFS provides hourly forecast wave data at user-selected locations in Lake Erie for the period of 2006 to present. As the WIS information spans a longer time period, which is more applicable for statistical analysis, the data from the WIS (Station 92243 - Figure C-1) will be used. Water elevation data at select U.S. locations on Lake Erie have been collected for over a century. Hourly water elevation data for Lake Erie near Buffalo are available from January 1960 to present.

C.1.2 WIS data

This section describes development of wave data for the hypothetical 2-year design storm (2-year wave and 2-year water level, Storm Condition 1), a

hypothetical 20-year design storm (20-year wave and 10-year water level, Storm Condition 2), and an actual storm (Storm Condition 3). The three angle classes are defined as viewed by an observer on shore. Class Angle 1 represents the mean wave approach angle greater than 30 deg to the right of the normal from shore. Class Angle 2 represents the mean wave approach angle within 30 deg to either side of the normal from shore. Class Angle 3 represents the mean wave approach angle greater than 30 deg to the left of the normal from shore. Due to the limited fetch distance for Class Angle 1 and 3, these will not be considered. Class Angle 2 waves encompass angles between 219 deg and 279 deg (Figure C-2). Table C-1 provides a list of storms during 1979–2012 with wave heights greater than 4 m (13.1 ft).

Figure C-1. Location of WIS Station 92243 (42.80º N, -78.96º W).

Figure C-2. Definition of Class Angle 2 wave directions.
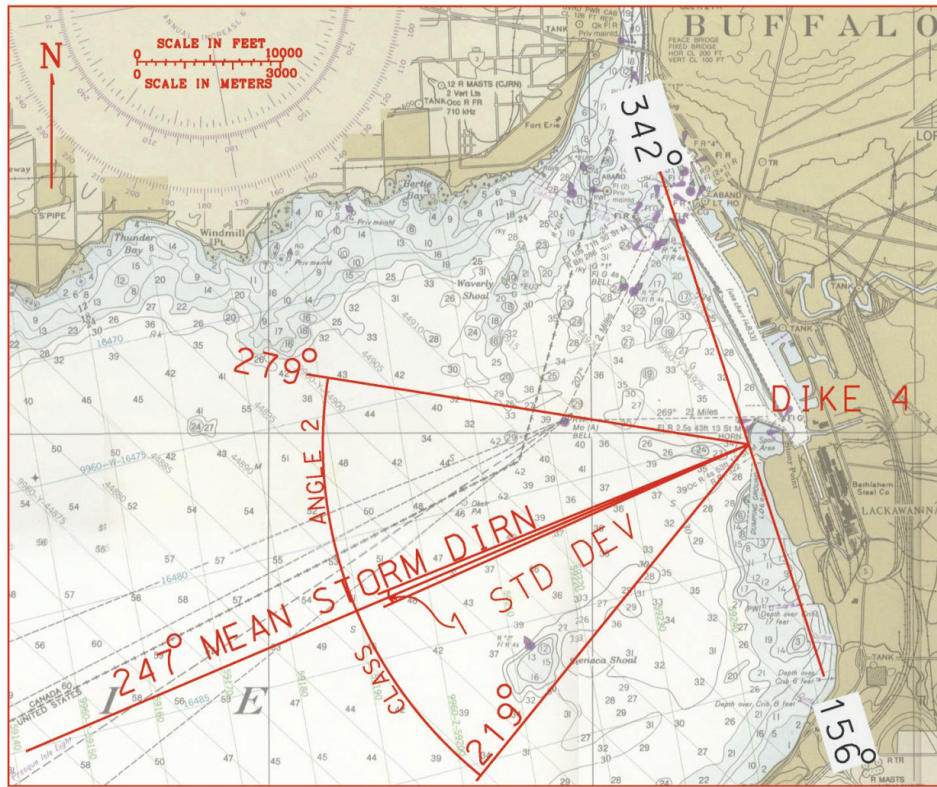
Table C-1. Storm list for wave heights greater than 4 m (13.1 ft) (1979–2012).

Rank	Start Date	Start Time	End Date	End Time	Peak Date	Peak Time	Peak Value H_{mo} (m)	T_P (sec)	Direction (deg)
1	2/24/2012	19:00	2/26/2012	7:00	2/25/2012	1:00	4.85	9.73	249
2	1/17/2012	17:00	1/18/2012	16:00	1/18/2012	1:00	4.73	9.23	248
3	2/1/2002	15:00	2/2/2002	6:00	2/1/2002	20:00	4.72	10.13	247
4	3/3/2012	4:00	3/4/2012	18:00	3/3/2012	13:00	4.68	10.02	247
5	1/28/2012	14:00	1/30/2012	17:00	1/28/2012	22:00	4.68	9.35	248
6	12/1/2006	20:00	12/3/2006	0:00	12/2/2006	3:00	4.59	10.25	247
7	1/1/2012	16:00	1/3/2012	5:00	1/2/2012	3:00	4.57	10.04	247
8	12/27/2008	15:00	12/29/2008	7:00	12/28/2008	19:00	4.48	10.03	248
9	10/14/2011	16:00	10/18/2011	10:00	10/15/2011	21:00	4.37	10.15	248
10	1/10/1982	15:00	1/12/1982	6:00	1/11/1982	12:00	4.37	10.17	247
11	12/1/1985	20:00	12/3/1985	13:00	12/2/1985	13:00	4.36	10.03	247
12	11/13/2003	3:00	11/14/2003	10:00	11/13/2003	14:00	4.33	10.92	247
13	1/4/1982	12:00	1/5/1982	21:00	1/5/1982	3:00	4.3	10.84	246
14	12/9/2009	14:00	12/12/2009	12:00	12/10/2009	5:00	4.29	10.78	246

Rank	Start Date	Start Time	End Date	End Time	Peak Date	Peak Time	Peak Value H$_{mo}$ (m)	T$_P$ (sec)	Direction (deg)
15	12/15/1987	14:00	12/17/1987	6:00	12/16/1987	8:00	4.27	10.97	246
16	12/17/2000	15:00	12/18/2000	20:00	12/18/2000	3:00	4.22	9.98	247
17	11/6/1990	3:00	11/6/1990	23:00	11/6/1990	11:00	4.15	10.42	247
18	4/28/2011	11:00	4/29/2011	3:00	4/28/2011	16:00	4.11	9.19	246
19	1/9/2008	5:00	1/10/2008	5:00	1/9/2008	13:00	4.11	8.48	249
20	2/5/2006	7:00	2/7/2006	12:00	2/5/2006	14:00	4.1	9.63	246
21	1/8/1989	4:00	1/9/1989	23:00	1/8/1989	20:00	4.06	9.73	248
22	1/13/2012	8:00	1/14/2012	11:00	1/13/2012	15:00	4.01	9.2	247

C.1.3 Wave height-recurrence interval

The significant wave height recurrence interval (return period) information for the Class Angle 2 was developed by sorting and ranking all storms for the period of record over 1 m (3.28 ft) (Figure C-3).

Figure C-3. Wave height vs. return period.
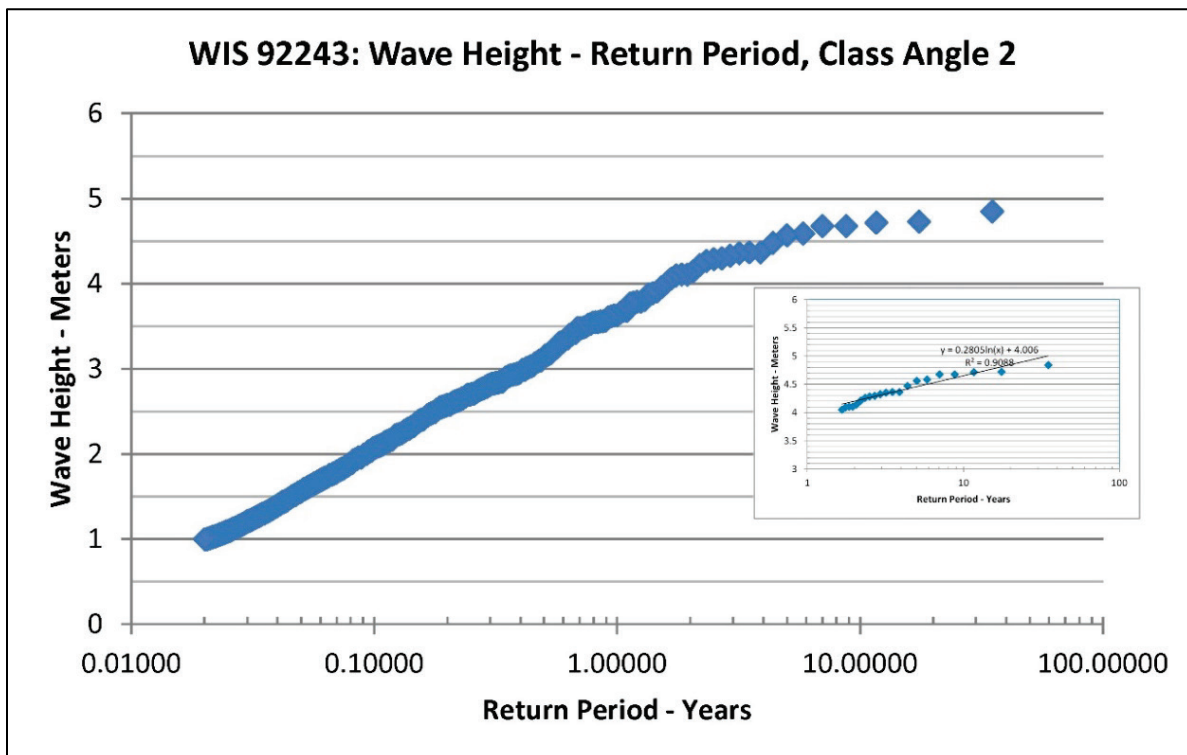
The best-fit curve for the waves above 4 m (13.1 ft) is defined as

$$H_{mo} = 0.2805 \ln(RI) + 4.006$$

where H_{mo} = wave height at WIS Station 92243 in meters and RI = "Recurrence Interval" or "Return Period" of wave in years.

C.1.4 Wave period

The corresponding wave period was identified by plotting all storm wave heights (H_{mo} > 1 m) and wave periods within the Class Angle 2 (Figure C-4). The best-fit curve to data is given by

$$T_p = -0.1407 H_{mo}^2 + 2.193 H_{mo} + 3.0877$$

Figure C-4. Wave period vs. wave height relation.
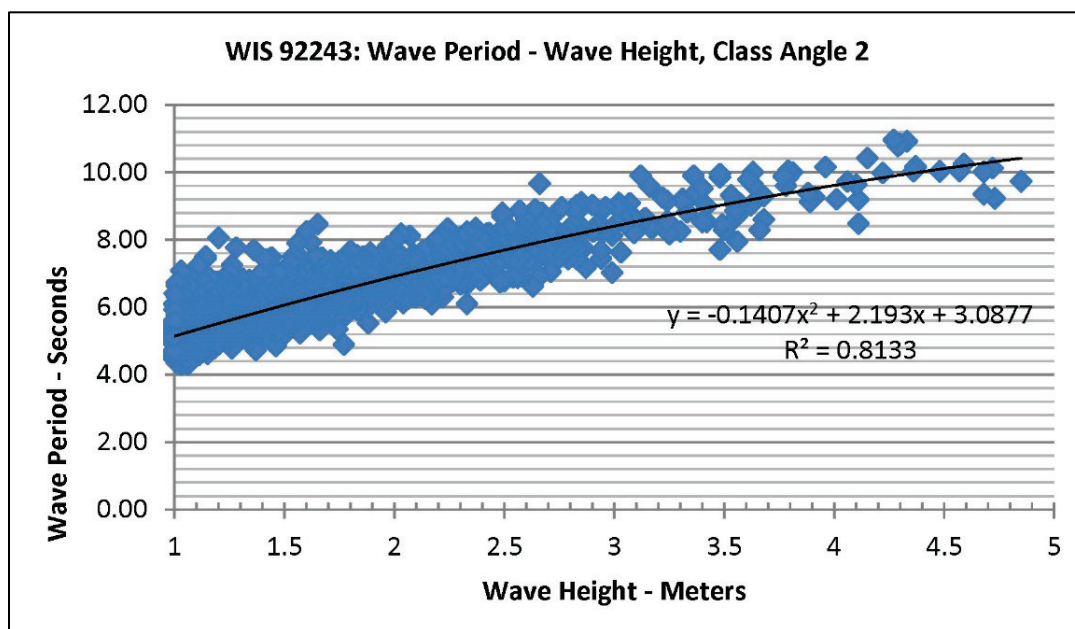
C.1.5 Wave direction distribution

The descriptive statistics for the direction of all peak storm waves greater than 4 m (13.1 ft), 3 m (9.8 ft), and 2 m (6.6 ft) were determined and presented in Table C-2. It was found that the mean wave direction for all major storms (greater than 4 m [13.1 ft]) approached from 247 deg azimuth with a standard deviation of approximately 1 deg (Figure C-2).

Table C-2. Descriptive statistics for storm wave direction.

Descriptive Statistic	Wave Direction - Degrees		
	Waves above 4 m	Waves above 3 m	Waves above 2 m
Mean	247.2	247.4	246.2
Standard error	0.193	0.131	0.689
Median	247	247	248
Mode	247	247	248
Standard deviation	0.907	1.190	13.617
Sample variance	0.823	1.416	185.413
Kurtosis	-0.308	0.211	234.494
Skewness	0.453	0.576	-13.883
Range	3	6	262
Minimum	246	245	10
Maximum	249	251	272
Sum	5438	20535	96283
Count	22	83	391

C.2 Data for the 2-year and 20-year storms

Table C-3 lists the wave recurrence interval information for the Class Angle 2 for the WIS station data.

Table C-3. Class Angle 2 recurrence interval for WIS Sta-92243.

RI - Years	H_{mo} M	T_P Sec
1	3.6	9.2
2	4.2	9.8
5	4.5	10.1
10	4.7	10.2
20	4.8	10.4
50	5.1	10.6

C.2.1 Storm selection

Three storms were used to create the typical storm pattern hydrographs for the 2-year and the 20-year waves based upon the events listed in Table C-1, which had peak wave height values close to those in Table C-3. For the actual storm, an event was selected from the storm list (Table C-1) that was not used in creating the synthetic storms, was relatively frequent

(3–5 years) and had a similar water level recurrence interval. The water level-frequency will be discussed subsequently.

For the 2-year storm, three storms from Table C-1 had a wave height vs. return period near 2 years. These include storms on 18 December 2000, 6 November 1990, and 28 April 2011. Three storms with the wave height-return period for the 20-year storms occurred on 25 December 2013, 18 January 2012, and 1 February 2002. Four storms were considered for the actual storm, which had a wave height recurrence interval between 3 to 5 years. These were storms on 15 October 2011 (3.5-year wave, ~1-year water level), 11 January 1982 (3.5-year wave, ~3-year water level), 2 December 1985 (3.2-year wave, water level highest for period of record), and 11 November 2003 (2.9-year wave, ~ 1-year water level). The 11 January 1982 storm was selected as the water level associated with this event demonstrated a peak elevation with a similar recurrence interval.

C.2.2 Wave height, period and direction data

Wave Height. The wave height hydrograph for the 2-year and the 20-year synthetic storms were created by plotting the three storms, adjusting the timing so all peaks align at same time, averaging the three storm wave heights, and then finally adjusting all wave heights based on ratio of average wave height at peak and the determined wave height for the 2-year or 20-year storm. Figures C-5 and C-6 present the three storms used to create the pattern hydrographs for the 2-year and 20-year wave, respectively. Figure C-13 to Figure C-15 present the wave height hydrographs for the 2-year wave and 2-year water level event, the 20-year wave and 10-year water level event, and the 11 January 1982 storm, respectively.

Figure C-5. Three storms used for 2-year wave height hydrograph (peaks aligned).

Three storms used for pattern storm
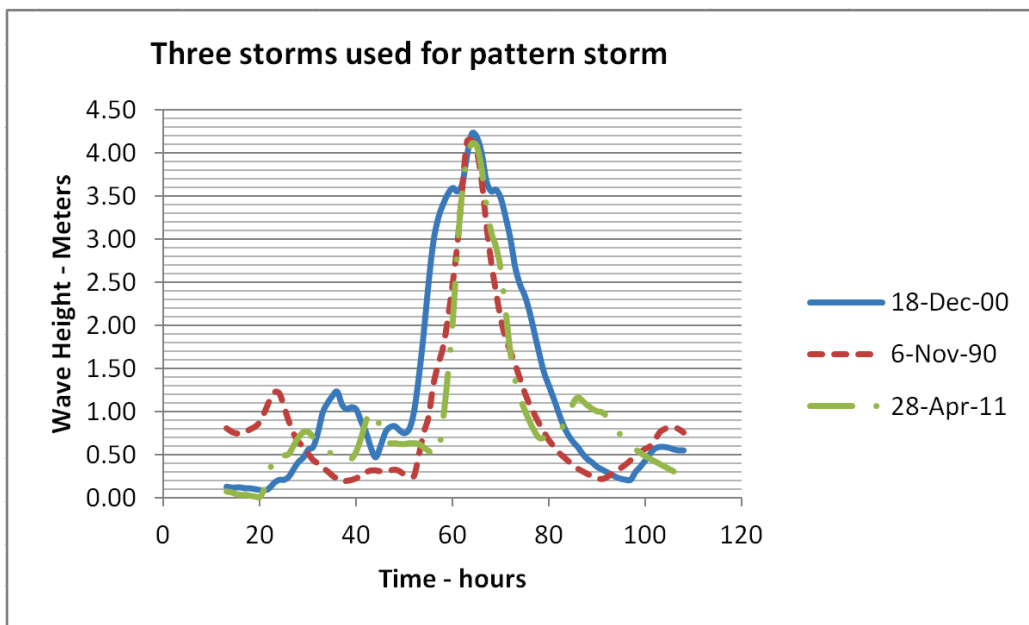
Figure C-6. Three storms used for 20-year wave height hydrograph (peaks aligned).

Three storms used for pattern storm
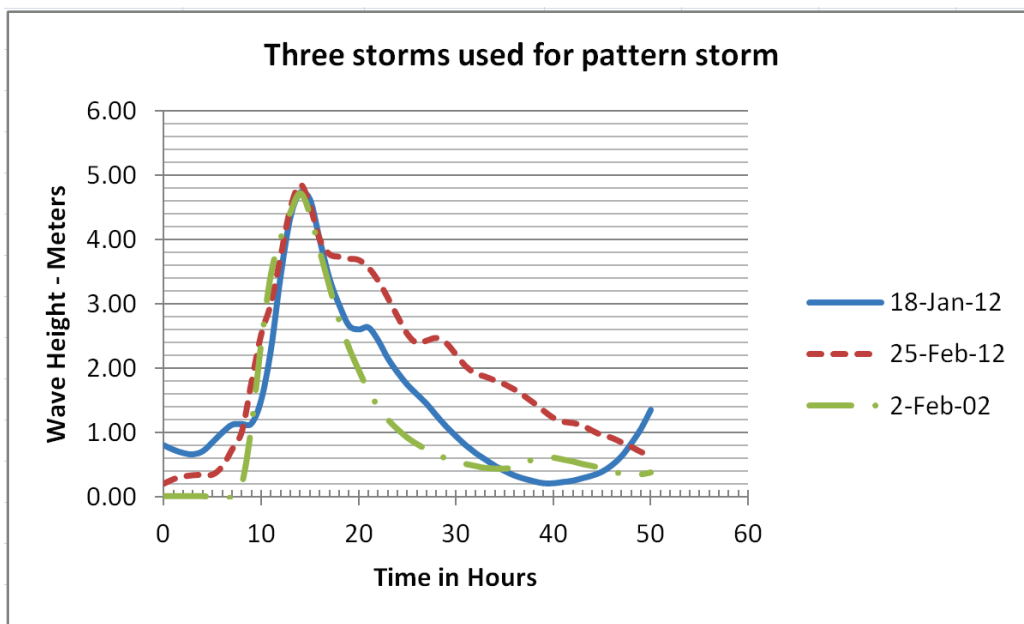
Wave Period. To develop the wave period pattern hydrograph, the three storms were plotted, the timing was adjusted as was done for the wave heights, the three storm wave period graphs were averaged, and the period adjusted by the ratio of the average wave period that occurs at the time of the peak wave height to the determined wave period for that frequency storm as presented in Table C-3. Note that the highest wave period did not occur at the same time as the highest wave, but usually afterwards (1–2 hr).

Figure C-7 and Figure C-8 present the three storms used to create the pattern hydrographs for the 2-year and 20-year wave, respectively. Figures C-13 to C-15 present the wave period graphs for the 2-year wave and 2-year water level event, the 20-year wave and 10-year water level event, and the 11 January 1982 storm, respectively.

Figure C-7. Three storms used for 2-year wave period hydrograph (peaks aligned).
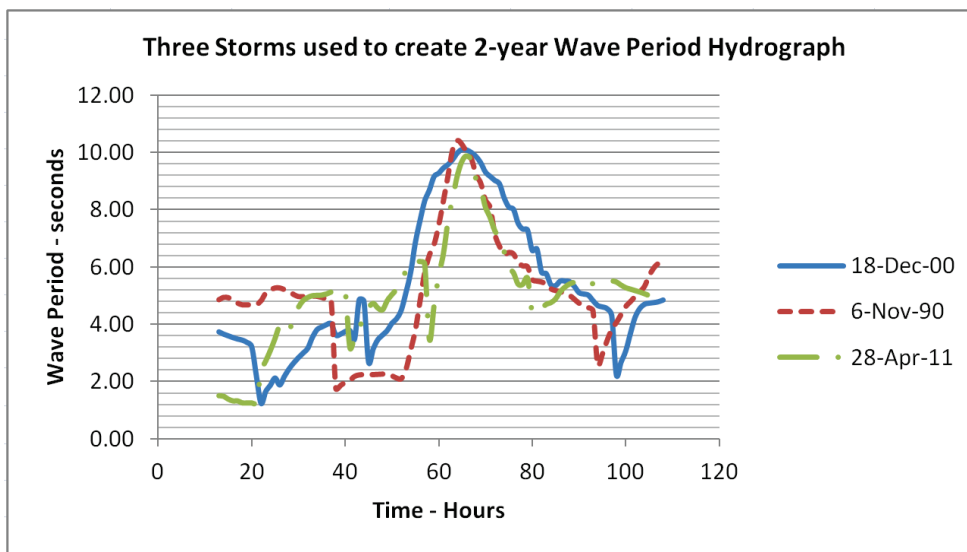
Figure C-8. Three storms used for 20-year wave period hydrograph (peaks aligned).
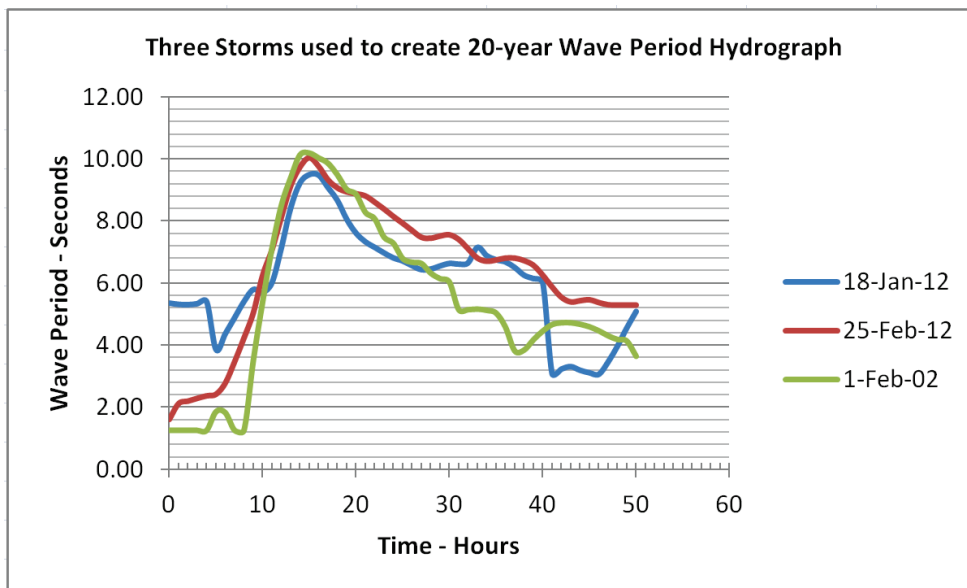
Direction. A constant wave direction of 247 deg was used for the synthetic storms based upon the descriptive statistics presented in Table C-2, and the actual values were used for the 11 January 1982 storm.

C.2.3 Wind speed

Some of the factors that affect the generation of waves are the wind speed, wind duration, fetch, water depth, bed roughness, water temperature, and air temperature. While the actual wind speed will be used for the *actual storm* modeled, a simple relation was created to select the wind speed corresponding with the waves for the synthetic storms. Using the WIS hourly data, waves from 247 deg were plotted with the accompanying wind speed. The following best-fit equation was developed and was used to generate a wind speed hydrograph to accompany the synthetic storms:

$$Wind\ Speed\ =\ 4.2957 H_{mo}\ +\ 2.5385$$

Figure C-14 illustrates the adopted wave height-wind speed relation. Figures C-13 to C-15 present the wind speed graphs for the 2-year wave and 2-year water level event, the 20-year wave and 10-year water level event, and the 11 January 1982 storm, respectively.

Figure C-9. Wave height vs.wind speed at constant wind direction of 247 deg.
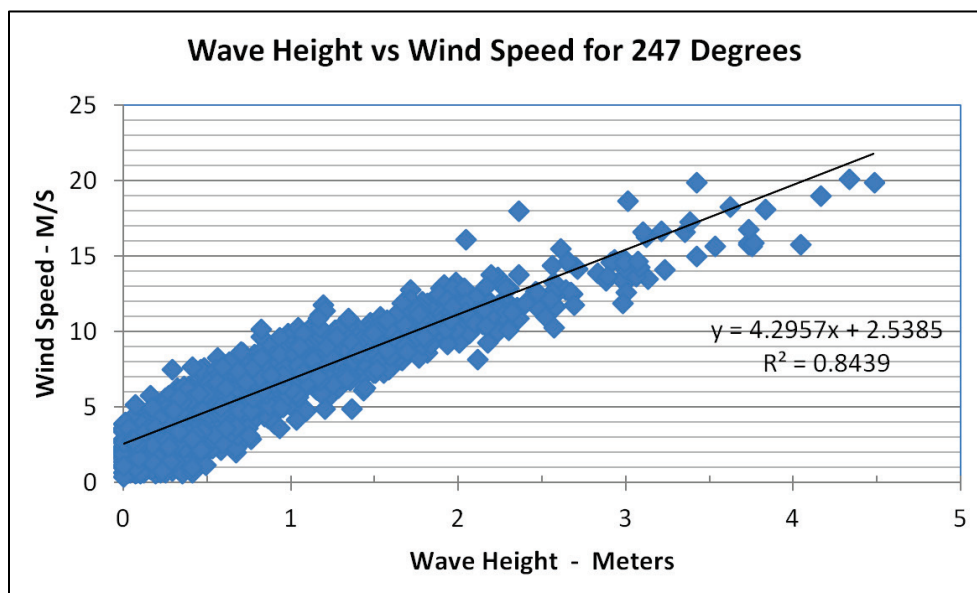
C.2.4 Wind direction

A constant wind direction of 247 deg was used for the synthetic storms (same as used for the wave direction), and the actual values were used for the 11 January 1982 storm.

C.2.5 Water level

NOAA Station 9063020 (42º-52.6'N and 78º-53.4'W) located on the south side of the Buffalo River, near the upriver end of the U.S. Coast Guard base, had collected hourly water level data since 1960. Annual maximum and minimum water levels are available in digital form since 1900. The lake level recurrence interval (return period) information was developed by sorting and ranking all annual maximum water levels for the period of record of 1900–2014 (Figure C-10). The 2-year, 10-year, 20-year, and 50-year lake levels are listed in Table C-4.

Table C-4. Return period for lake level.

Return Period - Years	Water Level – M IGLD 1985
2	175.80
10	176.45
20	176.56
50	176.74

Figure C-10. Lake Erie water elevation at Buffalo, NY (return period relation).
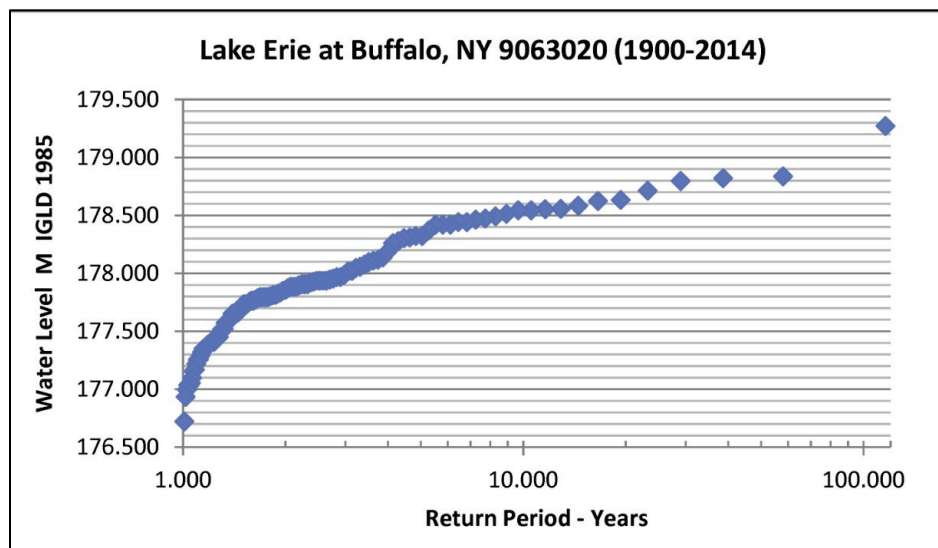
C.2.6 Storm hydrographs

Three storms were used to create the typical storm pattern hydrograph for the 2-year and the 10-year water levels based upon events that had peak water elevation values close to those in Table C-4. As discussed previously, the actual storm used will be the 11 January 1982 event.

Three storms that had a water level-return period near 2 years were 13 November 2003, 7 October 2009, and 25 December 2014. Three storms that had a wave height-return period near 10-years were 1 December 2006, 10 March 2002, and 12 December 2000. The water level hydrographs for the 2-year and the 10-year synthetic events were created by plotting the three storms, adjusting the timing so all peaks align at same time, averaging the three storm water levels, and then finally adjusting all water levels based on ratio of average water elevation at peak and the determined water elevation for the 2-year or 10-year event. Figures C-11 and C-12 present the three storms used to create the pattern hydrographs for the 2-year and 10-year water level, respectively. Figures C-13 to C-15 present the water level graphs for the 2-year wave and 2-year water level event, the 20-year wave and 10-year water level event, and the 11 January 1982 storm, respectively.

Figure C-11. Three storms used to create the 2-year water level hydrograph.
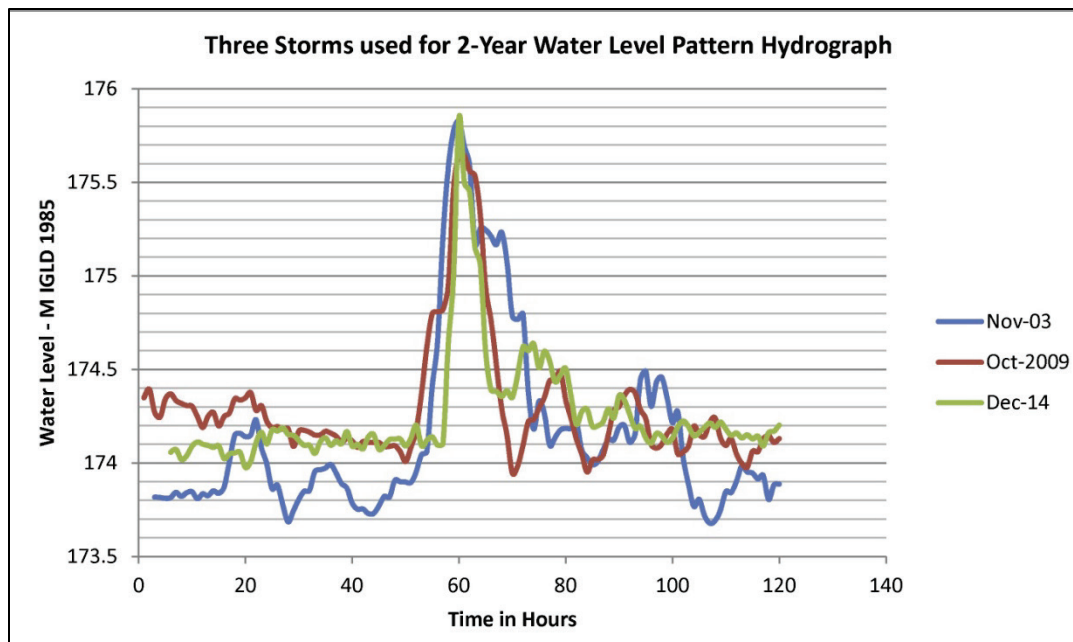
Figure C-12. Three storms used to create the 10-year water level hydrograph.
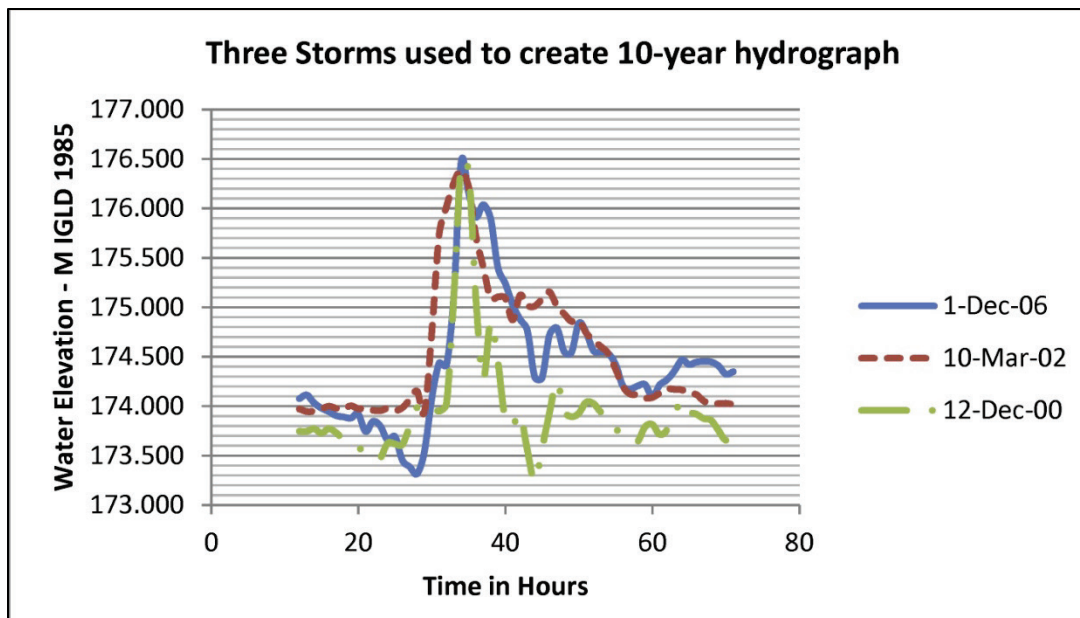
In the creation of the design storm hydrographs, it was assumed that the peak of the waves occurs coincident with the peak of the water level.

C.2.7 Storm summary

Three storms will be modeled representing (a) 2-year wave and 2-year water level, (b) 20-year wave and 10-year water level, and (c) the 11 January 2008 event. Tables C-5, C-6, and C-7 and Figures C-13, C-14, and C-15 provide hourly data of wave height, wave period, wave direction, wind speed, wind direction, and water level for each storm, respectively.

Table C-5. Hourly data for 2-year wave and 2-year water level storm.

Time - Hours	H_{mo} - M	T_P - Sec	Wave Direction Degrees Azimuth	Wind Speed - m/s	Wind Direction Degrees Azimuth	Water Level M IGLD 1985
0	0.55	3.73	247	4.4	247	174.02
1	0.57	3.82	247	4.4	247	174.03
2	0.64	4.01	247	4.8	247	174.06
3	0.86	4.44	247	5.7	247	174.05
4	1.10	4.99	247	6.8	247	174.02
5	1.34	5.58	247	7.8	247	174.06
6	1.61	6.16	247	8.9	247	174.13
7	1.78	6.70	247	9.6	247	174.19

Time - Hours	Hmo - M	Tₚ - Sec	Wave Direction Degrees Azimuth	Wind Speed - m/s	Wind Direction Degrees Azimuth	Water Level M IGLD 1985
8	2.04	6.15	247	10.6	247	174.29
9	2.37	6.81	247	11.9	247	174.47
10	2.73	7.43	247	13.3	247	174.54
11	3.17	8.02	247	14.9	247	174.73
12	3.63	8.74	247	16.5	247	175.07
13	4.06	9.36	247	17.9	247	175.44
14	4.20	9.80	247	18.4	247	175.80
15	4.14	9.96	247	18.2	247	175.63
16	3.87	9.93	247	17.3	247	175.55
17	3.45	9.77	247	15.9	247	175.31
18	3.15	9.32	247	14.8	247	175.23
19	2.99	9.04	247	14.2	247	174.95
20	2.76	8.52	247	13.4	247	174.81
21	2.44	8.27	247	12.2	247	174.71
22	2.15	7.77	247	11.1	247	174.65
23	1.88	7.49	247	10.0	247	174.56
24	1.69	7.09	247	9.2	247	174.38
25	1.54	6.82	247	8.6	247	174.43
26	1.38	6.71	247	7.9	247	174.52
27	1.23	6.32	247	7.3	247	174.42
28	1.08	6.21	247	6.7	247	174.37
29	0.98	6.26	247	6.2	247	174.40
30	0.93	5.49	247	6.0	247	174.42
31	0.85	5.48	247	5.7	247	174.38
32	0.78	5.25	247	5.4	247	174.36
33	0.72	5.25	247	5.1	247	174.40
34	0.70	5.09	247	5.0	247	174.36
35	0.71	5.11	247	5.1	247	174.28
36	0.70	5.23	247	5.0	247	174.20
37	0.65	5.26	247	4.8	247	174.15
38	0.61	5.27	247	4.6	247	174.11
39	0.57	5.19	247	4.4	247	174.09
40	0.54	5.05	247	4.3	247	174.10
41	0.52	4.97	247	4.2	247	174.13

Time - Hours	H$_{mo}$ - M	T$_P$ - Sec	Wave Direction Degrees Azimuth	Wind Speed - m/s	Wind Direction Degrees Azimuth	Water Level M IGLD 1985
42	0.50	4.94	247	4.1	247	174.21
43	0.47	4.88	247	4.0	247	174.23
44	0.45	4.22	247	3.9	247	174.30
45	0.43	4.33	247	3.8	247	174.32
46	0.42	4.47	247	3.8	247	174.27
47	0.42	4.52	247	3.8	247	174.26
48	0.45	3.90	247	3.9	247	174.33
49	0.47	4.10	247	4.0	247	174.31
50	0.50	4.29	247	4.1	247	174.19

Table C-6. Hourly data for 20-year wave and 10-year water level storm.

Time - Hours	H$_{mo}$ - M	T$_P$ - Sec	Wave Direction Degrees Azimuth	Wind Speed - m/s	Wind Direction Degrees Azimuth	Water Level M IGLD 1985
0	0.34	2.94	247	3.4	247	173.84
1	0.34	3.10	247	3.4	247	173.77
2	0.34	3.13	247	3.4	247	173.77
3	0.34	3.17	247	3.4	247	173.75
4	0.36	3.23	247	3.5	247	173.77
5	0.40	2.91	247	3.7	247	173.77
6	0.50	3.21	247	4.1	247	173.69
7	0.62	3.43	247	4.7	247	173.76
8	0.79	3.89	247	5.4	247	173.83
9	1.36	5.12	247	7.9	247	173.85
10	2.16	6.20	247	11.1	247	174.29
11	2.95	7.22	247	14.1	247	174.72
12	3.77	8.48	247	17.0	247	174.83
13	4.45	9.63	247	19.2	247	175.51
14	4.80	10.40	247	20.2	247	176.45
15	4.54	10.63	247	19.4	247	176.27
16	3.96	10.45	247	17.6	247	175.58
17	3.50	10.10	247	16.0	247	175.25
18	3.17	9.72	247	14.9	247	175.29
19	2.91	9.30	247	13.9	247	174.99

Time - Hours	H$_{mo}$ - M	T$_P$ - Sec	Wave Direction Degrees Azimuth	Wind Speed - m/s	Wind Direction Degrees Azimuth	Water Level M IGLD 1985
20	2.77	9.06	247	13.4	247	174.74
21	2.63	8.73	247	12.9	247	174.58
22	2.41	8.51	247	12.1	247	174.65
23	2.16	8.16	247	11.1	247	174.46
24	1.94	7.94	247	10.2	247	174.19
25	1.74	7.66	247	9.4	247	174.33
26	1.61	7.47	247	8.9	247	174.61
27	1.54	7.33	247	8.6	247	174.70
28	1.47	7.23	247	8.3	247	174.49
29	1.37	7.22	247	7.9	247	174.44
30	1.24	7.23	247	7.4	247	174.56
31	1.12	6.84	247	6.8	247	174.52
32	1.03	6.75	247	6.5	247	174.43
33	0.97	6.83	247	6.2	247	174.37
34	0.92	6.68	247	6.0	247	174.33
35	0.87	6.62	247	5.8	247	174.20
36	0.83	6.45	247	5.6	247	174.04
37	0.80	6.11	247	5.5	247	173.99
38	0.77	6.00	247	5.3	247	174.00
39	0.72	6.04	247	5.1	247	174.04
40	0.69	5.97	247	5.0	247	174.01
41	0.66	4.86	247	4.8	247	174.03
42	0.65	4.81	247	4.8	247	174.08
43	0.64	4.79	247	4.8	247	174.16
44	0.62	4.75	247	4.7	247	174.24
45	0.60	4.70	247	4.6	247	174.18
46	0.61	4.60	247	4.6	247	174.17
47	0.62	4.66	247	4.7	247	174.14
48	0.65	4.80	247	4.8	247	174.12
49	0.71	5.00	247	5.1	247	174.07
50	0.80	5.01	247	5.5	247	174.01

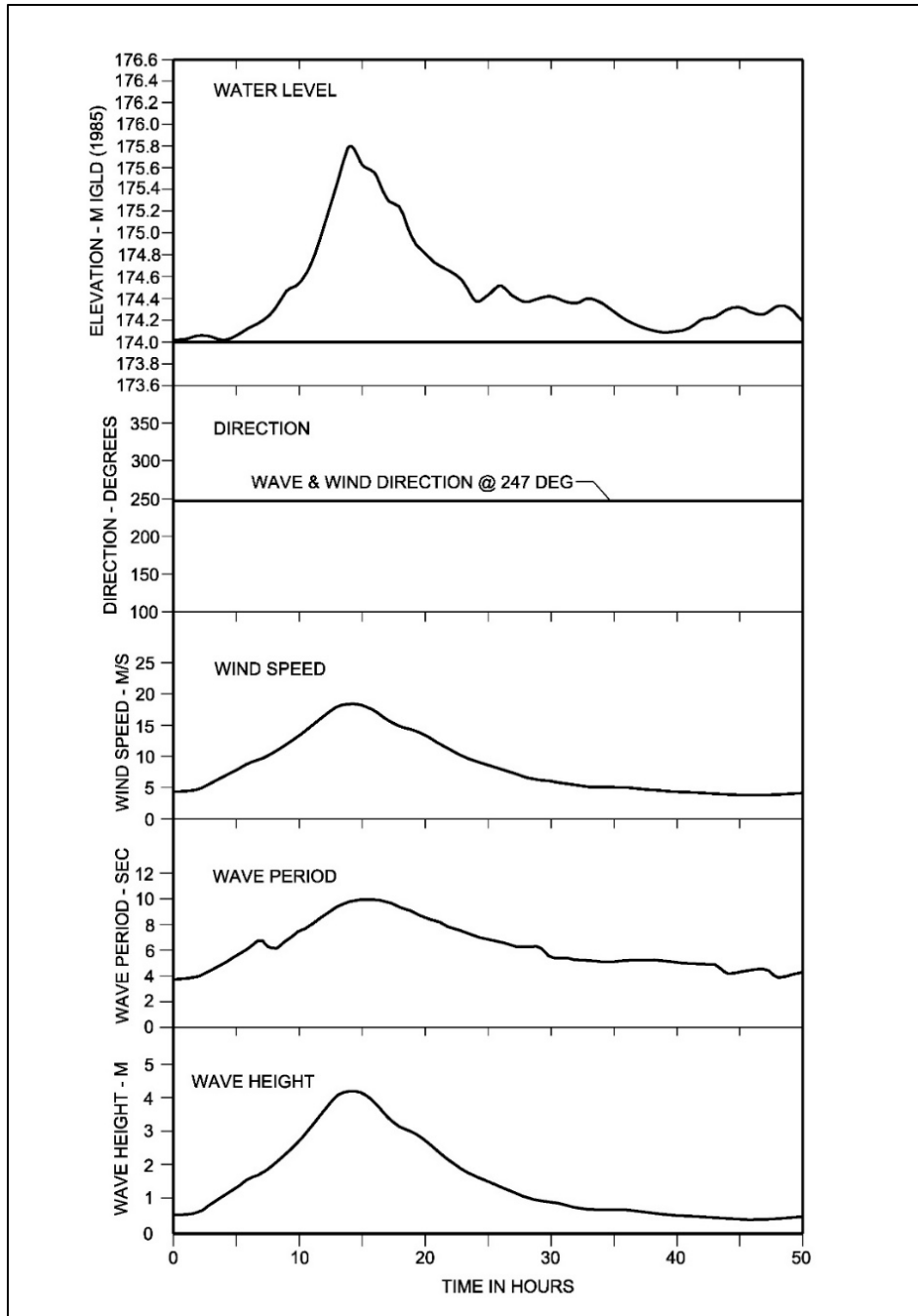Figure C-13. Time series data for the 2-year wave and 2-year water level storm.

Figure C-14. Time series data for the 20-year wave and 10-year water level storm.
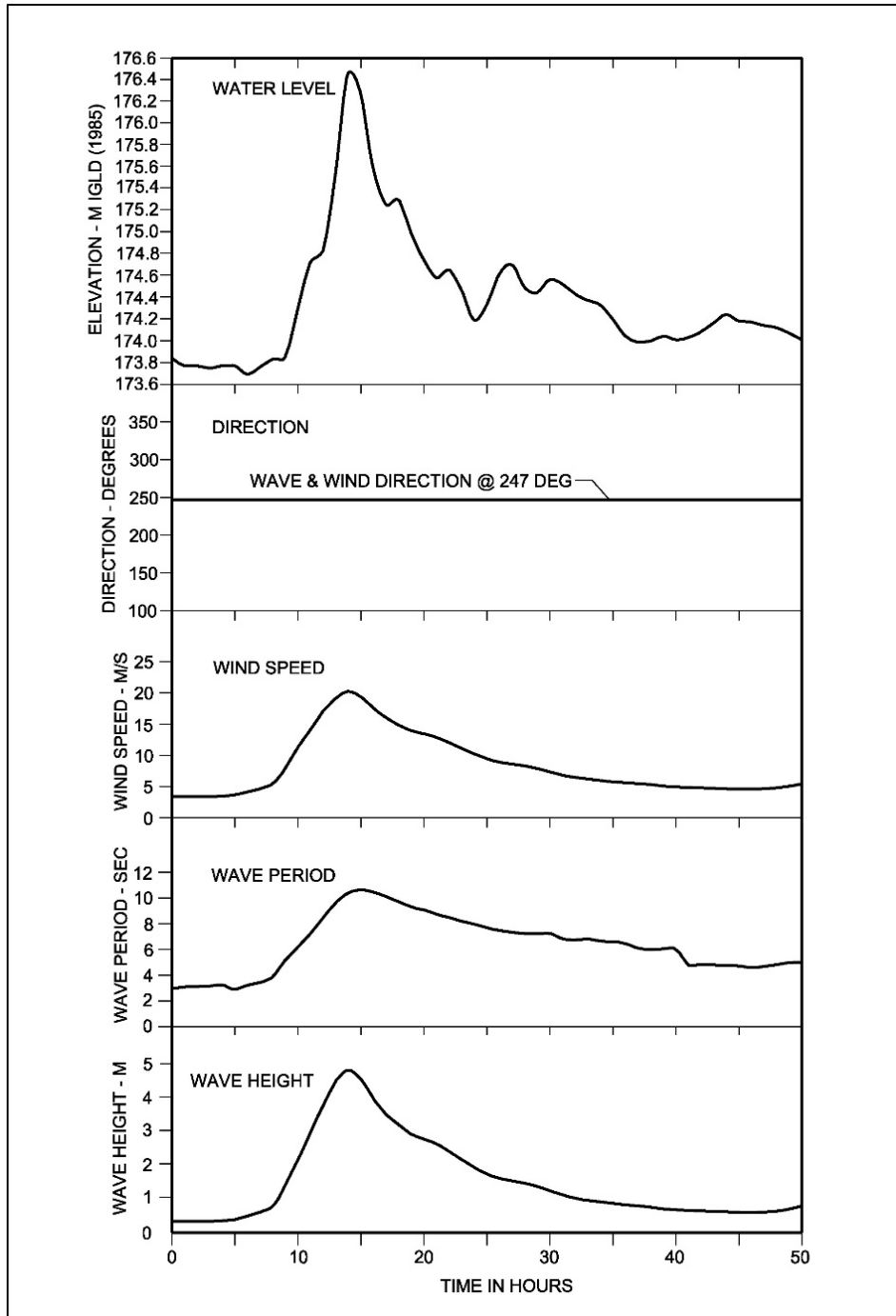
Table C-7. Hourly data for the 11 January 1982 storm.

Date and Time	H$_{mo}$ - M	T$_P$ - Sec	Wave Direction Degrees Azimuth	Wind Speed - m/s	Wind Direction Degrees Azimuth	Water Level M IGLD 1985
1/10/1982 15:00	1.06	3.90	260	11.6	286	174.637
1/10/1982 16:00	1.47	4.94	260	12.4	276	174.917
1/10/1982 17:00	1.93	5.82	257	13.4	270	175.119
1/10/1982 18:00	2.52	6.66	254	15.2	262	175.116
1/10/1982 19:00	2.97	7.46	252	15.8	261	175.027
1/10/1982 20:00	3.19	8.24	252	15.8	260	175.609
1/10/1982 21:00	3.24	8.82	251	15.4	258	175.981
1/10/1982 22:00	3.34	9.15	249	15.9	253	176.149
1/10/1982 23:00	3.56	9.59	249	16.7	249	176.191
1/11/1982 0:00	3.86	9.98	247	19.8	233	176.362
1/11/1982 1:00	4.28	10.20	248	20.3	243	176.176
1/11/1982 2:00	4.34	10.46	248	19.2	244	176.048
1/11/1982 3:00	4.12	10.67	248	18.4	243	175.844
1/11/1982 4:00	3.93	10.65	247	17.5	242	175.804
1/11/1982 5:00	3.69	10.44	247	16.5	241	175.652
1/11/1982 6:00	3.47	10.20	247	15.6	243	175.567
1/11/1982 7:00	3.35	10.00	247	16.1	242	175.466
1/11/1982 8:00	3.37	9.84	247	16.7	241	175.582
1/11/1982 9:00	3.52	9.76	248	17.8	240	175.707
1/11/1982 10:00	3.82	9.80	248	19.4	240	175.801
1/11/1982 11:00	4.20	10.00	248	20.4	240	175.820
1/11/1982 12:00	4.37	10.17	247	21.2	229	175.978
1/11/1982 13:00	4.25	10.30	247	18.7	245	176.015
1/11/1982 14:00	3.70	10.30	248	14.6	263	175.844
1/11/1982 15:00	3.03	10.12	248	12.0	284	175.719
1/11/1982 16:00	2.63	9.98	248	12.2	282	175.579
1/11/1982 17:00	2.59	9.92	247	12.5	279	175.399
1/11/1982 18:00	2.77	9.86	248	13.4	275	175.557
1/11/1982 19:00	2.91	9.86	248	13.5	278	175.469
1/11/1982 20:00	2.85	9.86	248	12.3	282	175.271
1/11/1982 21:00	2.63	9.80	248	11.0	284	175.213
1/11/1982 22:00	2.38	9.66	248	9.8	290	175.158
1/11/1982 23:00	2.15	9.34	247	8.7	297	174.911

Date and Time	H_{mo} - M	T_P - Sec	Wave Direction Degrees Azimuth	Wind Speed - m/s	Wind Direction Degrees Azimuth	Water Level M IGLD 1985
1/12/1982 0:00	1.97	9.16	247	7.9	297	174.814
1/12/1982 1:00	1.81	9.09	247	7.1	316	174.735
1/12/1982 2:00	1.66	9.04	246	7.1	334	174.597
1/12/1982 3:00	1.51	8.96	246	6.7	349	174.515
1/12/1982 4:00	1.35	8.70	246	5.9	355	174.515
1/12/1982 5:00	1.21	8.38	246	5.5	3	174.478
1/12/1982 6:00	1.09	8.28	246	4.9	3	174.411
1/10/1982 15:00	1.06	3.90	260	11.6	286	174.637
1/10/1982 16:00	1.47	4.94	260	12.4	276	174.917
1/10/1982 17:00	1.93	5.82	257	13.4	270	175.119
1/10/1982 18:00	2.52	6.66	254	15.2	262	175.116

Figure C-15. Time series data for the 11 January 1982 storm.
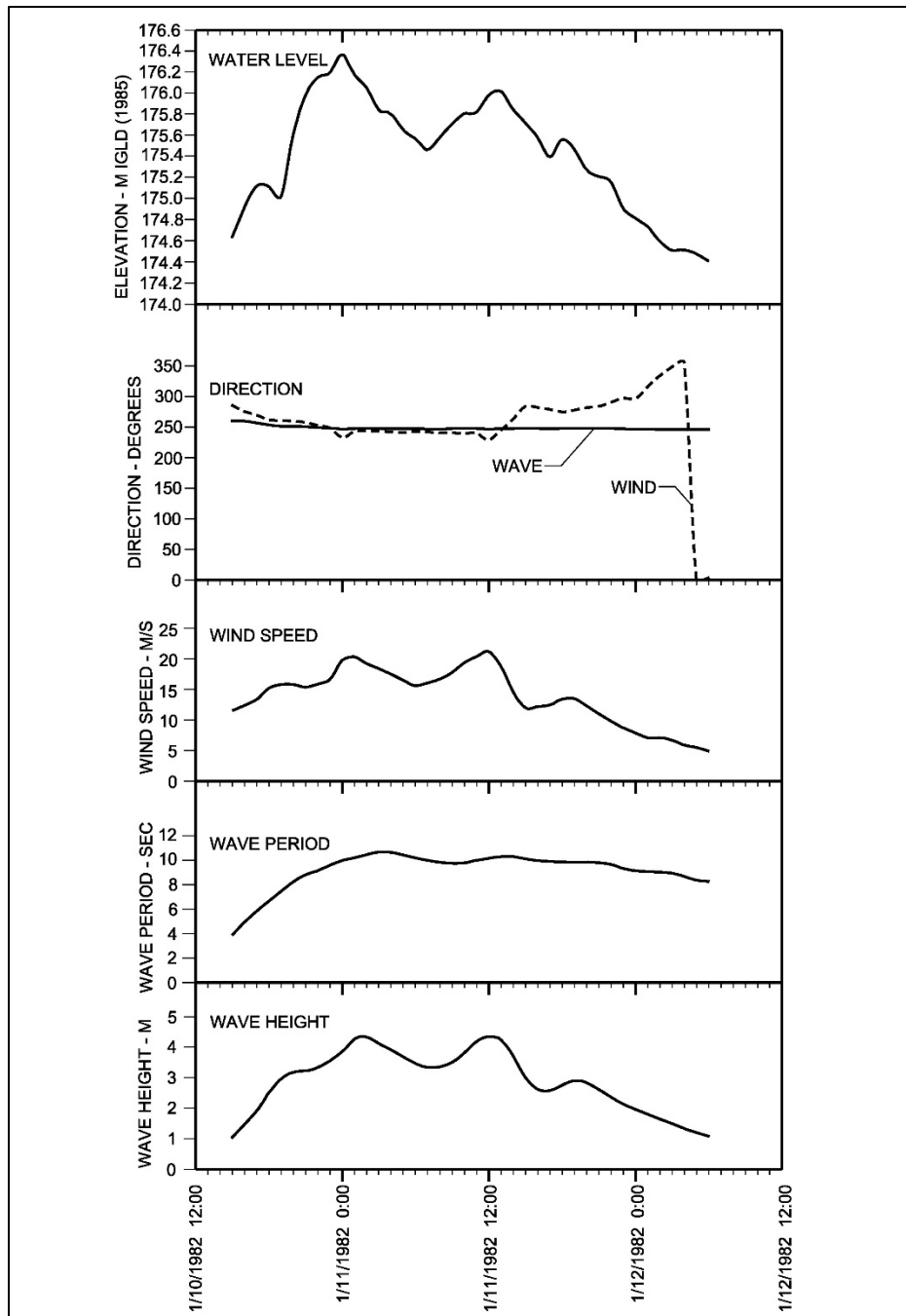
Unit Conversion Factors

Multiply	By	To Obtain
acres	4,046.873	square meters
cubic yards	0.7645549	cubic meters
feet	0.3048	meters
knots	0.5144444	meters per second
miles per hour	0.44704	meters per second
miles (U.S. nautical)	1.852	kilometers
miles (U.S. statute)	1.609347	kilometers

REPORT DOCUMENTATION PAGE

Form Approved OMB No. 0704-0188

The public reporting burden for this collection of information is estimated to average 1 hour per response, including the time for reviewing instructions, searching existing data sources, gathering and maintaining the data needed, and completing and reviewing the collection of information. Send comments regarding this burden estimate or any other aspect of this collection of information, including suggestions for reducing the burden, to Department of Defense, Washington Headquarters Services, Directorate for Information Operations and Reports (0704-0188), 1215 Jefferson Davis Highway, Suite 1204, Arlington, VA 22202-4302. Respondents should be aware that notwithstanding any other provision of law, no person shall be subject to any penalty for failing to comply with a collection of information if it does not display a currently valid OMB control number. **PLEASE DO NOT RETURN YOUR FORM TO THE ABOVE ADDRESS.**

1. REPORT DATE May 2019	2. REPORT TYPE Final Report	3. DATES COVERED *(From - To)*
4. TITLE AND SUBTITLE Design Water Levels and Waves for Repairs of Buffalo Harbor North and South Breakwaters and LaSalle Park Seawall, Buffalo, New York		**5a. CONTRACT NUMBER**
		5b. GRANT NUMBER
		5c. PROGRAM ELEMENT NUMBER 280H46
6. AUTHOR(S) Zeki Demirbilek, Lihwa Lin, Okey G. Nwogu, Weston P. Cross, Colleen M. O'Connell, Shanon Chader, Michael C. Mohr, Geoffrey K. Hintz, Sheila E. Hint, and Michael G. Draganac		**5d. PROJECT NUMBER**
		5e. TASK NUMBER
		5f. WORK UNIT NUMBER
7. PERFORMING ORGANIZATION NAME(S) AND ADDRESS(ES) Coastal and Hydraulics Laboratory U.S. Army Engineer Research and Development Center 3909 Halls Ferry Road Vicksburg, MS 39180-6199		**8. PERFORMING ORGANIZATION REPORT NUMBER** ERDC/CHL TR-19-8
9. SPONSORING/MONITORING AGENCY NAME(S) AND ADDRESS(ES) Buffalo District, U.S. Army Corps of Engineers 1776 Niagara Street Buffalo, NY 14207		**10. SPONSOR/MONITOR'S ACRONYM(S)** LRB
		11. SPONSOR/MONITOR'S REPORT NUMBER(S)

12. DISTRIBUTION/AVAILABILITY STATEMENT
Approved for public release; distribution is unlimited

13. SUPPLEMENTARY NOTES

14. ABSTRACT
Details of modeling approach for developing estimates of design water levels and waves for two U.S. Army Corps of Engineers (USACE) Buffalo District repair projects are described in this report. The estimates are for (1) the existing Buffalo Harbor (BH) South Breakwater (SB) and its two repair alternatives, and the existing BH North Breakwater, and (2) the LaSalle Park seawall along the northeast shore of the harbor that connects to the Niagara River canal. Two classes of wave models were used to develop these estimates for structural repairs: (1) CMS-Wave, a spectral wind-wave generation, growth, and transformation model, and (2) a nonlinear Boussinesq-type wave model BOUSS-2D. Estimates were developed for the 10-year maximum design water level condition of 3 meters (m) (9.8 feet ft) Low Water Datum and the 20-year design storm conditions with incident wave heights of 3.85 m (12.6 ft) and 4.15 m (13.6 ft), peak period of 10 seconds, and three incident wave directions of 233, 240, and 247 degrees. Study details, including data used, numerical modeling investigations, and analysis of results, are presented in this report.

15. SUBJECT TERMS

Boussinesq Modeling, Buffalo (N.Y.) Harbor, Breakwaters—Maintenance and repair, Coastal engineering, Harbors, Overtopping, Repairs, Runup, Seawall, Structural, Water level, Water waves

16. SECURITY CLASSIFICATION OF:			17. LIMITATION OF ABSTRACT	18. NUMBER OF PAGES	19a. NAME OF RESPONSIBLE PERSON Zeki Demirbilek
a. REPORT Unclassified	**b. ABSTRACT** Unclassified	**c. THIS PAGE** Unclassified	Unclassified	136	
					19b. TELEPHONE NUMBER *(Include area code)* 601.634.2834

Standard Form 298 (Rev. 8/98)
Prescribed by ANSI Std. Z39.18